nature immunology

Article

https://doi.org/10.1038/s41590-022-01367-z

Adaptive immune responses to SARS-CoV-2 persist in the pharyngeal lymphoid tissue of children

Received: 18 March 2022

Accepted: 21 October 2022

Published online: 19 December 2022

Check for updates

A list of authors and their affiliations appears at the end of the paper

Most studies of adaptive immunity to SARS-CoV-2 infection focus on peripheral blood, which may not fully reflect immune responses at the site of infection. Using samples from 110 children undergoing tonsillectomy and adenoidectomy during the COVID-19 pandemic, we identified 24 samples with evidence of previous SARS-CoV-2 infection, including neutralizing antibodies in serum and SARS-CoV-2-specific germinal center and memory B cells in the tonsils and adenoids. Single-cell B cell receptor (BCR) sequencing indicated virus-specific BCRs were class-switched and somatically hypermutated, with overlapping clones in the two tissues. Expanded T cell clonotypes were found in tonsils, adenoids and blood post-COVID-19, some with CDR3 sequences identical to previously reported SARS-CoV-2-reactive T cell receptors (TCRs). Pharyngeal tissues from COVID-19-convalescent children showed persistent expansion of germinal center and antiviral lymphocyte populations associated with interferon (IFN)-γ-type responses, particularly in the adenoids, and viral RNA in both tissues. Our results provide evidence for persistent tissue-specific immunity to SARS-CoV-2 in the upper respiratory tract of children after infection.

SARS-CoV-2 induces humoral and cellular immune responses in children, primarily noted by assessing antibody and T cell responses in peripheral blood[1,2]; however, little is known about immune responses to the virus in lymphoid tissues of the upper respiratory tract, where initial infection and viral replication take place[3,4]. The palatine tonsils and adenoids are secondary lymphoid structures at the mucosal surface of the naso- and oropharynx, in which tissue-specific T and B cell responses to antigens in the upper respiratory tract can be generated[5,6]. Here, collaborative interactions between follicular helper T (T_{FH}) cells and B cells enable immunoglobulin (Ig) gene class switching and formation of germinal centers (GCs), where B cells undergo somatic hypermutation of Ig genes and affinity maturation and results in the production of high-affinity antibodies and memory B cells. As tonsillectomy and adenoidectomy are among the most common pediatric surgeries, these tissues offer an accessible secondary lymphoid tissue to study immune responses to SARS-CoV-2 (ref. [7]). Using in-depth immune profiling, we characterized adaptive immune responses to SARS-CoV-2 in the tonsils and adenoids of children after COVID-19 infection and described antigen-specific responses, as well as long-term alterations in tissue-specific B and T lymphocyte populations involved in GC and antiviral memory responses following COVID-19 infection.

Results

SARS-CoV-2 induces robust GC responses

We collected blood, tonsils and adenoids from 110 children who underwent tonsillectomy and/or adenoidectomy primarily between September 2020 and January 2021 in the Washington DC metropolitan area (Fig. 1a and Supplementary Tables 1–3). All participants were required to have a negative SARS-CoV-2 polymerase chain reaction (PCR) test from a nasopharyngeal swab within 72 h before surgery. Eleven participants had a previous diagnosis of COVID-19 confirmed by PCR or antigen detection, ranging from 25 to 303 d before surgery (average 102 d), with only 7 of these 11 participants (64%) reporting symptoms at the time of positive testing (Fig. 1b and Supplementary Table 3). Thirteen

e-mail: pams@nih.gov; kalpana.manthiram@nih.gov

additional participants were identified as having been infected with SARS-CoV-2 through serological testing and/or identification of B cells that bound probes for both the S1 and receptor-binding domains (RBD) of the SARS-CoV-2 spike protein ($S1^+RBD^+$ B cells), resulting in a total of 24 participants with evidence of previous COVID-19 (post-COV; Fig. 1a and Supplementary Table 4). The remaining 86 participants were used as uninfected controls (UCs).

During the sample collection period, the dominant circulating SARS-CoV-2 strains in the Washington DC area were the D614G variant (similar to WA-1) until November 2020 and Alpha after December 2020 (refs. [8,9]). Accordingly, neutralizing antibodies against WA-1, B.1.1.7 (Alpha) and B.1.429 (Epsilon) were detected in the serum of all seropositive individuals, but not UCs; fewer post-COV individuals had neutralizing antibodies to other variants of concern, including B.1.617.2 (Delta, 21 of 23) and B.1.1.529 (Omicron, 9 out of 23) (Fig. 1c and Supplementary Table 4). Neutralizing titers were highest against the WA-1 strain and inversely correlated with the time since a positive PCR/antigen test in participants with previous testing (Fig. 1d). Overall, 80% of participants were seropositive to the common cold coronaviruses HCoV-OC43 and HCoV-HKU1, with no differences between post-COV and UC groups (Supplementary Table 4).

We detected $S1^+RBD^+$ B cells in peripheral blood mononuclear cells (PBMCs), tonsils and adenoids of all seropositive individuals (Fig. 1e), although responses were heterogeneous. Donors CNMC91 and CNMC104 had very few $S1^+RBD^+$ binding B cells in PBMCs and the lowest serum-neutralizing antibody titers to WA-1 among our cohort, whereas another participant (CNMC32) had high serum-neutralizing titers, but very low percentages of $S1^+RBD^+$ B cells, particularly in the tonsils and adenoids (Extended Data Fig. 1a).

High-dimensional flow cytometry analyses of B cells from post-COV PBMCs, tonsils and adenoids indicated that the majority of $S1^+RBD^+$ B cells were Ig class-switched $IgD^-CD38^-CD27^+$ memory B cells (hereafter, $CD27^+$ B_{SM} cells) (Fig. 1f,g, Extended Data Fig. 1b and Supplementary Figs. 1 and 2) that were present up to 10 months post-infection (Extended Data Fig. 1c) and were primarily IgG^+ (81% in PBMC, 82% adenoids, 84% tonsil; Extended Data Fig. 1d); fewer were IgA^+ relative to the total $CD27^+$ B_{SM} cells even in the adenoid and tonsil (14% versus 34% in adenoid, $P < 0.001$; 14% versus 28% in tonsil, $P < 0.001$) (Extended Data Fig. 1d). Of note, the percentage of $S1^+RBD^+$ B cells (0.2% in adenoids and tonsils) among $CD27^+$ B_{SM} cells in the pharyngeal tissues of post-COV individuals was comparable to that reported in the lung and lung-draining lymph nodes from organ donors who were post-COVID-19 (Extended Data Fig. 1e)[10].

Postmortem analyses of adults with fatal COVID-19 revealed loss of GCs in lymphoid organs[11]; however, we observed similar numbers and sizes of GCs, with discrete dark and light zones, in adenoids and tonsils from post-COV and UC children using multiplex immunofluorescence microscopy (Fig. 1h and Extended Data Fig. 1f,g). We also found a substantial portion of $IgD^-CD38^{int}CD19^+$ GC B cells (hereafter, GC B cells) among the $S1^+RBD^+$ B cells in both tissues (19% adenoid and 18% tonsil, range 2–47%; Fig. 1g). Paired analyses indicated more $S1^+RBD^+$ B cells among both total and GC B cells in adenoids compared to tonsils from the same donor (Extended Data Fig. 1h,i). The frequencies of $S1^+RBD^+$ B cells in adenoids, but not tonsils or PBMCs, also correlated significantly with serum neutralization titers for B.1.351 (Beta), B.1.526 (Iota), B.1.617.2 (Delta) and B.1.1.529 (Omicron) variants (Extended Data Fig. 1j), suggesting an important role for the adenoids in generating immune responses to SARS-CoV-2.

Early responses to SARS-CoV-2 in symptomatic patients are dominated by extrafollicular responses, characterized by expansion of $IgD^-CD27^-CD38^-CD19^+$ B cells (double-negative (DN) B cells)[12,13]. Although we saw expansion of DN B cells among $S1^+RBD^+$ B cells in post-COV adenoids and tonsils (Fig. 1g), most were $CD21^+CD11c^-$ DN B cells (known as DN1 cells; 81% in adenoid and 87% tonsil), which are derived from GCs (Fig. 1i). Only a small proportion (1.3% in adenoid and 1.5% tonsil) were $CD21^-CD11c^+$ DN2 B cells, which originate from extrafollicular B cell activation and were reported to expand in acute severe COVID-19 (ref. [12]). Thus, robust humoral responses to SARS-CoV-2 are generated and maintained in the tonsils and adenoids after COVID-19 infection.

CITE-seq of $S1^+$ B cells revealed their distinct features

To further investigate B cell responses, we sorted S1-binding ($S1^+$) and non-binding ($S1^-$) B cells from tonsils, adenoids and PBMCs from two post-COV individuals (CNMC71 and CNMC89) and one UC (CNMC99) (Supplementary Fig. 3a,b) and characterized these by cellular indexing of transcriptomes and epitopes by sequencing (CITE-seq), which simultaneously measured the expression of 22 B cell surface markers and sequenced the transcriptome and V(D)J/BCR in single cells. Over 1,860 $S1^+$ B cells and 25,000 $S1^-$ B cells were captured and analyzed. Surface antibody staining patterns evaluated with unsupervised clustering were concordant with the cell types suggested by gene expression signatures (memory B cells, GC B cells and plasma cells/plasmablasts)[14] in each cluster (Fig. 2a–e and Extended Data Fig. 2a,b). Confirming our flow analyses, the majority of $S1^+$ B cells in tonsils and adenoids were in cluster 2, which represented $CD27^+$ B_{SM} cells (Fig. 2c–e) with a smaller, but clear proportion of $S1^+$ B cells in cluster 4, which had a GC B cell gene expression signature and surface protein profile (Fig. 2a–e and Extended Data Fig. 2a,b). In contrast, $S1^+$ B cells in the blood were primarily in cluster 9 (Fig. 2a–c,e), which was a $CD27^+IgD^-$ cell population (Fig. 2e) but had distinct surface marker and gene expression profile compared to the $CD27^+IgD^-$ B_{SM} cells in the lymphoid tissues (Fig. 2e and Extended Data Fig. 2a-b). $S1^+$ memory B cells in cluster 2 had higher expression of *CXCR3* and *HOPX*, genes known to be induced by T-bet in T cells[15], and lower expression of several inhibitory receptors, including *FCGR2B*, *FCRL2*, *FCRL3* and *TNFRSF13B* (encoding TACI)[16] than $S1^-$ B cells (Supplementary Table 5 and Extended Data Fig. 2c), suggesting distinct features of the SARS-CoV-2-specific B cells.

BCR sequence analysis confirmed that $S1^+$ B cells were primarily IgG1 and IgA1 class-switched cells (Fig. 3a and Extended Data Fig. 2d), with high frequencies of somatic hypermutation (SHM) in V_H genes (Fig. 3b and Extended Data Fig. 2e) and low clonal diversity compared to $S1^-$ B cells (Fig. 3c), indicative of antigen-driven clonal expansion and GC origin. Overall, 44 $S1^+$ B cells had the same V and J genes and 80% similarity of their heavy chain CDR3 amino acid (aa) sequence to sequences publicly reported in the CoV-AbDab database[17], including one clone similar to 37 published antibody sequences (Supplementary Table 6 and Supplementary Fig. 4a–c).

A proportion of $S1^+$ B cell clones (83 B cells from 29 clones, 20 clones from CNMC89 and 9 from CNMC71) were present in both the tonsils and adenoids (Fig. 3d). The shared $S1^+$ B cell clones were nearly all isotype-switched (Extended Data Fig. 2f) and consisted primarily of $CD27^+$ B_{SM} cells (cluster 2; Fig. 2e); however, four cells among the shared clones in the tonsil of one donor were GC B cells (cluster 4) (Fig. 2e and Supplementary Table 7). Clonal lineage trees (Fig. 3e) suggested that class switching could occur before, during or after SHM. Thus, multimodal single cell analysis of SARS-CoV-2-specific B cells confirms their emergence from GCs and suggests migration of clonally expanded B cells between pharyngeal lymphoid tissues.

GC populations are expanded post-COVID-19

To determine whether SARS-CoV-2 infection could alter the immune landscape of mucosal tissues beyond acute infection, we used both unsupervised analyses (controlled for age and sex) and manual gating of high-dimensional flow cytometry data to compare immune cell profiles of tonsils, adenoids and PBMCs from post-COV and UC participants (Supplementary Table 2). $CD19^+$ B, $CD4^+$ T and $CD8^+$ T lymphocytes were gated and analyzed independently. Adenoids and tonsils were evaluated together, whereas PBMCs were examined separately, to increase sensitivity for detecting distinct populations in tissues and peripheral

https://doi.org/10.1038/s41590-022-01367-z

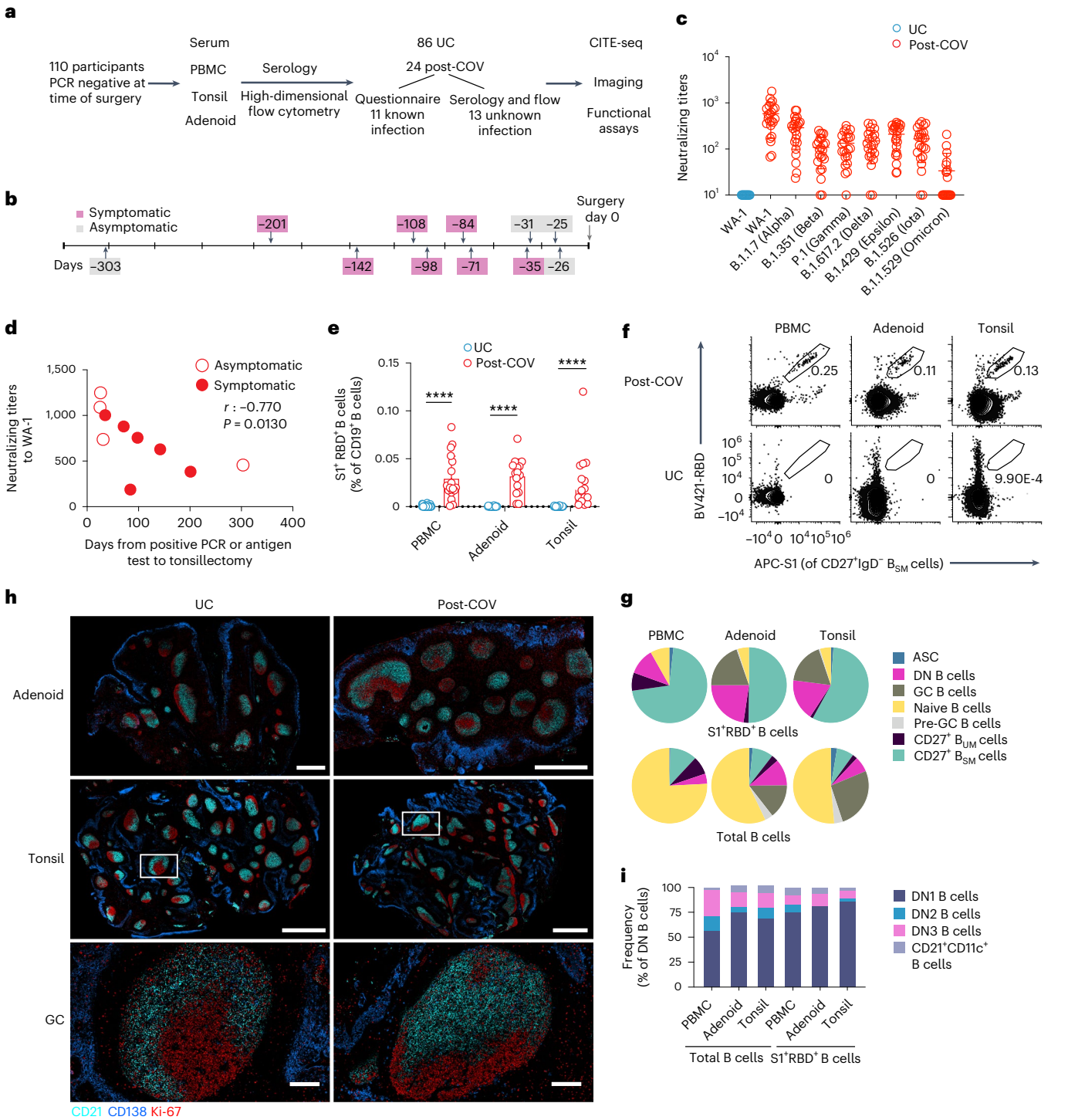

Fig. 1 | SARS-CoV-2 elicits robust humoral immune responses in children. **a**, Enrollment of post-COV and UC individuals and study design. **b**, Time from previous positive SARS-CoV-2 PCR/antigen test to tonsillectomy and/or adenoidectomy in 11 individuals with known previous infection. **c**, Neutralizing antibody titers (PsVNA50) against the early isolate WA-1 and seven other SARS-CoV-2 variants of interest (post-COV, $n = 23$; UC, $n = 14$). **d**, Correlation between neutralizing antibody titers to WA-1 and days from positive SARS-CoV-2 test to surgery ($n = 10$). Spearman's rank correlation (r) and P values are noted. **e**, Frequency of SARS-CoV-2-specific ($S1^+RBD^+$) cells among total $CD19^+$ B cells from PBMCs, adenoids and tonsils from post-COV and UC donors (PBMCs post-COV, $n = 18$; UC, $n = 33$; adenoids post-COV, $n = 16$; UC, $n = 27$; and tonsil post-COV, $n = 16$; UC, $n = 30$; all $P < 10^{-6}$). **f**, Representative flow cytometry plots showing the percentage of $S1^+RBD^+$ cells among $IgD^-CD38^-CD27^+CD19^+$ switched memory B cells ($CD27^+ B_{SM}$) in post-COV PBMCs, adenoids and tonsils. **g**, Composition of $S1^+RBD^+$ B cells and total B cells from post-COV PBMCs ($n = 18$), adenoids ($n = 16$) and tonsils ($n = 16$). Mean frequency of each B cell subset (defined in Supplementary Figs. 1 and 2) shown in pie chart. ASC, antibody secreting cells equivalent to plasma cells and plasmablasts; $CD27^+ B_{UM}$, $CD27^+IgD^+$ unswitched memory B. **h**, Images of adenoids and tonsils showing GCs from one post-COV donor and one UC, representative of three post-COV and three UC donors. Inset shows close-up of GC and light (CD21, follicular dendritic cells, cyan) and dark zones (Ki-67, dividing cells, red). CD138 (plasma cell and epithelial cell marker) in blue. Scale bars, 1 mm (top), 2 mm (middle) and 200 µm (bottom). **i**, Composition of $S1^+RBD^+ IgD^-CD27^-CD38^-CD19^+$ DN B cells and total DN B cells from post-COV PBMCs ($n = 18$), adenoids ($n = 16$) and tonsils ($n = 16$). Mean frequency of each DN subset is shown in bar chart. Mean ± s.d. are displayed in bar and scatter-plots. Each dot represents one donor. Significance calculated with two-sided Mann–Whitney U-test. ****$P < 0.0001$.

https://doi.org/10.1038/s41590-022-01367-z

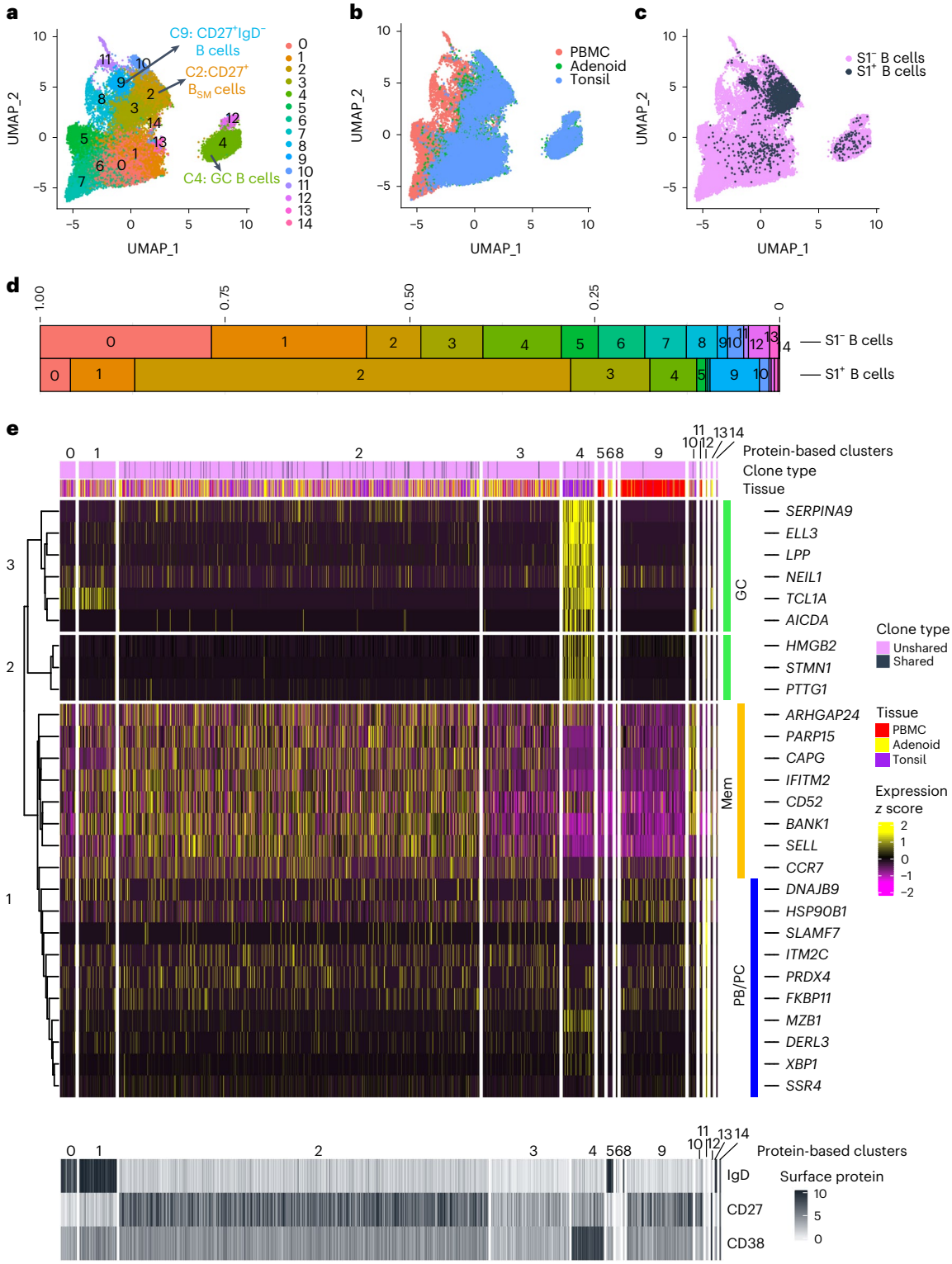

Fig. 2 | CITE-seq analysis of SARS-CoV-2 antigen-specific B cells. a, Uniform Manifold Approximation and Projection (UMAP) showing 15 clusters of sorted S1$^+$ and S1$^-$ B cells (Supplementary Fig. 3) from tonsils, adenoids and PBMCs from two post-COV (CNMC71 and CNMC89) and one UC (CNMC99) donors clustered according to CITE-seq surface antibody expression. **b**, Tissue distribution of S1$^+$ and S1$^-$ B cells in **a**. **c**, Distribution of S1$^+$ B cells among clusters in **a**. **d**, Proportion of each of the 15 clusters among S1$^-$ and S1$^+$ B cells in **a**. **e**, Heat map showing expression of signature gene sets for GC B cells, memory B cells (Mem) and plasma cells/plasmablasts (PC/PB)[14] among S1$^+$ B cells organized by cluster. IgD, CD38 and CD27 CITE-seq antibody expression are shown in the bottom heat map in gray. Tissue origin is shown in purple (tonsil), yellow (adenoid) and red (PBMC). Clones shared between tonsil and adenoid are marked in black in the top bar.

blood. Unsupervised analysis of B cells in post-COV versus UC samples revealed more significant differences in cluster frequencies in adenoids than tonsils (Fig. 4a,b and Extended Data Fig. 3a,b). Clusters 3 and 10, representing IgG$^+$ and IgM$^+$ GC B cells, respectively, were significantly increased in post-COV adenoids (Fig. 4b). In addition, a naive-type B cell cluster (cluster 14) was decreased in both post-COV tissues compared

https://doi.org/10.1038/s41590-022-01367-z

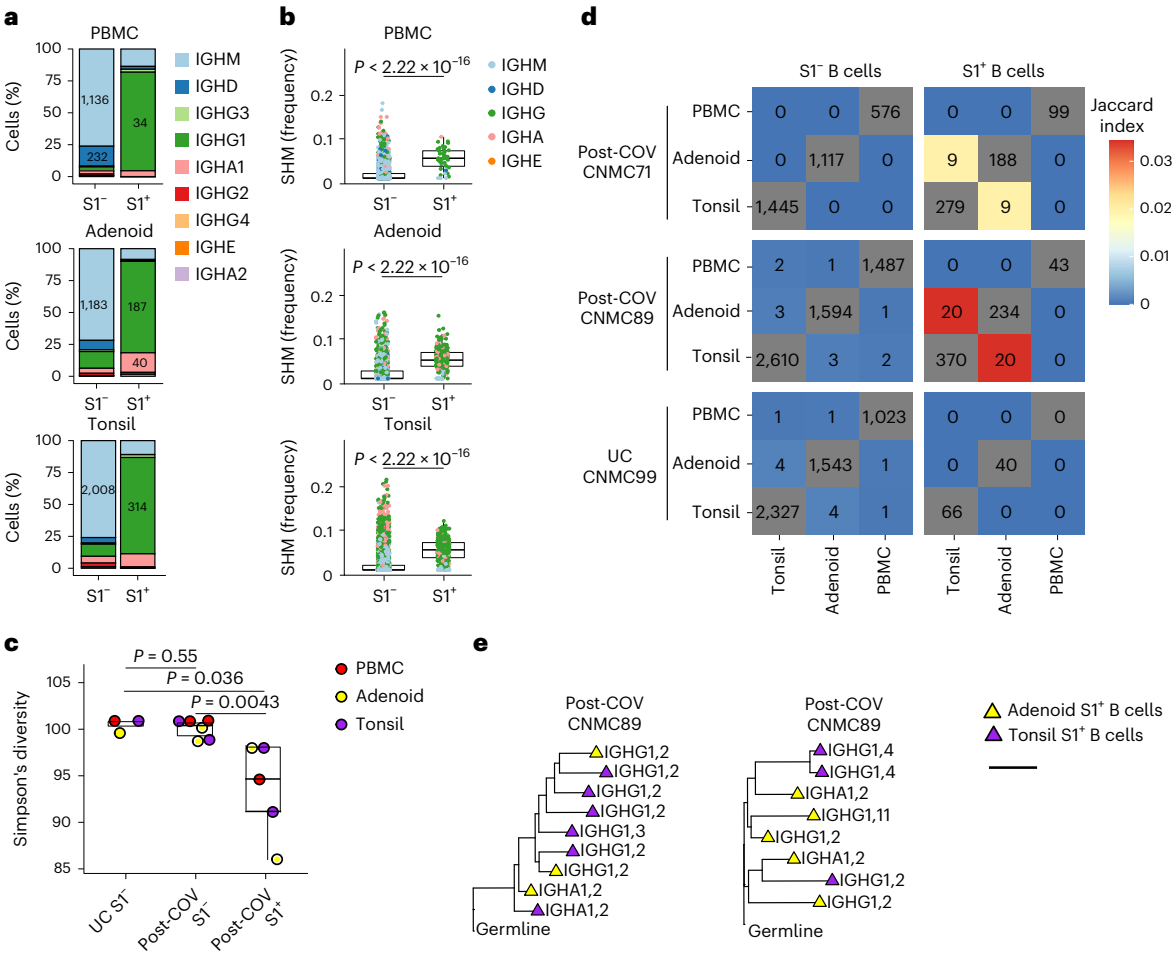

Fig. 3 | Single-cell BCR sequencing of SARS-CoV-2 antigen-specific B cells. **a**, Sub-isotype percentages among sorted S1$^+$ and S1$^-$ B cells from PBMC, adenoid and tonsil of one post-COV donor (CNMC89). Labels show the raw number of cells with a given sub-isotype and are only included for sub-isotypes that make up at least 10% of a given category. **b**, SHM frequency among sorted S1$^+$ and S1$^-$ B cells from PBMC, adenoid and tonsil of CNMC89 (PBMC S1$^+$ $n = 44$, S1$^-$ $n = 1{,}491$ cells; adenoid S1$^+$ $n = 261$, S1$^-$ $n = 1{,}647$ cells; tonsil S1$^+$ $n = 416$, S1$^-$ $n = 2{,}644$ cells). Mutation frequency calculated in V gene. Medians ± quartiles and *P* values are shown in the box plots. **c**, Simpson's diversity of S1$^+$ and S1$^-$ B cells from PBMCs, adenoids and tonsils from two post-COV donors (CNMC71 and 89) and S1$^-$ B cells from one UC (CNMC99). Lower Simpson's diversity values indicate a greater frequency of large clones. **d**, Overlap of B cell clones among PBMCs, tonsils and adenoids from post-COV and UC donors. Off-diagonal elements are colored by the Jaccard index of clonal overlap between the two tissues and are labeled by the raw number of overlapping clones. Diagonal elements are labeled by the total number of clones within a particular tissue. **e**, Clonal lineage trees from two of the largest S1$^+$ B cell clones shared between tonsil and adenoid from CNMC89. Triangles indicate S1$^+$ cells and tip color indicates tissue of origin (purple, tonsil; yellow, adenoid). Isotype and CITE-seq cluster of each cell are listed next to the symbol. Branch lengths represent SHM frequency/codon in VDJ sequence according to the scale bar. Significance calculated with two-sided Mann–Whitney *U*-test.

to UC (Fig. 4a,b). CD127$^+$IgD$^+$ B cells were also decreased in post-COV PBMCs (Fig. 4c,d and Supplementary Fig. 5a,b), as confirmed by manual gating of CD127$^+$ B cells (Fig. 4e). Thus, changes in B cell populations, including persistent enrichment of GC B cells in the adenoids, were detected after COVID-19 infection.

T_{FH} cell populations are expanded after COVID-19

Acute SARS-CoV-2 infection is associated with peripheral T cell lymphopenia[18]. We found post-COV adenoids had lower percentages of CD3$^+$ and CD4$^+$ T cells compared to UC (29.2% versus 34.1% for CD3$^+$; 23.2% versus 27.9% for CD4$^+$ T cells) (Extended Data Fig. 4a and gating in Supplementary Fig. 6). Unsupervised analysis of CD4$^+$ T cells showed a reduction in cluster 9, which represented CD45RA$^+$CCR7$^+$CD4$^+$ naive cells, in post-COV tonsils and adenoids compared to UC (Fig. 5a,b and Extended Data Fig. 4b,c); decreased percentages of naive CD4$^+$ T cells were also detected by manual gating (Fig. 5c). Conversely, cluster 3, a CD57$^+$PD-1^{hi}CD4$^+$ T cell subset, was significantly enriched in post-COV adenoids and tonsils (Fig. 5a,b), as confirmed by manual gating in adenoids (Fig. 5d). CD57 is a marker of T cell senescence associated with chronic infection, but is also found on some tonsillar CXCR5$^+$PD-1^{hi} GC T_{FH} cells[19,20]. Compared to the total CD4$^+$ T cell population in adenoids and tonsils from both post-COV and UC individuals, CD57$^+$PD-1^{hi} CD4$^+$ T cells exhibited higher expression of CXCR5, indicative of a T_{FH} cell phenotype and CD69, characteristic of tissue-resident memory T cells (T_{RM} cells) (Fig. 5e)[6]. Immunofluorescence microscopy indicated that CD57$^+$PD-1^{hi} CD4$^+$ T cells were located within tonsil and adenoid GCs (Fig. 5f) and their frequency positively correlated with the proportion of GC B cells in these tissues (both post-COV and UC samples analyzed) (Extended Data Fig. 5a,b). Phorbol myristate acetate (PMA) and ionomycin stimulation induced production of interleukin (IL)-21 and IL-10, cytokines that facilitate GC formation and B cell antibody secretion, in CD57$^+$PD-1^{hi} CD4$^+$ T cells (Extended Data Fig. 5c,d). Moreover, percentages of CD4$^+$ T cells in cluster 3 positively correlated with percentages of S1$^+$RBD$^+$ B cells that were GC B cells specifically in adenoids (Extended

https://doi.org/10.1038/s41590-022-01367-z

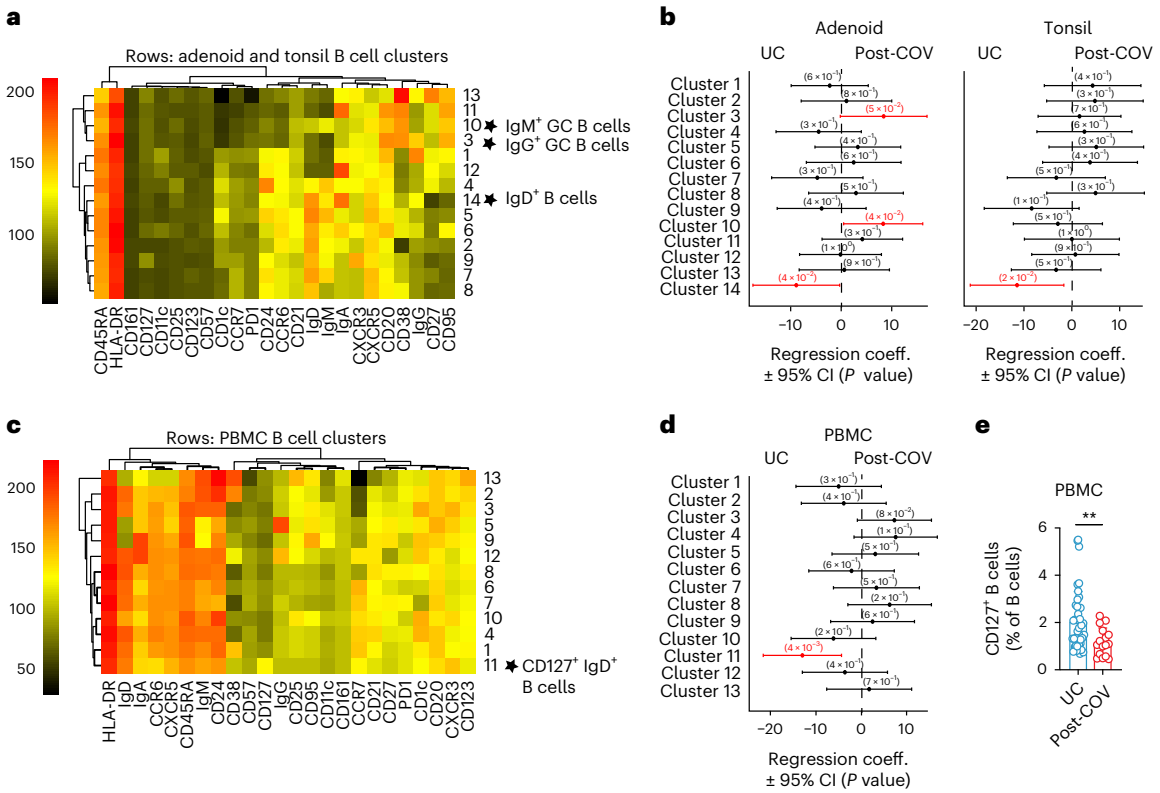

Fig. 4 | GC B cells are expanded in adenoids after COVID-19. a–**d**, Unsupervised clustering of CD19$^+$ B cells from adenoids and tonsils (**a**) and PBMCs (**c**) according to flow cytometric surface markers. Quantification of the effect of previous SARS-CoV-2 infection on CD19$^+$ B cell clusters in adenoids and tonsils (**b**) and PBMCs (**d**) showing regression coefficients ± 95% confidence intervals (CI) and *P* values, estimated with a linear model controlling for age and sex. Significantly different clusters ($P < 0.05$) between post-COV and UC groups are indicated with a star or highlighted in red. Adenoids, post-COV $n = 11$; UC $n = 33$; tonsils, post-COV $n = 15$; UC $n = 42$; PBMC, post-COV $n = 14$; UC $n = 36$. **e**, Frequency of CD127$^+$ B cells in post-COV ($n = 16$) and UC ($n = 41$) PBMCs, $P = 0.006$. Significance calculated with two-sided Mann–Whitney *U*-test. Each symbol represents one donor. Mean ± s.d. are displayed. $^{**}P < 0.01$.

Data Fig. 5e), supporting their role in the generation and persistence of SARS-CoV-2-specific GC responses.

Manual gating also revealed more CD25$^+$CXCR5$^+$PD-1^{hi} cells among CD4$^+$ T cells in post-COV tonsils compared to UC (Extended Data Fig. 5f); these CD25$^+$CXCR5$^+$PD-1^{hi} cells produced more IL-21 and IL-10 after PMA and ionomycin stimulation compared to their CD25$^-$ counterparts (Extended Data Fig. 5g) and their frequencies correlated with percentages of GC B cells in the tonsils (Extended Data Fig. 5h), suggesting they were activated cells important for GC generation[21]. Cluster 6, which contained a population of CD45RA$^-$CXCR5$^+$PD-1^{int} pre-T$_{FH}$ cells that were CXCR3$^+$CCR6$^-$ (Extended Data Fig. 4b,c), a combination of markers associated with IFN-γ and T$_H$1 cytokine production[22], was also significantly increased in post-COV adenoids (but not tonsils) compared to UC; this was confirmed by manual gating (Fig. 5a,b and Extended Data Fig. 5i). A high percentage of CXCR3$^+$CCR6$^-$ pre-T$_{FH}$ cells produced IFN-γ after PMA and ionomycin stimulation (Extended Data Fig. 5j,k), suggesting that type 1 T cell responses were induced as part of the antiviral response to SARS-CoV-2 in adenoids.

Stimulation with PMA and ionomycin revealed several combinations of cytokines had higher expression in CD4$^+$ T cells in post-COV tonsils and adenoids than UC (Fig. 5g and Supplementary Fig. 7). Two of these combinations (categories 33 and 41) included IL-21, suggesting they were produced by T$_{FH}$ cells; category 33 also included IL-10 (Fig. 5g). Increased IFN-γ was part of a cytokine pattern (category 27) specifically enriched in post-COV adenoids compared to UC (Fig. 5g), consistent with the enrichment of CXCR3$^+$CCR6$^-$ pre-T$_{FH}$ cells in post-COV adenoids. We also noted more robust IFN-γ production by CD4$^+$ T cells in adenoids than tonsils (post-COV and UC analyzed together) (Extended Data Fig. 5l), indicating inherent differences between T cells in these tissues.

In PBMCs, unsupervised analysis revealed that two clusters (5 and 11) of CD45RA$^-$CXCR5$^+$PD-1$^+$ circulating T$_{FH}$-like cells (cT$_{FH}$ cells) expressing the activation marker CD38 (ref. [23]) were increased in post-COV samples compared to UC (Fig. 5h,i and Extended Data Fig. 6a,b); cluster 11 was also CXCR3$^+$. Although percentages of total cT$_{FH}$ cells were not increased in post-COV PBMCs compared to UC, manual gating indicated that cT$_{FH}$ cells were skewed to a CXCR3$^+$CCR6$^-$phenotype (Fig. 5j and gating in Supplementary Fig. 8); these cells produced IFN-γ upon stimulation with PMA and ionomycin (Extended Data Fig. 6c). We also observed a higher frequency of CD45RA$^+$CCR7$^+$CD28$^+$CD27$^+$CD95$^+$ stem cell-like memory CD4$^+$ T cells (T$_{SCM}$ cells) (Extended Data Fig. 6d) in post-COV PBMCs than UC, perhaps reflecting long-lived memory T cells previously reported in children after COVID-19 infection[24]. Thus, expansion of functional T$_{FH}$ cells with IFN-γ-associated skewing suggests prolonged immune activation in the upper respiratory tract and PBMCs of children weeks to months after COVID-19 infection.

CD8$^+$ T$_{RM}$ cells are expanded post-COVID-19

Similar to CD4$^+$ T cells, we observed reduced percentages of a naive CD8$^+$ T cell cluster (cluster 1) in adenoids from post-COV donors compared to UC (Fig. 6a,b and Extended Data Figs. 7a,b and 8a). Manual gating revealed a similar, although not significant trend, in both adenoids and tonsils, in addition to more effector memory CD8$^+$ T cells in post-COV tonsils compared to UC (Extended Data Fig. 8b,c). Adenoids and tonsils from post-COV donors exhibited non-statistically significant increases in clusters 2 and 3 compared to UCs, which represented

https://doi.org/10.1038/s41590-022-01367-z

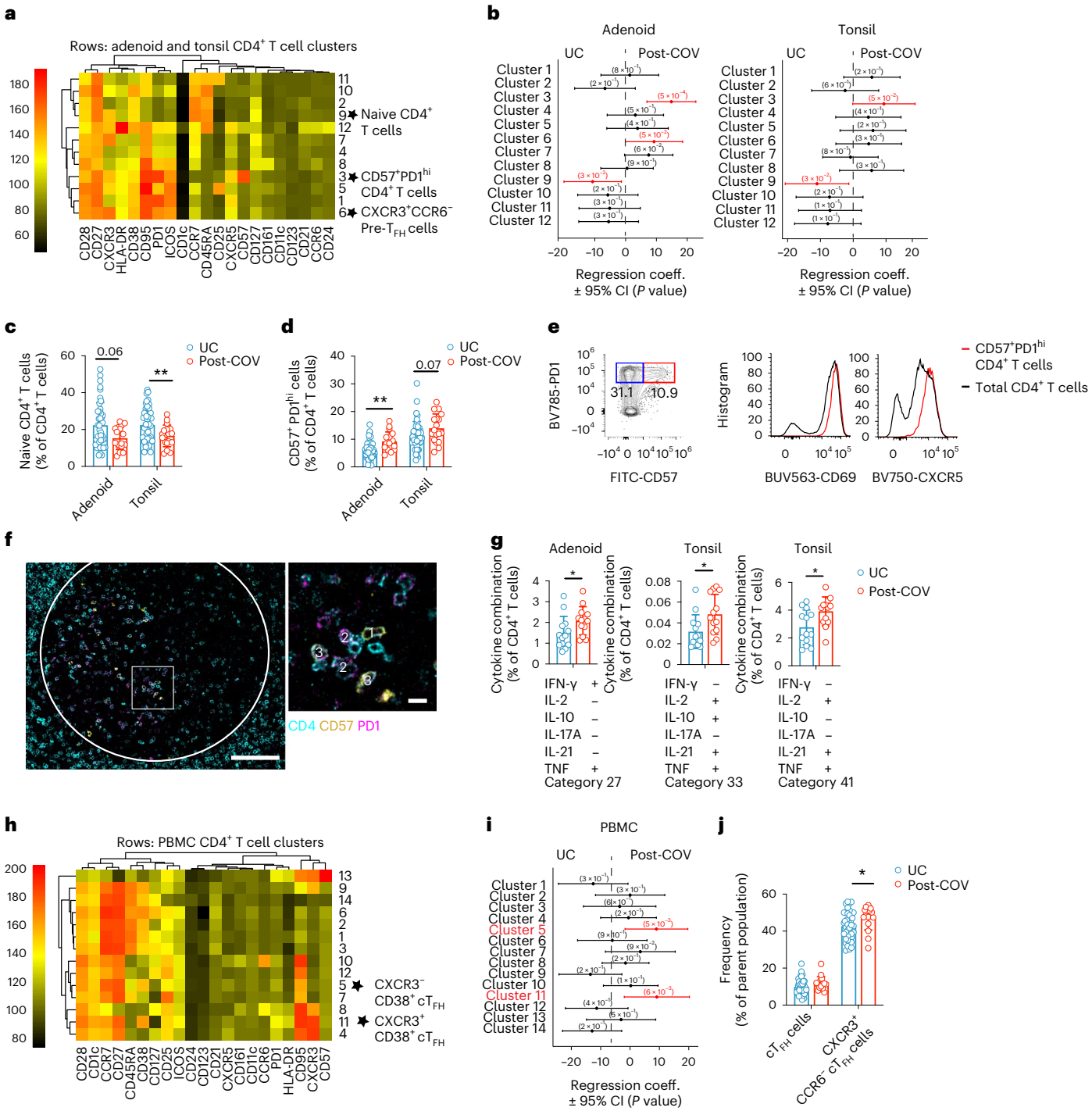

Fig. 5 | CD4$^+$ T_{FH} cells are expanded post-COVID-19. a,**b**, Unsupervised clustering of CD4$^+$ T cells from adenoids and tonsils according to flow cytometric surface markers (**a**). Quantification of the effect of previous SARS-CoV-2 infection on CD4$^+$ T cell clusters showing regression coefficients ± 95% CI and *P* values, estimated with a linear model controlling for age and sex (**b**). Significantly different clusters ($P < 0.05$) between post-COV and UC groups are indicated with a star or highlighted in red. Adenoids, post-COV $n = 12$, UC n = 38; tonsils, post-COV $n = 15$, UC $n = 43$. **c**,**d**, Frequencies of manually-gated CD45RA$^+$CCR7$^+$ naive CD4$^+$ T cells ($P = 0.022$ for tonsils) (**c**) and CD57$^+$PD-1^{hi} CD4$^+$ T cells ($P = 0.001$ for adenoid) (**d**) in post-COV and UC adenoids and tonsils (adenoids, post-COV $n = 17$, UC $n = 42$; tonsils, post-COV $n = 18$, UC $n = 46$). **e**, Plots of CD69 and CXCR5 expression on CD57$^+$PD-1^{hi} CD4$^+$ T cells and total CD4$^+$ T cells from one tonsil, representative of tonsils and adenoids from 26 donors. **f**, Image of post-COV adenoid showing CD57$^+$PD-1^{hi} CD4$^+$ T cells in one GC, representative of tonsils and adenoids from six donors. Magnification of square inset shown on the right. CD4 in cyan, CD57 in yellow and PD-1 in magenta. GC boundaries defined using Ki-67 (Fig. 1h). 1 indicates CD4$^+$CD57$^+$; 2 indicates CD4$^+$PD-1$^+$; 3 indicates CD4$^+$CD57$^+$PD-1$^+$ cells. Scale bars, 100 µm (left) and 10 µm (right). **g**, Cytokine combinations (IFN-γ, IL-2, IL-10, IL-17A, IL-21 and TNF as analyzed by SPICE) produced by tonsillar or adenoid CD4$^+$ T cells from post-COV ($n = 13$) and UC ($n = 13$) donors following PMA and ionomycin stimulation (category 27: $P = 0.04$, 33: $P = 0.01$, 41: $P = 0.03$). **h**,**i**, Unsupervised clustering of CD4$^+$ T cells from PBMC (**h**) and quantification of the effect of previous SARS-CoV-2 infection (**i**) as described in **a**,**b** (post-COV $n = 13$, UC $n = 34$). **j**. Frequencies of CD45RA$^-$CXCR5$^+$PD-1$^+$ circulating T_{FH} (cT_{FH}) and CXCR3$^+$CCR6$^-$ cT_{FH} cells in post-COV ($n = 16$) and UC ($n = 16$) PBMCs, $P = 0.032$ for CXCR3$^+$CCR6$^-$ cT_{FH} cells. Sample list for **a**–**d** and **h**–**j** in Supplementary Table 2 and for **g** in Supplementary Table 11. Each symbol represents one donor. Mean ± s.d. displayed in bar plots. Significance calculated with two-sided Mann–Whitney *U*-test. *$P < 0.05$, **$P < 0.01$.

https://doi.org/10.1038/s41590-022-01367-z

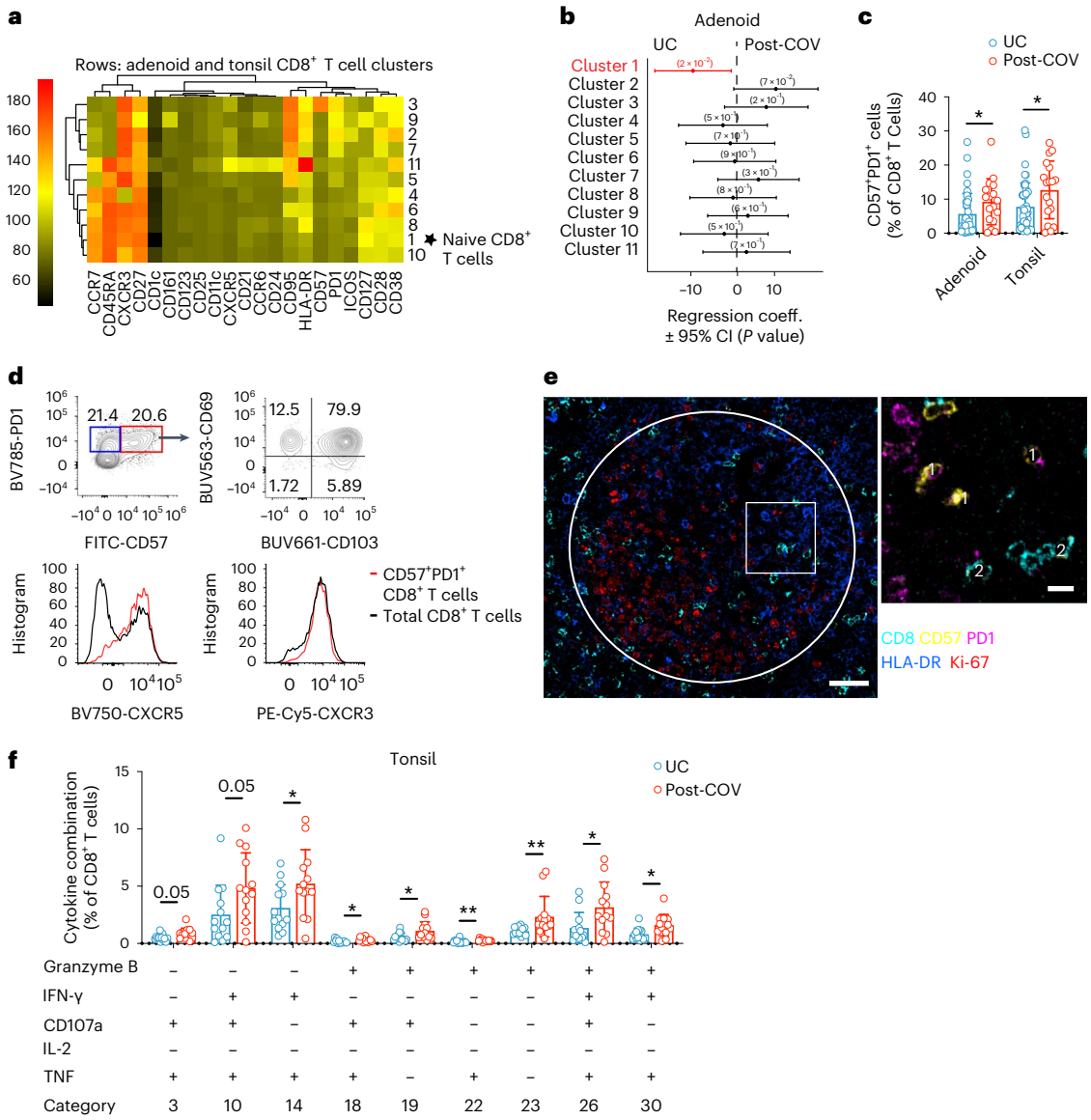

Fig. 6 | Tissue-resident memory CD8⁺ T cells are expanded post-COVID-19. **a**,**b**, Unsupervised clustering of CD8⁺ T cells from adenoids and tonsils according to flow cytometric surface markers (**a**). Quantification of the effect of previous SARS-CoV-2 infection on CD8⁺ T cell clusters showing regression coefficients ± 95% CI and *P* values, estimated with a linear model controlling for age and sex (**b**). Significantly different clusters ($P < 0.05$) between post-COV and UC groups are indicated with a star or highlighted in red. Adenoids post-COV $n = 12$, UC $n = 35$; tonsils post-COV $n = 15$, UC $n = 42$. **c**, Frequency of CD57⁺PD-1⁺CD8⁺ T cells in post-COV and UC adenoids (post-COV $n = 17$, UC $n = 42$, $P = 0.044$) and tonsils (post-COV $n = 18$, UC $n = 46$, $P = 0.030$) **d**, Flow cytometry plots showing CD69, CD103, CXCR5 and CXCR3 expression on CD57⁺PD-1⁺CD8⁺ T cells from one tonsil, representative of tonsils and adenoids from 26 donors. **e**, Adenoid from post-COV donor showing the location of CD57⁺PD-1⁺CD8⁺ T in one GC, representative of six samples. GC is circled, magnification of square is in inset. CD8 is cyan, CD57 is yellow, PD-1 is pink. HLA-DR (blue) stains follicles and Ki-67 (red) stains GC. 1 indicates CD8⁺CD57⁺PD-1⁺; 2 indicates CD8⁺CD57⁺ cells. Scale bars, 50 µm (left) and 10 µm (right). **f**, Cytokine/cytotoxic factor combinations (involving granzyme B, IFN-γ, CD107a, IL-2 and TNF, analyzed by SPICE) produced by tonsillar CD8⁺ T cells from post-COV ($n = 13$) and UC ($n = 13$) donors following PMA and ionomycin stimulation (category 3, $P = 0.049$; 10, $P = 0.051$; 14, $P = 0.035$; 18, $P = 0.020$; 19, $P = 0.032$; 22, $P = 0.007$; 23, $P = 0.001$; 26, $P = 0.017$; 30, $P = 0.025$). Sample list for **a**–**c** is in Supplementary Table 2 and **e**,**f** in Supplementary Table 11. Each symbol represents one donor. Mean ± s.d. are displayed in bar plots. Significance calculated using two-sided Mann–Whitney *U*-test. *$P < 0.05$.

HLA-DR⁺CD38⁺CXCR3⁺CCR7⁻CD45RA⁻ activated effector memory CD8⁺ T cells that were either CD38^{hi} or CD57⁺ (Fig. 6a,b). Manual gating showed significantly more CD57⁺PD-1⁺CD8⁺ T cells in post-COV adenoids and tonsils (Fig. 6c) and more CXCR3⁺CCR6⁻CD8⁺ T cells (Tc1 skewed) in post-COV adenoids than samples from UC (Extended Data Fig. 8d). In addition, CD8⁺ T cells from adenoids produced more IFN-γ than those from tonsils upon PMA and ionomycin stimulation (post-COV and UC analyzed together) (Extended Data Fig. 8e).

CD8⁺ T cells expressing CD57 and PD-1 are expanded in the peripheral blood of adults with moderate and severe COVID-19 (ref. [25]); however, their function is unclear. CD57⁺PD-1⁺CD8⁺ T cells in post-COV adenoids and tonsils exhibited robust production of IFN-γ, tumor necrosis factor (TNF), IL-2, granzyme B and perforin following PMA and ionomycin stimulation (Extended Data Fig. 8f,g), expressed the tissue-resident markers CD103 and CD69 in addition to CXCR5 (Fig. 6d) and were found in the GC (Fig. 6e). Moreover, tonsillar CD8⁺ T cells from post-COV donors had higher expression of multiple combinations of cytokines/cytotoxic factors compared to those from UC (Fig. 6f and Supplementary Fig. 9). Thus, activated CD8⁺ T cell populations were enriched in the pharyngeal lymphoid tissues after COVID-19 infection.

In contrast, the only significant finding among CD8$^+$ T cell populations in PBMCs (Extended Data Fig. 8h,i and Supplementary Fig. 10a,b) were more abundant CD45RA$^+$CCR7$^+$CD28$^+$CD27$^+$CD95$^+$CD8$^+$ T_{SCM} cells seen by manual gating in post-COV relative to UC samples (Extended Data Fig. 8j) as noted by others[26]. Thus, activated and cytotoxic CD8$^+$ T_{RM} cells in the GC were enriched in the tonsils and adenoids post-COVID-19, whereas fewer significant changes were detected in PBMCs.

Expanded T cell clonotypes may be SARS-CoV-2 specific

To evaluate whether changes in T cell populations reflected SARS-CoV-2 antigen-specific responses, we stimulated post-COV tonsils, adenoids and PBMCs with spike (S), membrane (M) and nucleocapsid (N) peptide pools and assessed activation-induced markers on T cells. SARS-CoV-2-reactive CD4$^+$ T cells in PBMCs had the greatest responses to the S-peptide pool (Fig. 7a,b). Concatenation of all peptide-activated CD4$^+$ T cells indicated that SARS-CoV-2-responsive CD4$^+$ T cells in PBMCs were primarily memory cells that were enriched for CD45RA$^-$CXCR5$^+$PD-1$^+$ cT_{FH} cells that were CXCR3$^+$ (Fig. 7c).

Due to the highly activated nature of T cells in the adenoids and tonsils even without stimulation, we were unable to precisely identify and phenotype SARS-CoV-2-specific T cells in these tissues using peptide pool stimulations (Extended Data Fig. 9a,b), nor were we able to identify antigen-specific CD8$^+$ T cells in PBMCs, adenoids or tonsils. As an alternative approach, we used single-cell T cell receptor (TCR) sequencing to identify clonally expanded SARS-CoV-2-specific T cells and compared these to TCRβ sequences previously reported to recognize SARS-CoV-2 antigens. Non-naive (activated) CD95$^+$CD8$^+$ T cells and CD95$^+$CD4$^+$ T cells were sorted from tonsils, adenoids and PBMCs from the same two post-COV and one UC individuals described above and characterized by CITE-seq, assessing ten T cell surface markers, the transcriptome and TCR sequences of each cell. Analysis of about 13,000 CD8$^+$ T cells and 12,000 CD4$^+$ T cells indicated a higher frequency of expanded clonotypes (>1% clonotype frequency at the CDR3β aa level) among CD8$^+$ T cells in post-COV tonsils, adenoids and PBMCs compared to UC samples (Fig. 7d). By unsupervised clustering of cell surface protein expression, expanded clonotypes were primarily in five clusters (Fig. 7e–i). Clusters 2, 6 and 9 represented CD57$^+$CD8$^+$ T cells from PBMCs (Fig. 7e–g), corresponding to T cell subsets reported to be enriched in peripheral blood during acute COVID-19 (refs. [25,27]). Clusters 1 and 12 contained activated CD38$^+$HLA-DR$^+$ T_{RM} cells expressing CXCR5 and PD-1 from tonsils and adenoids, with cluster 12 additionally expressing CD57 (Fig. 7e–g), resembling the activated CD8$^+$ T_{RM} cells we found enriched in post-COV tonsils and adenoids, suggesting these represented clones that expanded in response to SARS-CoV-2.

We then compared TCR CDR3β aa sequences in the expanded clones to those previously reported in databases of SARS-CoV-2-specific TCR sequences (immuneCODE[28] and VDJdb[29]). In one post-COV participant with symptomatic COVID-19 71 d before surgery (CNMC71), 24% of the expanded CD8$^+$ TCRs matched sequences in these databases (13% tonsil, 10% adenoid, 30% PBMC), including the most abundant clonotype (111 cells, detected in PBMCs) (Supplementary Table 8 and Extended Data Fig. 9c,d). Although we identified TCRβ sequences reported to recognize a wide variety of SARS-CoV-2 epitopes among all activated CD8$^+$ T cells (Extended Data Fig. 9e), among the expanded clones, S and ORF1ab were the primary antigens recognized (Fig. 7j), similar to other studies[27,30]. The S epitopes recognized by these expanded clonotypes were located in the S2 subunit and were among the most reported immunodominant epitopes recognized by CD8$^+$ T cells (Supplementary Table 8)[30].

We observed fewer clones with >1% frequency among CD4$^+$ T cells (Supplementary Table 8), suggesting less proliferation among CD4$^+$ T cells compared to CD8$^+$ T cells. Therefore, we used a less stringent definition for expanded CD4$^+$ T cells clones (frequency >0.1% and absolute count ≥3 in a sample). In addition, because more prominent clonally expanded motifs have been noted among TCRα sequences than among TCRβ in SARS-CoV-2-specific CD4$^+$ T cells[31], we analyzed both TCR chains (Extended Data Fig. 9f,g and Supplementary Table 8). Unsupervised clustering of activated CD95$^+$CD4$^+$ T cells showed that expanded clonotypes were primarily in cluster 12 in PBMCs, which represented CD57$^+$PD-1$^+$CD4$^+$ T cells (Extended Data Fig. 9h–l) with higher expression of T_H1 and cytotoxic genes, including *IFNG*, *TBX21*, *CCL4*, *NKG7*, *PRF1* and *GZMB* compared to other PBMC clusters (Supplementary Table 8), similar to other studies[25,32–34]. In tonsils and adenoids, most expanded clones were in the T_{FH}-like clusters 1 and 4 (Extended Data Fig. 9h–l). Differential gene expression indicated that cluster 4 had high *IFNG* expression (Supplementary Table 8).

Among the expanded CD4$^+$ T cell clones, four had CDR3β aa sequences present in the TCRβ-centric database immuneCODE and recognized epitopes in ORF1ab, ORF7b, ORF10 and S (Supplementary Table 8). We also identified ten clones with SARS-CoV-2-specific TCRα sequences reported in VDJdb and the literature[31–33,35], including the most abundant clone (14 cells from CNMC89 PBMCs), which was paired with the most highly-expanded CD4$^+$ TCRβ sequence (Extended Data Fig. 9m and Supplementary Table 8). Several of the SARS-CoV-2-specific CDR3α sequences we found were shared among two donors (Supplementary Table 8), suggesting that they may recognize immunodominant or public epitopes.

Furthermore, we found overlap of CD8$^+$ T cell clones in post-COV tonsils and adenoids, including some that were SARS-CoV-2-reactive (Fig. 7k and Supplementary Table 8); less clonotype overlap was noted among CD4$^+$ T cells (Extended Data Fig. 9n), perhaps due to their limited expansion. Thus, SARS-CoV-2-specific T cells in the blood and tissue showed persistent clonal expansion and significant sharing of CD8$^+$ T cell clones among tonsils and adenoids after COVID-19 infection.

Fig. 7 | SARS-CoV-2 antigen-specific T cells. a, Representative flow cytometry plots showing gating of antigen-specific CD4$^+$ T cells from post-COV PBMCs expressing activation-induced markers (AIM$^+$, CD40L$^+$4-1BB$^+$) following stimulation with SARS-CoV-2 peptide pools of S, M and N. Dimethylsulfoxide (DMSO) (vehicle, V) was the negative control, PHA-L was the positive control. **b**, Frequencies of AIM$^+$CD4$^+$ T cells from six post-COV PBMCs as in **a** (V versus S, $P = 0.031$; V versus M, $P = 0.031$; V versus N, $P = 0.031$). Significance calculated with two-sided Wilcoxon signed-rank test for paired samples from the same donor. **c**, Flow cytometry plots showing frequency of memory T cells (shown in box on left), CD45RA$^-$CXCR5$^+$PD-1$^+$ cT_{FH} cells and CXCR3$^+$CCR6$^-$ cT_{FH} cells from concatenated antigen-specific CD4$^+$ T cells from S, M and N peptide pool stimulations from six donors compared to total CD4$^+$ T cells in PBMC. **d**, Frequency of CD8$^+$ T cells that are part of expanded clonotypes (frequency > 0.01, clone defined by identical CDR3β aa sequence) in tonsils, adenoids and PBMCs from two post-COV donors (CNMC71 and CNMC89) and one UC (CNMC99) assessed by CITE-seq and TCR sequencing. **e**–**g**, UMAP (**e**), tissue distribution (**f**) and CITE-seq surface antibody expression (**g**) of 16 clusters of CD95$^+$CD8$^+$ T cells from tonsils, adenoids and PBMCs of the three donors in **d**. **h**–**i**, Expanded clonotypes (**h**) and the distribution of expanded and non-expanded clones across clusters (**i**) of CD95$^+$CD8$^+$ T cells in **e**. **j**, Antigens recognized by four expanded CD8$^+$ T cell clones (each represented by a slice) with CDR3β sequences matching those reported to be SARS-CoV-2-specific in public databases; percentage of cells in each clone noted. Clones recognizing spike epitopes in green and ORF1ab epitopes in red. Clones reported to recognize >1 antigen not shown. Nested epitopes recognized by spike- and ORF1ab-specific TCRs are depicted below the pie chart (Supplementary Table 8). **k**, Overlap of CD8$^+$ T cell clones among PBMCs, tonsils and adenoids from two post-COV donors and one UC; degree of overlap between TCRα/β CDR3 aa sequences was calculated with the Morisita index (shown in plot), ranging from 0 to 1, with 0 indicating no sharing and 1 indicating full overlap. *$P < 0.05$.

https://doi.org/10.1038/s41590-022-01367-z

SARS-CoV-2 viral RNA persisted in post-COV tissue

Because we observed prolonged immune activation and clonal expansion after COVID-19, we assessed viral RNA persistence in pharyngeal lymphoid tissues. Using droplet digital PCR, we found SARS-CoV-2 nucleocapsid RNA in 7 out of 9 adenoid and 15 out of 22 tonsil formalin-fixed, paraffin-embedded tissue blocks from post-COV individuals, despite negative nasopharyngeal swab PCRs at the time of surgery (Fig. 8a and Supplementary Table 9). Viral RNA was not found in any UC (Fig. 8a). In four post-COV donors, their nasopharyngeal swab PCR had been positive over 100 d before surgery, including one 303 d before surgery. Viral RNA copies significantly correlated with the percentages of S1$^+$RBD$^+$ B cells among GC B cells in post-COV tonsils

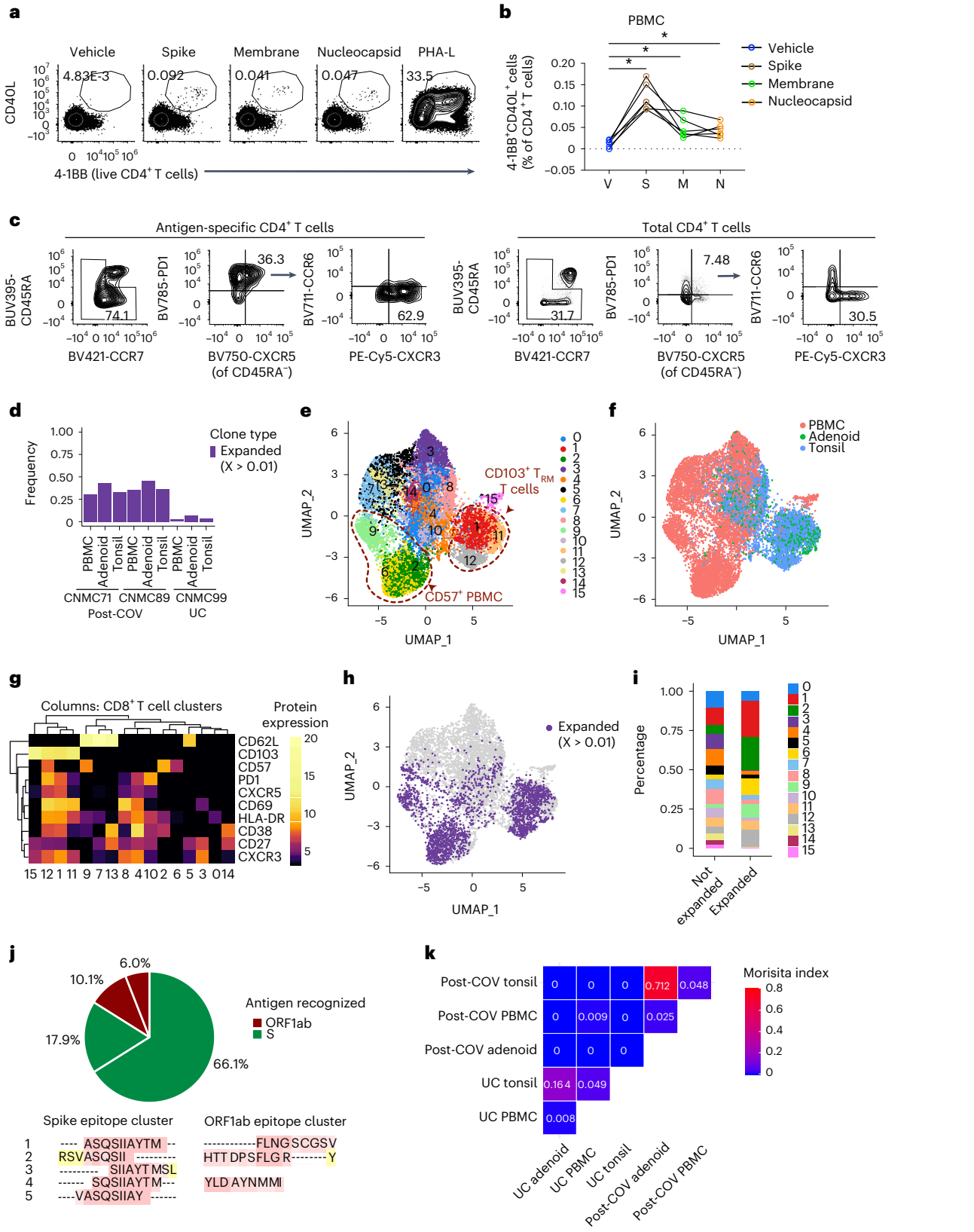

https://doi.org/10.1038/s41590-022-01367-z

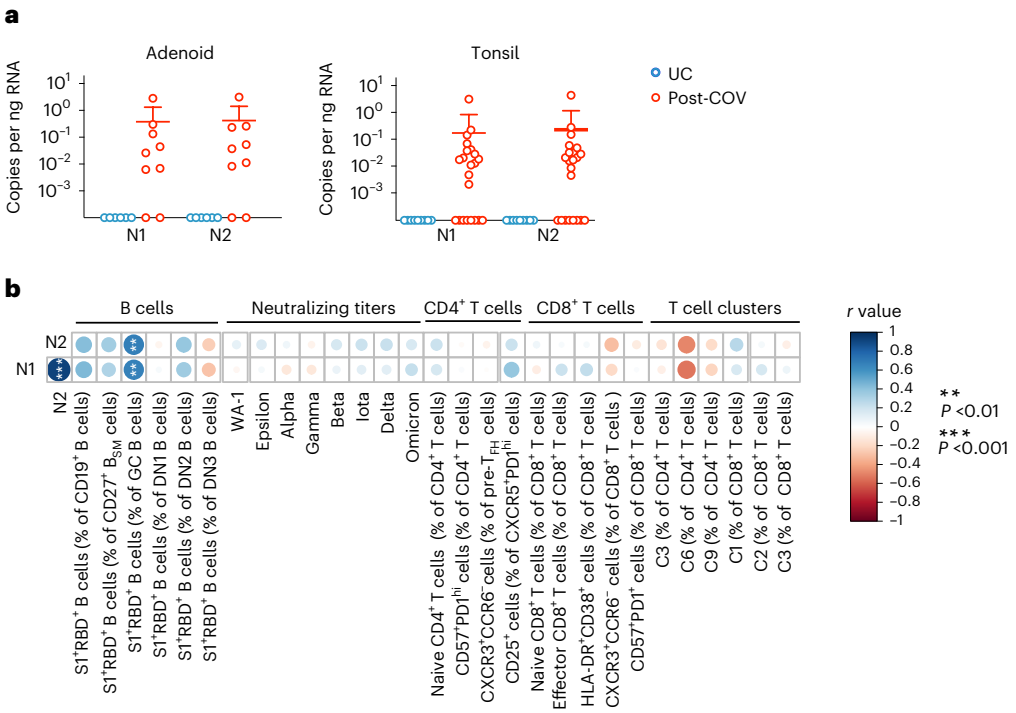

Fig. 8 | Persistence of SARS-CoV-2 RNA in the pharyngeal tissues post-COVID-19. a, Quantification of SARS-CoV-2 nucleocapsid RNA by droplet digital PCR (ddPCR) from adenoid and tonsil formalin-fixed paraffin-embedded (FFPE) tissue blocks (adenoids post-COV $n = 9$ and UC $n = 6$; tonsils post-COV $n = 22$ and UC $n = 9$). N1 and N2 represent two regions of the gene encoding the SARS-CoV-2 nucleocapsid. Each symbol represents one donor. Mean ± s.d. are displayed. Analyzed samples are listed in Supplementary Table 9. **b**, Summary of correlations among various subsets of SARS-CoV-2 antigen-specific B cells, serum-neutralizing antibody titers and T cell populations of interest versus copies of nucleocapsid (N1 and N2) RNA in post-COV tonsils. Correlations assessed with Spearman's rank correlation (copies N1 versus N2 $P < 10^{-5}$; percentage of $S1^+RBD^+$ B cells among GC B cells versus N1 $P = 0.004$ and versus N2 $P = 0.005$). *P* values were not corrected for multiple comparisons. $^{**}P < 0.01$; $^{***}P < 0.001$.

(Fig. 8b), raising the possibility that antigen persistence contributes to prolonged lymphoid and GC responses in post-COV donors.

Discussion

Using samples from pediatric tonsillectomies and adenectomies, we found evidence of persistent immune responses to SARS-CoV-2 in the pharyngeal lymphoid tissues, including antigen-specific memory B and T cells and prolonged changes in lymphocyte populations after infection. The high percentage of seropositive children in our cohort in late 2020 to early 2021, before vaccine availability, underscored the extent of COVID-19 in this urban population[36]. The variation in memory B cell frequencies and serum-neutralizing antibody titers we observed further highlighted heterogeneity of responses that may leave some children prone to repeat infection. Whether immunization generates immunity to SARS-CoV-2 in the upper respiratory tract and how this compares to natural infection are important questions.

Lasting changes in immune cell populations in the PBMCs and nasal mucosa of adults have been reported months after COVID-19 (refs. [37–40]). We saw more prominent changes in the pharyngeal tissues compared to PBMCs and many of the enriched lymphocyte populations we noted in the tissues were tissue-resident populations that remain at these sites for months and even years[41,42]. These populations, including T_{FH} cells and $CD8^+$ T_{RM} cells, some of which were likely SARS-CoV-2-specific, exhibited an IFN-γ-type bias that likely led to upregulation of *CXCR3* and *HOPX* in SARS-CoV-2-specific B cells. Strong local type 1 and type 2 IFN responses have been reported in the airways of infected children, which may lead to enhanced viral control compared to adults[43]. Many of the expanded populations we noted in the tissues expressed CXCR5 and were located in GCs, including $CXCR5^+CD8^+$ T cells, which resemble stem-like progenitor cells that maintain antiviral responses in chronic viral infections[44–46]. We also found enrichment of various $CD57^+$ T cell populations, which are found following repeated antigen exposure in chronic infections[47]. The role of these $CXCR5^+$ and $CD57^+$ cells in the response to an acute respiratory virus like SARS-CoV-2 is less clear, but their enrichment raises the question of whether prolonged antigen exposure contributes to these expanded populations[48].

Longitudinal studies suggest continued affinity maturation of SARS-CoV-2-specific B cells in GCs months after infection, possibly due to antigen persistence[13,38,49]; however, few studies have demonstrated SARS-CoV-2-specific GCs[10,50]. Our analyses provide direct evidence of ongoing SARS-CoV-2-specific GC reactions with expanded T_{FH} cell populations in adenoids and tonsils weeks to months after acute infection.

Our evaluation of multiple tissues from the same individual further revealed immunologic connections among the pharyngeal lymphoid tissues that may mediate tissue immunity. These findings parallel previous studies that noted B and $CD8^+$ T cell clones distributed across multiple lymph tissues, whereas $CD4^+$ T cell clones were more restricted in distribution[51–54]. Nonetheless, our results indicate more significant changes in adenoids than tonsils following COVID-19 infection. Adenoids are located in the nasopharynx and have a respiratory epithelium, whereas palatine tonsils are located in the oropharynx and have a stratified squamous epithelium. These factors, as well as differences in immune cell populations[55], may make adenoids more susceptible to immune activation during respiratory infections such as COVID-19, but also raise questions as to whether adenoidectomy and/or tonsillectomy affect immune responses to SARS-CoV-2.

A limitation of our study is the lack of information about dates of infection and symptoms in participants who were unaware of having COVID-19. We also do not have longitudinal samples to precisely map

the duration of immunological changes; instead, we relied on time from positive testing to surgery as a proxy. Although we could not identify antigen-specific T cells in the tonsils and adenoids by peptide stimulation due to T cell activation in these chronically inflamed environments, we identified potential antigen-specific T cells by matching TCR sequences to those publicly previously reported to recognize SARS-CoV-2. Lastly, COVID-19-convalescent participants underwent tonsillectomy for sleep-disordered breathing (SDB) or obstructive sleep apnea (OSA) due to hypertrophy of the adenoids and/or tonsils, which may influence local immune responses to SARS-CoV-2 (ref. [50]); we used control samples from children with the same conditions to address this concern.

Our findings offer insights into how viral infections shape the mucosal immune tissues in children; maintenance of activated tissue-resident T cells may aid responses against future infectious insults; however, activated cells in these tissues after infection may also contribute to delayed or prolonged sequelae of COVID-19, including long-COVID-19 and multisystem inflammatory syndrome in children, which is characterized by IFN-γ-induced signatures in PBMCs and has mucocutaneous findings, including pharyngeal erythema[56,57]. Our repository of pharyngeal tissues may facilitate evaluation of these and other important questions.

Online content

Any methods, additional references, Nature Portfolio reporting summaries, source data, extended data, supplementary information, acknowledgements, peer review information; details of author contributions and competing interests; and statements of data and code availability are available at https://doi.org/10.1038/s41590-022-01367-z.

References

1. Weisberg, S. P. et al. Distinct antibody responses to SARS-CoV-2 in children and adults across the COVID-19 clinical spectrum. *Nat. Immunol.* **22**, 25–31 (2021).
2. Pierce, C. A. et al. Immune responses to SARS-CoV-2 infection in hospitalized pediatric and adult patients. *Sci. Transl. Med.* **12**, eabd5487 (2020).
3. Wölfel, R. et al. Virological assessment of hospitalized patients with COVID-2019. *Nature* **581**, 465–469 (2020).
4. Huang, N. et al. SARS-CoV-2 infection of the oral cavity and saliva. *Nat. Med.* **27**, 892–903 (2021).
5. Wagar, L. E. et al. Modeling human adaptive immune responses with tonsil organoids. *Nat. Med.* **27**, 125–135 (2021).
6. Kumar, B. V. et al. Human tissue-resident memory T Cells are defined by core transcriptional and functional signatures in lymphoid and mucosal sites. *Cell Rep.* **20**, 2921–2934 (2017).
7. Mitchell, R. B. et al. Clinical practice guideline: tonsillectomy in children (update). *Otolaryngol. Head Neck Surg.* **160**, S1–S42 (2019).
8. Korber, B. et al. Tracking changes in SARS-CoV-2 spike: evidence that D614G increases infectivity of the COVID-19 virus. *Cell* **182**, 812–827 (2020).
9. Chan, W. S. et al. Geographical prevalence of SARS-CoV-2 variants, August 2020 to July 2021. *Sci. Rep.* **12**, 4704 (2022).
10. Poon, M. M. L. et al. SARS-CoV-2 infection generates tissue-localized immunological memory in humans. *Sci. Immunol.* **6**, eabl9105 (2021).
11. Kaneko, N. et al. Loss of Bcl-6-expressing T follicular helper cells and germinal centers in COVID-19. *Cell* **183**, 143–157 (2020).
12. Woodruff, M. C. et al. Extrafollicular B cell responses correlate with neutralizing antibodies and morbidity in COVID-19. *Nat. Immunol.* **21**, 1506–1516 (2020).
13. Sokal, A. et al. Maturation and persistence of the anti-SARS-CoV-2 memory B cell response. *Cell* **184**, 1201–1213 (2021).
14. Attaf, N. et al. FB5P-seq: FACS-based 5-prime end single-cell RNA-seq for integrative analysis of transcriptome and antigen receptor repertoire in B and T Cells. *Front. Immunol.* **11**, 216 (2020).
15. Albrecht, I. et al. Persistence of effector memory T_H1 cells is regulated by Hopx. *Eur. J. Immunol.* **40**, 2993–3006 (2010).
16. Ben Mkaddem, S., Benhamou, M. & Monteiro, R. C. Understanding Fc receptor involvement in inflammatory diseases: from mechanisms to new therapeutic tools. *Front. Immunol.* **10**, 811 (2019).
17. Raybould, M. I. J., Kovaltsuk, A., Marks, C. & Deane, C. M. CoV-AbDab: the coronavirus antibody database. *Bioinformatics* **37**, 734–735 (2021).
18. Ding, Y., Yan, H. & Guo, W. Clinical characteristics of children with COVID-19: a meta-analysis. *Front. Pediatrics* **8**, 431 (2020).
19. Kim, C. H. et al. Subspecialization of CXCR5+ T cells: B helper activity is focused in eagerminal center-localized subset of CXCR5+ T cells. *J Exp Med.* https://pubmed.ncbi.nlm.nih.gov/11413192/(2001).
20. Padhan, K., Moysi, E., Noto, A. & Petrovas, C. Acquisition of optimal TFH cell function is defined by specific molecular, positional, and TCR dynamic signatures. *Proc. Natl Acad. Sci. USA* https://www.pnas.org/doi/full/10.1073/pnas.2016855118 (2021).
21. Li, H. & Pauza, C. D. $CD25^{+}Bcl6^{low}$ T follicular helper cells provide help to maturing B cells in germinal centers of human tonsil. *Eur. J. Immunol.* **45**, 298–308 (2015).
22. Mahnke, Y. D., Brodie, T. M., Sallusto, F., Roederer, M. & Lugli, E. The who's who of T-cell differentiation: Human memory T-cell subsets. *Eur. J. Immunol.* **43**, 2797–2809 (2013).
23. Piedra-Quintero, Z. L., Wilson, Z., Nava, P. & Guerau-de-Arellano, M. CD38: an immunomodulatory molecule in inflammation and autoimmunity. *Front. Immunol.* **11**, 597959 (2020).
24. Jung, J. H. et al. SARS-CoV-2-specific T cell memory is sustained in COVID-19 convalescent patients for 10 months with successful development of stem cell-like memory T cells. *Nat. Commun.* **12**, 1–12 (2021).
25. De Biasi, S. et al. Marked T cell activation, senescence, exhaustion and skewing towards TH17 in patients with COVID-19 pneumonia. *Nat. Commun.* **11**, 3434 (2020).
26. Adamo, S. et al. Signature of long-lived memory $CD8^{+}$ T cells in acute SARS-CoV-2 infection. *Nature* **602**, 148–155 (2022).
27. Saini, S. K. et al. SARS-CoV-2 genome-wide T cell epitope mapping reveals immunodominance and substantial $CD8^{+}$ T cell activation in COVID-19 patients. *Sci. Immunol.* **6**, eabf7550 (2021).
28. Nolan, S. et al. A large-scale database of T-cell receptor β (TCRβ) sequences and binding associations from natural and synthetic exposure to SARS-CoV-2. *Res. Sq.* https://doi.org/10.21203/rs.3.rs-51964/v1 (2020).
29. Bagaev, D. V. et al. VDJdb in 2019: database extension, new analysis infrastructure and a T-cell receptor motif compendium. *Nucleic Acids Res.* **48**, D1057–D1062 (2019).
30. Grifoni, A. et al. SARS-CoV-2 human T cell epitopes: adaptive immune response against COVID-19. *Cell Host Microbe* **29**, 1076–1092 (2021).
31. Mudd, P. A. et al. SARS-CoV-2 mRNA vaccination elicits a robust and persistent T follicular helper cell response in humans. *Cell* **185**, 603–613 (2022).
32. Bacher, P. et al. Low-avidity CD4(⁺) T cell responses to SARS-CoV-2 in unexposed individuals and humans with severe COVID-19. *Immunity* **53**, 1258–1271 (2020).
33. Meckiff, B. J. et al. Imbalance of regulatory and cytotoxic SARS-CoV-2-reactive CD4(+) T cells in COVID-19. *Cell* **183**, 1340–1353 (2020).

34. Al Balushi, A. et al. Immunological predictors of disease severity in patients with COVID-19. *Int. J. Infect. Dis.* **110**, 83–92 (2021).
35. Lu, X. et al. Identification of conserved SARS-CoV-2 spike epitopes that expand public cT_{FH} clonotypes in mild COVID-19 patients. *J. Exp. Med.* **218**, e20211327 (2021).
36. Mudd, P. et al. Examining multi-level immune response to determine prevalence of COVID-19 in pediatric tonsillectomy. *Laryngoscope* https://doi.org/10.1002/lary.30382 (2022).
37. Files, J. K. et al. Sustained cellular immune dysregulation in individuals recovering from SARS-CoV-2 infection. *J. Clin. Investig.* **131**, e140491 (2021).
38. Gaebler, C. et al. Evolution of antibody immunity to SARS-CoV-2. *Nature* **591**, 639–644 (2021).
39. Breton, G. et al. Persistent cellular immunity to SARS-CoV-2 infection. *J. Exp. Med.* **218**, e20202515 (2021).
40. Roukens, A. H. E. et al. Prolonged activation of nasal immune cell populations and development of tissue-resident SARS-CoV-2-specific $CD8^+$ T cell responses following COVID-19. *Nat. Immunol.* **23**, 23–32 (2022).
41. Smith, N. et al. Distinct systemic and mucosal immune responses during acute SARS-CoV-2 infection. *Nat. Immunol.* **22**, 1428–1439 (2021).
42. Szabo, P. A., Miron, M. & Farber, D. L. Location, location, location: tissue-resident memory T cells in mice and humans. *Sci. Immunol.* **4**, eaas9673 (2019).
43. Yoshida, M. et al. Local and systemic responses to SARS-CoV-2 infection in children and adults. *Nature* **602**, 321–327 (2022).
44. He, R. et al. Follicular CXCR5-expressing $CD8^+$ T cells curtail chronic viral infection. *Nature* **537**, 412–416 (2016).
45. Leong, Y. A. et al. $CXCR5^+$ follicular cytotoxic T cells control viral infection in B cell follicles. *Nat. Immunol.* **17**, 1187–1196 (2016).
46. Yu, D. & Ye, L. A portrait of $CXCR5^+$ follicular cytotoxic $CD8^+$ T cells. *Trends Immunol.* **39**, 965–979 (2018).
47. Focosi, D., Bestagno, M., Burrone, O. & Petrini, M. $CD57^+$ T lymphocytes and functional immune deficiency. *J. Leukoc. Biol.* **87**, 107–116 (2010).
48. Kim, T. S., Hufford, M. M., Sun, J., Fu, Y. X. & Braciale, T. J. Antigen persistence and the control of local T cell memory by migrant respiratory dendritic cells after acute virus infection. *J. Exp. Med.* **207**, 1161–1172 (2010).
49. Chertow, D. et al. SARS-CoV-2 infection and persistence throughout the human body and brain. *Nat. Portfolio* https://doi.org/10.21203/rs.3.rs-1139035/v1 (2022).
50. Tan, H.-X. et al. Cutting edge: SARS-CoV-2 infection induces robust germinal center activity in the human tonsil. *J. Immunol.* **208**, 2267–2271 (2022).
51. Seay, H. R. et al. Tissue distribution and clonal diversity of the T and B cell repertoire in type 1 diabetes. *JCI Insight* **1**, e88242 (2016).
52. Bergqvist, P. et al. Re-utilization of germinal centers in multiple Peyer's patches results in highly synchronized, oligoclonal, and affinity-matured gut IgA responses. *Mucosal Immunol.* **6**, 122–135 (2013).
53. Meng, W. et al. An atlas of B-cell clonal distribution in the human body. *Nat. Biotechnol.* **35**, 879–884 (2017).
54. Ohm-Laursen, L. et al. B cell mobilization, dissemination, fine tuning of local antigen specificity and isotype selection in asthma. *Front. Immunol.* **12**, 702074 (2021).
55. Boyaka, P. N. et al. Human nasopharyngeal-associated lymphoreticular tissues. Functional analysis of subepithelial and intraepithelial B and T cells from adenoids and tonsils. *Am. J. Pathol.* **157**, 2023–2035 (2000).
56. Feldstein, L. R. et al. Characteristics and outcomes of US children and adolescents with multisystem inflammatory syndrome in children (MIS-C) compared with severe acute COVID-19. *JAMA* **325**, 1074–1087 (2021).
57. Sacco, K. et al. Immunopathological signatures in multisystem inflammatory syndrome in children and pediatric COVID-19. *Nat. Med.* **28**, 1050–1062 (2022).

Qin Xu[1], Pedro Milanez-Almeida[2,24], Andrew J. Martins[3,24], Andrea J. Radtke[4,24], Kenneth B. Hoehn[5,24], Cihan Oguz[6,7], Jinguo Chen[2], Can Liu[3], Juanjie Tang[8], Gabrielle Grubbs[8], Sydney Stein[9,10], Sabrina Ramelli[9], Juraj Kabat[4], Hengameh Behzadpour[11], Maria Karkanitsa[12], Jacquelyn Spathies[13], Heather Kalish[13], Lela Kardava[14], Martha Kirby[15], Foo Cheung[2], Silvia Preite[1], Patrick C. Duncker[16], Moses M. Kitakule[17], Nahir Romero[18], Diego Preciado[11,18], Lyuba Gitman[11,18], Galina Koroleva[2], Grace Smith[19], Arthur Shaffer[20], Ian T. McBain[1], Peter J. McGuire[15], Stefania Pittaluga[19], Ronald N. Germain[4,21], Richard Apps[2], Daniella M. Schwartz[17], Kaitlyn Sadtler[12], Susan Moir[14], Daniel S. Chertow[9,10], Steven H. Kleinstein[5,22,23], Surender Khurana[8], John S. Tsang[2,3], Pamela Mudd[11,18], Pamela L. Schwartzberg[1,15] ✉ & Kalpana Manthiram[1] ✉

[1]Cell Signaling and Immunity Section, Laboratory of Immune System Biology (LISB), National Institute of Allergy and Infectious Diseases (NIAID), National Institutes of Health (NIH), Bethesda, MD, USA. [2]Center for Human Immunology, NIAID, NIH, Bethesda, MD, USA. [3]Multiscale Systems Biology Section, LISB, NIAID, NIH, Bethesda, MD, USA. [4]Center for Advanced Tissue Imaging, LISB, NIAID, NIH, Bethesda, MD, USA. [5]Department of Pathology, Yale School of Medicine, New Haven, CT, USA. [6]NIAID Collaborative Bioinformatics Resource (NCBR), NIAID, NIH, Bethesda, MD, USA. [7]Axle Informatics, Bethesda, MD, USA. [8]Division of Viral Products, Center for Biologics Evaluation and Research (CBER), Food and Drug Administration (FDA), Silver Spring, MD, USA. [9]Emerging Pathogens Section, Critical Care Medicine Department, Clinical Center (CC), NIH, Bethesda, MD, USA. [10]Laboratory of Immunoregulation, NIAID, NIH, Bethesda, MD, USA. [11]Division of Pediatric Otolaryngology, Children's National Hospital, Washington, DC, USA. [12]Laboratory of Immuno-Engineering, National Institute of Biomedical Imaging and Bioengineering (NIBIB), NIH, Bethesda, MD, USA. [13]Trans-NIH Shared Resource on Biomedical Engineering and Physical Science, NIBIB, NIH, Bethesda, MD, USA. [14]B-cell Immunology Section, Laboratory of Immunoregulation, NIAID, NIH, Bethesda, MD, USA. [15]National Human Genome Research Institute (NHGRI), NIH, Bethesda, MD, USA. [16]Cytek Biosciences, Fremont, CA, USA.

[17]Laboratory of Allergic Diseases, NIAID, NIH, Bethesda, MD, USA. [18]Division of Otolaryngology, Department of Surgery, George Washington University School of Medicine and Health Sciences, Washington, DC, USA. [19]Laboratory of Pathology, Center for Cancer Research, National Cancer Institute (NCI), NIH, Bethesda, MD, USA. [20]Lymphoid Malignancies Branch, Center for Cancer Research, NCI, NIH, Bethesda, MD, USA. [21]Lymphocyte Biology Section, LISB, NIAID, NIH, Bethesda, MD, USA. [22]Program in Computational Biology and Bioinformatics, Yale University, New Haven, CT, USA. [23]Department of Immunobiology, Yale School of Medicine, New Haven, CT, USA. [24]These authors contributed equally: Pedro Milanez-Almeida, Andrew J. Martins, Andrea J. Radtke, Kenneth B. Hoehn. ✉e-mail: pams@nih.gov; kalpana.manthiram@nih.gov

Methods

Ethics statement

This study was approved by the Institutional Review Board at Children's National Hospital (protocol no. 00009806). Written informed consent was obtained from parent/guardians of all enrolled participants and assent was obtained from minor participants over 7 years of age.

Participant recruitment

We recruited 110 children undergoing tonsillectomy and/or adenoidectomy at Children's National Hospital (CNH). All children scheduled to undergo tonsillectomy at CNH were eligible. The first 102 participants were recruited from late September 2020 to early February 2021 without screening for previous COVID-19. An additional two participants were subsequently recruited with a known history of COVID-19, plus six additional individuals (one of whom turned out to be positive by serology) were recruited in May and June 2021. Because not all tissues or blood were available from each individual, we collected a total of 106 blood samples, 100 adenoids and 108 tonsils from 110 participants (Supplementary Table 2). No statistical methods were used to predetermine sample size. All participants had negative PCR with reverse transcription (RT–PCR) test from a nasopharyngeal swab for SARS-CoV-2 within 72 h of surgery. Demographic information and clinical data were collected through parental questionnaires and chart review and managed in REDCap, and biological samples were acquired in the operating room by the clinical team at CNH.

Eleven participants had previous confirmed SARS-CoV-2 infection with RT–PCR or antigen testing from nasopharyngeal swabs. Another 13 COVID-19-exposed participants were identified through serum antibody testing and/or identification of B cells that recognize the spike protein of SARS-CoV-2 by flow cytometry (described below). One participant (CNMC43) had SARS-CoV-2 detected by RT–PCR from the nasopharynx 20 d before surgery but had negative serology and no SARS-CoV-2-specific B cells in the tissue or blood. We excluded this individual from our subsequent analysis.

Control selection within the cohort

Controls for flow cytometric analyses were selected among individuals with no serological or cellular evidence of previous COVID-19. The primary indication for tonsillectomy in all 24 participants with previous COVID-19 was adenotonsillar hypertrophy leading to SDB or OSA (Supplementary Tables 1 and 3) except one participant who had eustachian tube dysfunction. Patients with SDB and OSA both have breathing difficulties during sleep (primarily snoring); however, patients with OSA had polysomnography documenting an apnea–hypopnea index greater than 1, whereas those with SDB did not undergo polysomnography testing and were diagnosed by clinical history alone. None of the 24 participants with prior COVID-19 had frequent recurrent tonsillitis (more than six episodes in a year) or other medical problems that directly affect the immune system aside from atopic disease, nor did they take immunomodulating medications aside from nasal/inhaled steroid or loratadine within 2 weeks of surgery. Therefore, individuals were excluded from the control group if they (1) had periodic fever, recurrent tonsillitis or chronic tonsillitis as primary indication for surgery ($n = 15$); (2) had more than six episodes of tonsillitis in a year ($n = 2$); (3) took immunomodulatory medications (including montelukast and cetirizine) aside from inhaled steroid or loratadine within 2 weeks of surgery ($n = 9$); (4) had sickle cell anemia ($n = 3$); or (5) did not have flow cytometry studies performed on their samples on the day of processing due to sample collection before panel finalization or technical problems with the flow cytometer on the day of acquisition. Controls were also excluded if they had indeterminate serological testing for SARS-CoV-2 infection and did not have any SARS-CoV-2-specific B cells in the tissue or blood ($n = 2$); both of these participants subsequently had negative neutralizing titers to SARS-CoV-2 as well. Samples included in unsupervised and manual gating analyses of flow cytometry data are listed in Supplementary Table 2.

Blood and tissue collection

Blood samples were obtained just before the surgical procedure in the operating room in serum separator tubes (BD) for serum collection and sodium heparin tubes (BD) for PBMC extraction. Once received in the laboratory, serum separator tubes were spun at 1,200*g* for 10 min and serum was aliquoted and stored at −80 °C. PBMCs were isolated the day after collection by density gradient centrifugation on lymphocyte separation medium (MP Biomedicals) at 300*g* for 30 min at room temperature with no brake and washed with PBS. If red blood cell contamination was present, cells were lysed with ACK buffer.

Tonsils and adenoids were stored in RPMI medium with 5% FBS (VWR), gentamicin 50 mg ml^{-1} (Gibco) and 1× antibiotic/antimycotic solution (Gibco) on ice immediately after collection. Tissues were processed the day after collection. A 3–5-mm portion of tonsil and adenoid tissue was cut and fixed in 5 ml of 10% buffered formalin (Avantik) for 24–48 h. The fixed tissue was then incubated in 70% ethanol until it was paraffin embedded. The remainder of the tissue was mechanically disrupted and filtered through a 100-µm cell strainer to create a single cell suspension, lysed with ACK buffer (Gibco) and washed with PBS three times. Freshly isolated PBMCs and tonsil and adenoid cells were surface stained and analyzed with flow cytometry as described below on the day of processing. The remaining cells were stored in liquid nitrogen in the presence of FBS with 10% DMSO.

SARS-CoV-2 serum antibody ELISA

After thawing frozen serum to room temperature, IgG and IgM antibodies against the S protein and RBD of the S protein of SARS-CoV-2 were analyzed using ELISA as previously described[58,59]. Positivity thresholds were based on mean optical density (absorbance) plus 3 s.d. The final criterion of S^+ and RBD^+ for any combination of positive IgG or IgM gave estimated sensitivity and specificity of 100% based on previous studies of this assay. Data are shown in Supplementary Table 4.

Pseudovirus neutralization assay

Antibody preparations were evaluated by SARS-CoV-2 pseudovirus neutralization assay (PsVNA) using WA-1, B.1.429 (Epsilon), B.1.1.7 (Alpha), P.1 (Gamma), B.1.351 (Beta), B.1.526 (Iota), B.1.617.2 (Delta) and B.1.1.529 (Omicron) strains. The PsVNA using the 293-ACE2-TMPRSS2 cell line was described previously[60–62].

Briefly, human codon-optimized complementary DNA encoding SARS-CoV-2 S glycoprotein of the WA-1, B.1.429, B.1.1.7, P.1, B.1.351, B.1.526, B.1.617.2 and B.1.1.529 strains were synthesized by GenScript and cloned into eukaryotic cell expression vector pcDNA 3.1 between the BamHI and XhoI sites. Pseudovirions were produced by co-transfection Lenti-X 293T cells with psPAX2 (gag/pol), pTrip-luc lentiviral vector and pcDNA 3.1 SARS-CoV-2-spike-DeltaC19, using Lipofectamine 3000. The supernatants were collected 48 h after transfection and filtered through 0.45-µm membranes and titrated using 293T-ACE2-TMPRSS2 cells (HEK 293T cells that express ACE2 and TMPRSS2 proteins).

For the neutralization assay, 50 µl of SARS-CoV-2 S pseudovirions were pre-incubated with an equal volume of medium containing serum at varying dilutions at room temperature (RT) for 1 h, then virus–antibody mixtures were added to 293T-ACE2-TMPRSS2 cells in a 96-well plate. The input virus with all SARS-CoV-2 strains used in the current study were the same (2×10^5 relative light units per 50 µl per well). After a 3-h incubation, the inoculum was replaced with fresh medium. Cells were lysed 24 h later and luciferase activity was measured using luciferin. Controls included cells only, virus without any antibody and positive sera. The cutoff value or the limit of detection for the neutralization assay was 1:10. Data are in Supplementary Table 4.

High-dimensional flow cytometry of SARS-CoV-2-specific B cells

Five million cells per sample of PBMC, adenoid or tonsil were resuspended in PBS with 2% FBS and 2 mM EDTA (FACS buffer). Biotinylated S1 and RBD probes (BioLegend) were crosslinked with fluorochrome-conjugated streptavidin in a molar ratio of 4:1. Fluorochrome-conjugated streptavidin was split into five aliquots and conjugated to biotinylated S1 and RBD probes by mixing for 20 min per aliquot at 4 °C. Cells were first stained with the viability dye, Zombie NIR (1:800 dilution, BioLegend) for 15 min at RT, washed twice and then incubated with True-Stain Monocyte Blocker (BioLegend) for 5 min. An antibody cocktail containing the rest of the surface antibodies, the fluorochrome-conjugated S1 and RBD probes and Brilliant Stain Buffer Plus (BD) were then added directly to the cells and incubated for 30 min at RT in the dark (200 µl staining volume). Cells were washed three times and fixed in 1% paraformaldehyde for 20 min at RT before washing again and collecting on a spectral flow cytometer (Aurora, Cytek) using SpectroFlo software (Cytek v.1.1). Antibodies are listed in Supplementary Table 10.

Broad 37 parameter immunophenotyping flow cytometry panel

Two million cells per sample of PBMCs and 5 million cells per adenoid or tonsil were resuspended in FACS buffer. Cells were first stained with LIVE/DEAD Blue (1:800 dilution, Thermo Fisher) for 15 min at RT, washed twice and then incubated with True-Stain Monocyte Blocker (BioLegend) for 5 min. Antibodies for chemokine receptors and TCRγδ were sequentially added at RT (anti-CCR7 for 10 min, anti-CCR6, anti-CXCR5 and anti-CXCR3 together with Brilliant Stain Buffer Plus for 5 min and anti-TCRγδ for 10 min). An antibody cocktail containing the rest of the surface antibodies and Brilliant Stain Buffer Plus was then added to the cells and incubated for 30 min at RT (total staining volume 182 µl). Cells were washed three times and stained with fluorescence-conjugated streptavidin for 15 min at RT. Then, cells were washed twice and fixed in 1% paraformaldehyde for 20 min at RT before washing again and acquiring on the Aurora spectral cytometer (Cytek) using SpectroFlo software (Cytek v.1.1). Antibodies are listed in Supplementary Table 10. Manual gating for both panels was conducted with FlowJo Software v.10 (BD Biosciences) based on previously described gating strategies[63].

Unsupervised analysis and statistical modeling

Data from the broad immunophenotyping flow cytometry panel with 37 parameters were analyzed with unsupervised clustering of surface antibody staining. $CD19^+$ B cells, $CD4^+$ T cells and $CD8^+$ T cells were analyzed separately. Tonsils and adenoids were merged and processed together, whereas PBMCs were processed separately due to pre-determined antibody concentration differences in staining required for optimal results in each organ. B cell analyses were based on surface expression of CCR6, CXCR5, CXCR3, CCR7, CD45RA, CD11c, IgD, CD20, IgM, IgG, CD27, HLA-DR, CD38, CD21, CD123, PD-1, CD57, CD25, CD24, CD95, IgA, CD1c, CD127 and CD161. $CD4^+$ and $CD8^+$ T cells analyses were based on the expression of CCR6, CXCR5, CXCR3, CCR7, CD45RA, CD161, CD28, PD-1, CD57, CD25, CD95, CD27, CD127, HLA-DR, CD38, ICOS, CD11c, CD24, CD1c, CD123 and CD21. FCS files (3.0) as well as FlowJo workspaces (v.10.7.2) were processed in R (v.4.1) via Rstudio (v.1.4.1717) and Bioconductor (v.3.13) using cytoverse (v.0.0.0.9000), including flowCore (v.2.4.0), flowWorkspace (v.4.4.0), ggcyto (v.1.20.0), openCyto (v.2.4.0), CytoML (v.2.4.0), cytolib (v.2.4.0) and cytoqc (v.0.99.2). Default options for biexponential data transformation were used. Outlier cells with expression values in the top or bottom 1×10^{-3} quantiles were excluded. Single cells in each sample were first clustered using *k*-means ($k = 500$, referred to as metacells), followed by merging cluster centroids from different samples with the same staining (tonsil/adenoids versus PBMC) for meta-clustering and dimensionality reduction. Specifically, 500 centroids from each sample (metacells) were merged followed by another run of *k*-means meta-clustering (again $k = 500$), which were finally used in Leiden clustering and to learn a *t*-UMAP model to project the metacells (single-cell level *k*-means centroids; shown in plots). Seurat (v.4.0.3), uwot (v.0.1.10) and Leiden (v.0.3.9) were used in shared nearest neighbors graph building, *t*-UMAP projection and meta-clustering, respectively, with default settings. Leiden meta-clusters were mapped back to the single-cell level and the ranked frequency of single cells in each Leiden meta-cluster in each sample was modeled linearly as a function of age, sex and history of COVID-19 (COVID status) (as in lm(rank(frequency) ~ age + sex + status). Before statistical modeling, principal-component analysis of frequencies was used to detect and exclude outlier samples. Sample sizes are described in the legend of each plot. *t*-UMAP projections as well as all CIs of coefficients and their *P* values (from two-tailed Student's *t*-tests of each coefficient within each model) are presented in plots built with ggplot2 (v.3.3.5). Data are in Supplementary Table 12.

Processing for CITE-seq

Banked PBMCs, tonsils and adenoids from two post-COV donors (CNMC71 and CNMC89) and one UC (CNMC99) were thawed from liquid nitrogen in a 37 °C water bath for 2–3 min. A total of 2 ml of medium consisting of RPMI with 10% of fetal bovine serum, 0.1 mg ml^{-1} DNase I (Roche) and 10 mM HEPES was added drop by drop to the thawed cells. Cells were further diluted by incremental addition of a 1:1 volume of medium up to 8 ml, then centrifuged at 300*g* for 5 min. Cells were then resuspended in 300 µl of medium, incubated at RT for 5 min, washed with medium without DNase I and filtered through a 100-µm strainer before spinning down and resuspending in staining buffer (PBS + 1% BSA). Cells were then incubated with Fc blocker (Human TruStain FcX, BioLegend), stained with TotalSeq-C human hashtag antibodies (BioLegend) to uniquely label the sample origin (by tissue and donor) and washed with PBS + 0.04% BSA. Adenoids and tonsils from the three donors (six samples in total) were pooled together and PBMCs from three were pooled together separately. The number of cells to pool from each tissue and donor was calculated with the aim of pooling a similar number of $S1^+$ B cells from each sample. Pooled cells were first incubated with Fc blocker at 4 °C for 10 min followed by CITE-seq and sorting antibody cocktails in the following order at 4 °C: TotalSeq anti-CXCR3 antibody for 10 min, TotalSeq chemokine cocktail (anti-CCR7, CCR6, CXCR5 antibodies) for 10 min and the rest of CITE-seq antibodies and fluorescence-labeled sorting antibodies and viability dye (Aqua) for 30 min (Supplementary Table 10). Cells were then washed with PBS + 0.04% BSA and resuspended in PBS + 2% FBS. $S1^+$ and $S1^-$ B cells, $CD95^+CD4^+$ and $CD95^+CD8^+$ T cells were sorted from each pool on a BD FACS Aria Fusion sorter for tonsil/adenoid pool and FACS Aria III sorter for the PBMC pool (BD Biosciences). Supplementary Fig. 3 details the sorting strategy. Cells were sorted into PBS + 2% FBS. Note that the antibody concentrations used for CITE-seq were optimized by the manufacturer based on healthy PBMC samples and thus may not be optimal for tissue samples. We have not independently verified the specificity of each antibody in our CITE-seq panel. Antibody concentrations were based on our titration from flow cytometry[64,65].

Sorted $S1^+$ and $S1^-$ B cells and $CD95^+CD4^+$ and $CD95^+CD8^+$ T cells were mixed with the reverse transcription mix and partitioned into single cell Gel-Bead in Emulsion (GEM) using 10x 5′ Chromium Single Cell Immune Profiling Next GEM v2 chemistry (10x Genomics). The reverse transcription step was performed in an Applied Materials Veriti 96-well thermocycler. 10x Genomics 5′ single-cell gene expression, cell surface protein and BCR or TCR libraries were prepared as instructed by 10x Genomics user guides (https://www.10xgenomics.com/resources/user-guides/). RNA quality and quantity in the libraries were measured using a bioanalyzer (Agilent) and a Qubit fluorometer (Thermo Fisher). Libraires were pooled at a concentration of 10 nM and sequenced on

Illumina NovaSeq platform (Illumina) using the following read lengths: Read 1, 26 bp; Index 1, 10 bp; Index 2, 10 bp; Read 2, 150 bp.

CITE-seq data processing and analysis

CellRanger (10x Genomics) v.6.0.0 was used to map cDNA libraries to the hg19 genome reference (10x Genomics hg19 CellRanger reference, v.1.2.0) and to count antibody tag features. Data were further processed using Seurat (v.4.0.1)[66] running in R v.4.0.3. After transforming the surface protein library counts using dsb[67], we demultiplexed the pooled samples using manual cutoffs on the hashtag antibody staining. We removed cells with fewer than 100 detected genes, greater than 30% mitochondrial reads or mRNA counts greater than 25,000. To exclude cells with extremely high surface antibody counts, we also removed the top 0.05% of cells in the surface antibody total count distribution. Cell clustering was performed by applying the FindNeighbors() function from Seurat on a distance matrix generated from the dsb-transformed surface protein data, followed by Louvain clustering on the resulting shared nearest neighbor graph using Seurat's FindClusters() algorithm, with a resolution parameter of 1. Expression of selected genes was visualized using the ComplexHeatmap package[68] and the percentage of cells per cluster for the $S1^+$ and $S1^-$ cells and T cell populations of interest was plotted using ggplot2 (ref. [69]). For the comparison of differentially expressed genes between the $S1^+$ and $S1^-$ B cells, we first downsampled the fastq files from the $S1^+$ sequencing library to more closely match the reads per cell obtained in the $S1^-$ sequencing libraries using seqtk v.1.3. Differential expression was then compared using the MAST algorithm with 'Donor' as a latent variable, as implemented in the Seurat FindMarkers function. For RNA-based clustering $S1^+$ and $S1^-$ B cells, we first downsampled the fastq files from the $S1^+$ sequencing library to more closely match the reads per cell obtained in the $S1^-$ sequencing libraries using seqtk v.1.3. Cells were then clustered using the top 15 principal components derived from the 2,000 most variable genes, selected by Seurat's FindVariableFeatures function using the 'vst' method. Clustering was performed using the Louvain method and a resolution of 1.15 in Seurat's FindClusters function.

BCR sequence analysis and clonal clustering

BCR repertoire sequence data were analyzed using the Immcantation (www.immcantation.org) framework. Starting with filtered CellRanger output, V(D)J genes for each sequence were aligned to the IMGT GENE-DB reference database v.3.1.29 (ref. [70]) using IgBlast v.1.16.0 (ref. [71]) and Change-O v.1.0.0 (ref. [72]). Nonproductive sequences, cells without associated constant region calls, cells identified as arising from doublets or negative wells and cells with multiple heavy chains were all removed. Samples within each individual were pooled and sequences were grouped into clonal clusters, which contain B cells that relate to each other by somatic hypermutations from a common V(D)J ancestor. Sequences were first grouped by common IGHV gene annotations, IGHJ gene annotations and junction lengths. Using the hierarchicalClones function of scoper v1.1.0 (ref. [73]), sequences within these groups differing by a length normalized Hamming distance of 0.1 within the CDR3 region were defined as clones using single-linkage hierarchical clustering[74]. This threshold was determined through manual inspection of distance to nearest neighbor plots using shazam v.1.1.0 (ref. [75]). These heavy chain-defined clonal clusters were further split if their constituent cells contained light chains that differed by V and J genes. Within each clone, germline sequences were reconstructed with D segment and N/P regions masked (replaced with 'N' nucleotides) using the createGermlines function within dowser v.0.1.0 (ref. [76]). All BCR analyses used R v.4.1.1 (R Core Team 2017) and plots were generated using ggpubr v.0.4.0 (ref. [77]) and ggplot2 v.3.3.5 (ref. [69]). After clonal clustering, only heavy chain sequences were used for subsequent analysis. Somatic hypermutation was calculated as the Hamming distance between each sequence's IMGT-gapped sequence alignment and its predicted unmutated germline ancestor along the V gene (IMGT positions 1–312).

Clonal diversity is an important metric of B cell repertoires and low B cell clonal diversity is consistent with an adaptive immune response. To quantify B cell clonal diversity, we calculated Simpson's diversity for each sample using the alphaDiversity function of alakazam v.1.1.0 (ref. [72]). Lower values of Simpson's diversity indicate a greater probability of two random sequences belonging to the same clone, consistent with more large clones. To account for differences in sequence depth, samples within each comparison were downsampled to the same number of sequences and the mean of 1,000 such re-sampling repetitions was reported. Only donor/tissue/cell sort samples with at least 100 B cells were included, which led to the exclusion of all $S1^+$ cells from CNMC99 (UC) and $S1^+$ PBMCs from CNMC89 (post-COV). Clonal overlap among tissues can be used as a measure of immunological connectivity. Clonal overlap was calculated using the Jaccard index, which for each pair of tissues is the number of unique clones found in both tissues (intersect) divided by the total number of unique clones among the two tissues (union). Clones were labeled as '$S1^{+}$' if they contained at least one $S1^+$ sorted B cell. To infer lineage trees, we estimated tree topologies, branch lengths and individual-wide substitution model parameters using maximum likelihood under the GY94 model[78,79]. Using fixed tree topologies estimated from the GY94 model, we then estimated branch lengths and donor-wide parameter values under the HLP19 model in IgPhyML v.1.1.3 (ref. [78]). Trees were visualized using dowser v.0.1.0 and ggtree v.3.0.4 (ref. [80]).

To identify convergent BCR sequences, heavy chain sequences were compared to previously published SARS-CoV-2 binding antibodies in the CoV-AbDab database[17]. BCR sequences were identified as convergent with a previously published antibody if they used the same V gene, J gene, CDR3 length and had an aa Hamming distance of no more than 20% in the CDR3.

TCR sequence analysis

TCR repertoire sequence data were analyzed using the scRepertoire package v.1.5.2 (ref. [81]) in R v.4.1.1 (R Core Team 2017). Starting with the filtered CellRanger contig annotations output, combineTCR and combineExpression functions were used for combining the TCR data from each sample and for integration of the combined TCR data with the single cell RNA-seq data (processed with Seurat v.4.1.0 (ref. [66])), respectively. Repertoire overlap between the samples was quantified as the Morisita index[82] with the clonalOverlap function of scRepertoire. CDR3 aa sequences previously reported in the ImmuneCODE[28] and VDJdb[29] databases and four recently published manuscripts[31–33,35] were matched to the CDR3α or β sequences in the data to identify SARS-CoV-2-specific cells. The logo plots and sequence alignment plots were generated using M-Coffee[83], respectively.

Tissue processing and staining for multiplexed imaging

The 5-µm tissue sections were cut from FFPE samples and placed onto glass slides. Following sectioning, glass slides (with tissue) were baked in a 60 °C oven for 1 h Deparaffinization was performed as described previously[84]: two exchanges of 100% xylene (10 min per exchange) followed by 100% ethanol for 10 min, 95% ethanol for 10 min, 70% ethanol for 5 min and 10% formalin for 15 min. Antigen retrieval was performed by incubating slides in AR6 buffer (Akoya Biosciences) for 40 min in a 95 °C water bath. After 40 min, slides were removed from the water bath and allowed to cool on the bench for 20 min. Sections were permeabilized, blocked and stained in PBS containing 0.3% Triton X-100 (Sigma-Aldrich), 1% bovine serum albumin (Sigma-Aldrich) and 1% human Fc block (BD Biosciences). Immunolabeling was performed with the PELCO BioWave Pro 36500-230 microwave equipped with a PELCO SteadyTemp Pro 50062 Thermoelectric Recirculating Chiller (Ted Pella) using a 2-1-2-1-2-1-2-1-2 program[84,85]. A complete list of antibodies and imaging panels with labeling steps can be found in Supplementary

Table 10. In general, primary antibodies were applied first, washed three times in PBS and incubated with appropriate secondary antibodies. Directly conjugated primary antibodies were applied last after blocking with host serum (5%). Endogenous biotin was blocked using the Avidin/Biotin Blocking kit (Abcam). Cell nuclei were visualized with Hoechst (Biotium) and sections were mounted using Fluoromount G (Southern Biotech).

Confocal microscopy, image analysis and histocytometry

Images were acquired using an inverted Leica TCS SP8 X confocal microscope equipped with a ×40 objective (NA 1.3), 4 HyD and 1 PMT detectors, a white light laser that produces a continuous spectral output between 470 and 670 nm as well as 405, 685 and 730 nm lasers. All images were captured at an eight-bit depth, with a line average of 3 and 1,024 × 1,024 format with the following pixel dimensions: x (0.284 µm), y (0.284 µm) and z (1 µm). Images from whole-tissue sections were tiled and merged using the LAS X Navigator software (v.3.5.5.19976). Fluorophore emission was collected on separate detectors with sequential laser excitation of compatible fluorophores (3–4 per sequential) used to minimize spectral spillover. The Channel Dye Separation module within the LAS X v.3.5.5.19976 (Leica) was then used to correct for any residual spillover. Threshold identification, voxel gating, surface creation and masking were performed as previously described using Imaris software (Imaris v.9.8.0, Bitplane AG)[86,87]. For publication quality images, Gaussian filters, brightness/contrast adjustments and channel masks were applied uniformly to all images.

A combination of automatic and manual surface/contour creation methods were used to define GC regions of interest (ROIs) with Imaris software (Imaris v.9.8.0, Bitplane AG). GCs were identified as aggregations of five or more Ki-67$^+$ nuclei. For each sample, whole-tissue ROIs were generated using the Hoechst channel and surface function of Imaris. The resulting metric, total area of tissue imaged, was then used to normalize the number and size of GCs between samples. Imaging data were exported and processed in Excel (Microsoft) and GraphPad Prism v.8.2.1.

Activated induced marker assay

Banked frozen PBMC and tonsil and adenoid cells were thawed as described above in 'Processing for CITE-seq.' Two million mononuclear cells from tonsil or adenoid or 1 million PBMCs from each donor were cultured in a 96-well round bottom plate at a concentration of 1×10^7 cells ml^{-1} in medium consisting of RPMI plus 5% human AB serum (Omega), 2 mM L-glutamine, 0.055 mM β-mercaptoethanol, 1% penicillin/streptomycin, 1 mM sodium pyruvate, 10 mM HEPES and 1% non-essential amino acids. Cells were blocked at 37 °C for 15 min before peptide pool stimulation with 0.5 µg ml^{-1} of anti-CD40 monoclonal antibody (Miltenyi). Following this, cells were stimulated with SARS-CoV-2 peptide pools for 18 h at 37 °C in 5% CO_2 incubator. The following peptide pools were reconstituted per instructions and used for stimulation (Miltenyi): PepTivator SARS-CoV-2 Prot_S+, PepTivator SARS-CoV-2 Prot_S1, PepTivator SARS-CoV-2 Prot_S, PepTivator SARS-CoV-2 Prot_N, PepTivator SARS-CoV-2 Prot_M. Prot_S+, Prot_S1 and Prot_S were pooled into one megapool of spike peptides at concentration of 0.6 nmol ml^{-1} for each pool. PHA-L (Millipore) at 5 µg ml^{-1} was used as positive control. Negative control wells lacking peptides were supplemented with an equivalent volume of DMSO and ddH_2O. After stimulation, cells were first stained with a viability dye (LIVE/DEAD Blue, Thermo Fisher) for 15 min at RT, washed twice and then incubated with True-Stain Monocyte Blocker (BioLegend) for 5 min. Antibodies for chemokine receptors (anti-CXCR3 for 10 min, anti-CCR7 for 10 min, anti-CXCR5 and anti-CCR6 together for 5 min) were sequentially added at RT. The antibody cocktail containing the rest of the surface antibodies and Brilliant Stain Buffer Plus (BD) was then added directly to the cells and incubated for 30 min at RT in the dark (total staining volume 180 µl). Stained cells were washed three times and fixed in 1% paraformaldehyde for 20 min at RT before collecting on the Aurora spectral cytometer (Cytek). Antibodies and reagents used in this assay are listed in Supplementary Table 10.

T cell functional assays: intracellular cytokine staining

Frozen cells were thawed as described in 'Processing for CITE-seq.' Two million PBMCs, adenoid or tonsil cells from each sample were resuspended in 200 µl of complete RPMI medium containing 10% FBS (VWR), 2 mM glutamine, 0.055 mM β-mercaptoethanol, 1% penicillin/streptomycin, 1 mM sodium pyruvate, 10 mM HEPES and 1% non-essential amino acids. Cells were stimulated with PMA (50 ng ml^{-1}, Sigma) and ionomycin (1,000 ng ml^{-1}, Sigma) for 2.5 h in the presence of anti-CD107a (BioLegend), GolgiSTOP (monensin, BD) and GolgiPlug (BFA, BD). After stimulation, surface markers were stained as described above in the AIM assay. Surface-stained cells were washed and fixed with Cytofix Fixation Buffer (BD) at RT for 20 min and washed with permeabilization buffer (eBioscience) twice. Then, the intracellular cytokine antibody mix was added for 30 min at RT (staining volume 50 µl). Stained cells were collected on the Aurora spectral cytometer (Cytek). Antibodies used in this assay are listed in Supplementary Table 10.

Viral quantification in FFPE blocks by ddPCR

RNA was extracted from scrolls cut from FFPE tonsil and adenoid tissues using the RNeasy FFPE kit (QIAGEN) according to the manufacturer's protocol. A NanoDrop ND-1000 Spectrophotometer (Thermo Fisher Scientific) was used to quantify RNA concentrations. The QX200 AutoDG Droplet Digital PCR System (Bio-Rad) was used to detect and quantify SARS-CoV-2 RNA using the SARS-CoV-2 Droplet Digital PCR kit (Bio-Rad), which contains a triplex assay of primers/probes aligned to the CDC markers for SARS-CoV-2 N1 and N2 genes and human *RPP30* gene. Ninety-six-well plates were prepared with technical replicates using the aforementioned kit according to the manufacturer's instructions. The QX200 Automated Droplet Generator (Bio-Rad) provided microdroplet generation and plates were sealed with the PX1 PCR Plate Sealer (Bio-Rad) before proceeding with RT–PCR on the C1000 Touch Thermal Cycler (Bio-Rad) according to the manufacturer's instructions. Plates were read on the QX200 Droplet Reader (Bio-Rad) and analyzed using the freely available QuantaSoft Analysis Pro Software (Bio-Rad) to quantify copies of N1, N2 and RP genes per well, which was then normalized to RNA concentration input. For samples to be considered positive for SARS-CoV-2 N1 or N2 genes, they needed to average the manufacturer's limit of detection of ≥0.1 copies per µl and two positive droplets per well.

Statistics and reproducibility

Previous sections provide a detailed description of statistical analysis of results from unsupervised analysis as well as where to find reproducible scripts. SPICE software (v.6, NIAID, NIH, https://niaid.github.io/spice/) was used to analyze flow cytometry data on T cell polyfunctionality[25]. Graphs were produced by Prism (v.8). Statistical analyses were performed using SPSS (IBM, v.28.0.0.0). We did not assume that the data were normally distributed and used nonparametric statistical tests. Differences between groups were compared using the Mann–Whitney U-test for independent values and Wilcoxon signed-ranks test for paired values. Correlations were assessed using the Spearman's rank correlation and visualized by corrplot (v.0.92). All statistical tests were two-sided. $P < 0.05$ was considered significant. Experiments were not repeated independently. Data collection and analysis were not performed blind to the conditions of the experiments.

Reporting summary

Further information on research design is available in the Nature Portfolio Reporting Summary linked to this article.

Data availability

Raw sequencing data are deposited to the Gene Expression Omnibus under accession no. GSE215802. All other source data are provided with the article or upon request from the corresponding authors. Source data are provided with this paper.

Code availability

The R scripts used in this paper are available at https://github.com/kalpanamanthiram/Covid-Tonsil.

References

58. Michael, S. et al. Standardization of ELISA protocols for serosurveys of the SARS-CoV-2 pandemic using clinical and at-home blood sampling. *Nat. Commun.* **12**, 113 (2021).
59. Kalish, H. et al. Undiagnosed SARS-CoV-2 seropositivity during the first 6 months of the COVID-19 pandemic in the United States. *Sci. Transl. Med.* **13**, eabh3826 (2021).
60. Zahra, F. T., Bellusci, L., Grubbs, G., Golding, H. & Khurana, S. Neutralisation of circulating SARS-CoV-2 delta and omicron variants by convalescent plasma and SARS-CoV-2 hyperimmune intravenous human immunoglobulins for treatment of COVID-19. *Ann. Rheum. Dis.* https://doi.org/10.1136/annrheumdis-2022-222115 (2022).
61. Ravichandran, S. et al. Antibody signature induced by SARS-CoV-2 spike protein immunogens in rabbits. *Sci. Transl. Med.* **12**, abc3539 (2020).
62. Tang, J. et al. Antibody affinity maturation and plasma IgA associate with clinical outcome in hospitalized COVID-19 patients. *Nat. Commun.* **12**, 1221 (2021).
63. Park, L. M., Lannigan, J. & Jaimes, M. C. OMIP-069: forty-color full spectrum flow cytometry panel for deep immunophenotyping of major cell subsets in human peripheral blood. *Cytom. A* **97**, 1044–1051 (2020).
64. Liu, C. et al. Time-resolved systems immunology reveals a late juncture linked to fatal COVID-19. *Cell* **184**, 1836–1857 (2021).
65. Kotliarov, Y. et al. Broad immune activation underlies shared set point signatures for vaccine responsiveness in healthy individuals and disease activity in patients with lupus. *Nat. Med.* **26**, 618–629 (2020).
66. Hao, Y. et al. Integrated analysis of multimodal single-cell data. *Cell* **184**, 3573–3587 (2021).
67. Mulè, M. P., Martins, A. J. & Tsang, J. S. Normalizing and denoising protein expression data from droplet-based single cell profiling. Preprint at *bioRxiv* https://doi.org/10.1101/2020.02.24.963603 (2021).
68. Gu, Z., Eils, R. & Schlesner, M. Complex heatmaps reveal patterns and correlations in multidimensional genomic data. *Bioinformatics* **32**, 2847–2849 (2016).
69. Wickham, H. *ggplot2: Elegant Graphics for Data Analysis*. 1st edn, (Springer, 2009).
70. Giudicelli, V., Chaume, D. & Lefranc, M. P. IMGT/GENE-DB: a comprehensive database for human and mouse immunoglobulin and T cell receptor genes. *Nucleic Acids Res.* **33**, D256–D261 (2005).
71. Ye, J., Ma, N., Madden, T. L. & Ostell, J. M. IgBLAST: an immunoglobulin variable domain sequence analysis tool. *Nucleic Acids Res.* **41**, W34–W40 (2013).
72. Gupta, N. T. et al. Change-O: a toolkit for analyzing large-scale B cell immunoglobulin repertoire sequencing data. *Bioinformatics* **31**, 3356–3358 (2015).
73. Nouri, N. & Kleinstein, S. H. A spectral clustering-based method for identifying clones from high-throughput B cell repertoire sequencing data. *Bioinformatics* **34**, i341–i349 (2018).
74. Gupta, N. T. et al. Hierarchical clustering can identify B cell clones with high confidence in Ig repertoire sequencing data. *J. Immunol.* **198**, 2489–2499 (2017).
75. Yaari, G. et al. Models of somatic hypermutation targeting and substitution based on synonymous mutations from high-throughput immunoglobulin sequencing data. *Front. Immunol.* **4**, 358 (2013).
76. Hoehn, K. B., Pybus, O. G. & Kleinstein, S. H. Phylogenetic analysis of migration, differentiation, and class switching in B cells. *PLoS Comput. Biol.* **18**, e1009885 (2022).
77. Kassambara, A. ggpubr: 'ggplot2' Based Publication Ready Plots v.0.4.0. https://github.com/kassambara/ggpubr (2020).
78. Hoehn, K. B. et al. Repertoire-wide phylogenetic models of B cell molecular evolution reveal evolutionary signatures of aging and vaccination. *Proc. Natl Acad. Sci. USA* **116**, 22664–22672 (2019).
79. Nielsen, R. & Yang, Z. Likelihood models for detecting positively selected amino acid sites and applications to the HIV-1 envelope gene. *Genetics* **148**, 929–936 (1998).
80. Yu, G., Smith, D. K., Zhu, H., Guan, Y. & Lam, T. T.-Y. ggtree: an R package for visualization and annotation of phylogenetic trees with their covariates and other associated data. *Methods Ecol. Evol.* **8**, 28–36 (2017).
81. Borcherding, N., Bormann, N. L. & Kraus, G. scRepertoire: an R-based toolkit for single-cell immune receptor analysis. *F1000Res* **9**, 47 (2020).
82. Greiff, V., Miho, E., Menzel, U. & Reddy, S. T. Bioinformatic and statistical analysis of adaptive immune repertoires. *Trends Immunol.* **36**, 738–749 (2015).
83. Wallace, I. M., O'Sullivan, O., Higgins, D. G. & Notredame, C. M-Coffee: combining multiple sequence alignment methods with T-Coffee. *Nucleic Acids Res.* **34**, 1692–1699 (2006).
84. Radtke, A. J. et al. IBEX: an iterative immunolabeling and chemical bleaching method for high-content imaging of diverse tissues. *Nat. Protoc.* **17**, 378–401 (2022).
85. Radtke, A. J. et al. IBEX: a versatile multiplex optical imaging approach for deep phenotyping and spatial analysis of cells in complex tissues. *Proc. Natl Acad. Sci. USA* **117**, 33455–33465 (2020).
86. Radtke, A. J. et al. Lymph-node resident CD8α$^+$ dendritic cells capture antigens from migratory malaria sporozoites and induce CD8$^+$ T cell responses. *PLoS Pathog.* **11**, e1004637 (2015).
87. Gerner, M. Y., Kastenmuller, W., Ifrim, I., Kabat, J. & Germain, R. N. Histo-cytometry: a method for highly multiplex quantitative tissue imaging analysis applied to dendritic cell subset microanatomy in lymph nodes. *Immunity* **37**, 364–376 (2012).

Acknowledgements

We thank the patients and their families for their generous participation; J. Reilley and N. Bansal for their technical assistance; A.J. Athman, R. Kissinger, R. Perry-Gottschalk and A. Stewart of the Research Technologies Branch of the National Institute of Allergy and Infectious Diseases (NIAID) for figure illustrations and formatting; the Division of Otolaryngology at CNH for helping with participant recruitment; the National Cancer Institute (NCI) Sequencing Facility for sequencing support; J. Lack, J. Cannons, A. Pichler, A.I. Lim, L. Notarangelo and Y. Belkaid (NIAID/National Institutes of Health (NIH)), S. Anderson and D. Kastner (National Human Genome Research Institute (NHGRI)/NIH) and K. Edwards (Vanderbilt) for insightful discussions. This work was supported in part by the Intramural Research Programs of NIAID, Clinical Center, NHGRI, NCI and National Institute of Biomedical Imaging and Bioengineering at NIH that supported individual investigators and the Intramural Research Programs of NIAID and other NIH Institutes that support the NIH Center for Human Immunology. The antibody response study was supported by the US Food and Drug Administration's Perinatal Health

Center of Excellence project grant no. GCBER005 to S.K. K.B.H. and S.H.K. were funded in part by NIAID/NIH grant no. R01AI104739. The funders had no role in study design, data collection and analysis, decision to publish or preparation of the manuscript.

Author contributions

K.M., P.M., P.L.S. and Q.X. conceived and designed the study. Q.X., K.M., A.J.R., J.C., J.T., G.G., S.S., S.R., J.K., M. Karkanitsa, J.S., H.K., M.M.K., M. Kirby, F.C., G.K., P.D. and G.S. performed experiments. Q.X, K.M., P.M.-A., A.J.M., A.J.R., K.B.H., C.O., C.L., J.K., S.S., S.R., F.C., A.S. and I.T.M. analyzed and interpreted results. K.M., P.M., H.B., N.R., D.P. and L.G. developed patient recruitment materials and/or recruited participants. Q.X., P.M.-A., A.J.M., A.J.R., K.B.H., L.K., S. Preite, R.A., P.J.M., D.M.S., S. Pittaluga, R.N.G., S.M., D.S.C., A.S., S.K., S.H.K., K.S., J.S.T., P.M., P.L.S. and K.M. provided critical scientific input and/or reagents. K.M., P.L.S. and Q.X. wrote the initial draft of the paper. All authors contributed to the final review and editing of the paper.

Competing interests

P.M.-A. is currently an employee of Novartis. S. Preite and A.S. are currently employees of AstraZeneca and may own stock or stock options. S.H.K. receives consulting fees from Peraton. K.B.H. receives consulting fees from Prellis Biologics. The remaining authors have no competing interests.

Additional information

Extended data is available for this paper at https://doi.org/10.1038/s41590-022-01367-z.

Supplementary information The online version contains supplementary material available at https://doi.org/10.1038/s41590-022-01367-z.

Correspondence and requests for materials should be addressed to Pamela L. Schwartzberg or Kalpana Manthiram.

Peer review information *Nature Immunology* thanks Olivier Schwartz and the other, anonymous, reviewer(s) for their contribution to the peer review of this work. Primary Handling Editor: Ioana Visan in collaboration with the *Nature Immunology* team. Peer reviewer reports are available.

https://doi.org/10.1038/s41590-022-01367-z

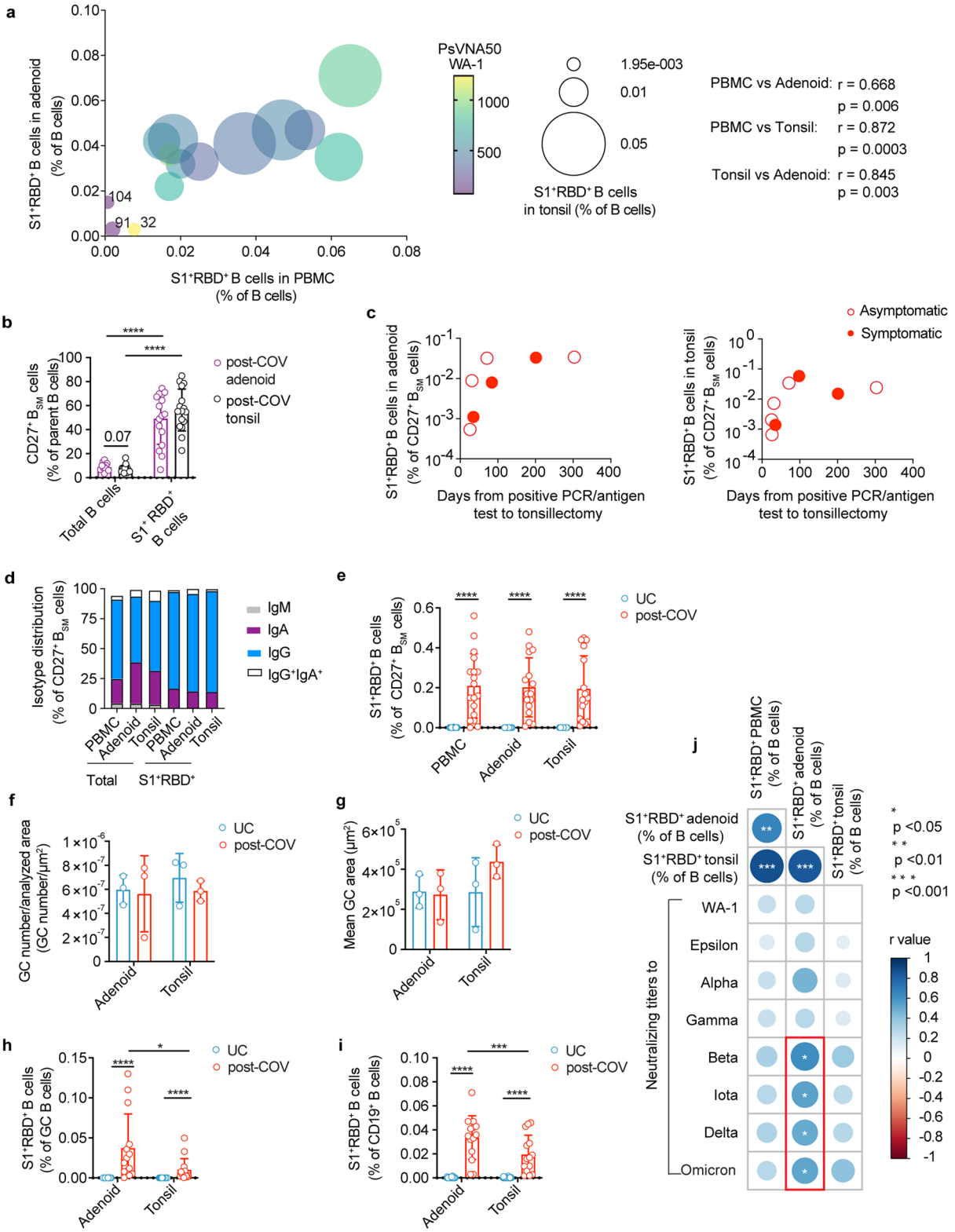

Extended Data Fig. 1 | See next page for caption.

https://doi.org/10.1038/s41590-022-01367-z

Extended Data Fig. 1 | Characterization of neutralization titers and S1$^+$RBD$^+$ B cells. a. Correlation of S1$^+$RBD$^+$ cell frequency among B cells in post-COV PBMCs, tonsils and adenoids. Data point color indicates neutralizing titers (PsVNA50) to WA-1. Donors with the lowest frequencies of S1$^+$RBD$^+$ B cells are labeled. Spearman's coefficient (r) noted. **b**. CD27$^+$ B_{SM} cell frequency among total B cells and among S1$^+$RBD$^+$ B cells from post-COV adenoids ($p < 0.0001$) and tonsils ($p < 0.0001$). **c**. S1$^+$RBD$^+$ B cell frequency among CD27$^+$ B_{SM} cells in post-COV adenoids and tonsils according to time from positive PCR/antigen test to surgery. **d**. Proportion of each isotype among S1$^+$RBD$^+$ CD27$^+$ B_{SM} cells and total CD27$^+$ B_{SM} cells in post-COV PBMCs, adenoids and tonsils. **e**. Percentage of S1$^+$RBD$^+$ B cells among CD27$^+$ B_{SM} cells from post-COV and UC PBMCs, adenoids and tonsils (all post-COV vs. UC $p < 10^{-6}$). **f,g** Mean number of GCs per total scanned tissue area (**f**) and mean GC area (total GC area/number of GCs in section) (**g**) from adenoids and tonsils from post-COV and UC donors (n = 3 each). **h,i**. Percentage of S1$^+$RBD$^+$ B cells among GC B cells (**h**) and total B cells (**i**) from 14 pairs of post-COV adenoids and tonsils (total B $p = 0.007$, GC B $p = 0.030$) and UC (UC adenoid n = 27; tonsil n = 30). All post-COV vs. UC comparisons $p < 10^{-6}$. **j**. Summary of correlations between frequencies of S1$^+$RBD$^+$ cells among CD19$^+$ B cells PBMCs, adenoids and tonsils and neutralizing titers (PsVNA50) to multiple variants. Spearman's correlation noted in color. % S1$^+$RBD$^+$ B in post-COV adenoid vs. PBMC $p = 0.006$, tonsil vs. PBMC $p = 0.00003$, tonsil vs. adenoid $p = 0.0003$; % S1$^+$RBD$^+$ B in post-COV adenoid vs. PsVNA50 Beta $p = 0.01$, Iota $p = 0.04$, Delta $p = 0.05$, Omicron $p = 0.04$). Panels **a**–**g,j**: PBMC post-COV n = 18, UC n = 33; adenoid post-COV n = 16, UC n = 27; and tonsil post-COV n = 16, UC n = 30. Each symbol represents one donor. Means ± S.D. displayed in bar plots. Significance calculated with two-sided Mann–Whitney U-test (unpaired) or Wilcoxon signed ranks test (paired). *$p < 0.05$, ***$p < 0.001$, ****$p < 0.0001$.

https://doi.org/10.1038/s41590-022-01367-z

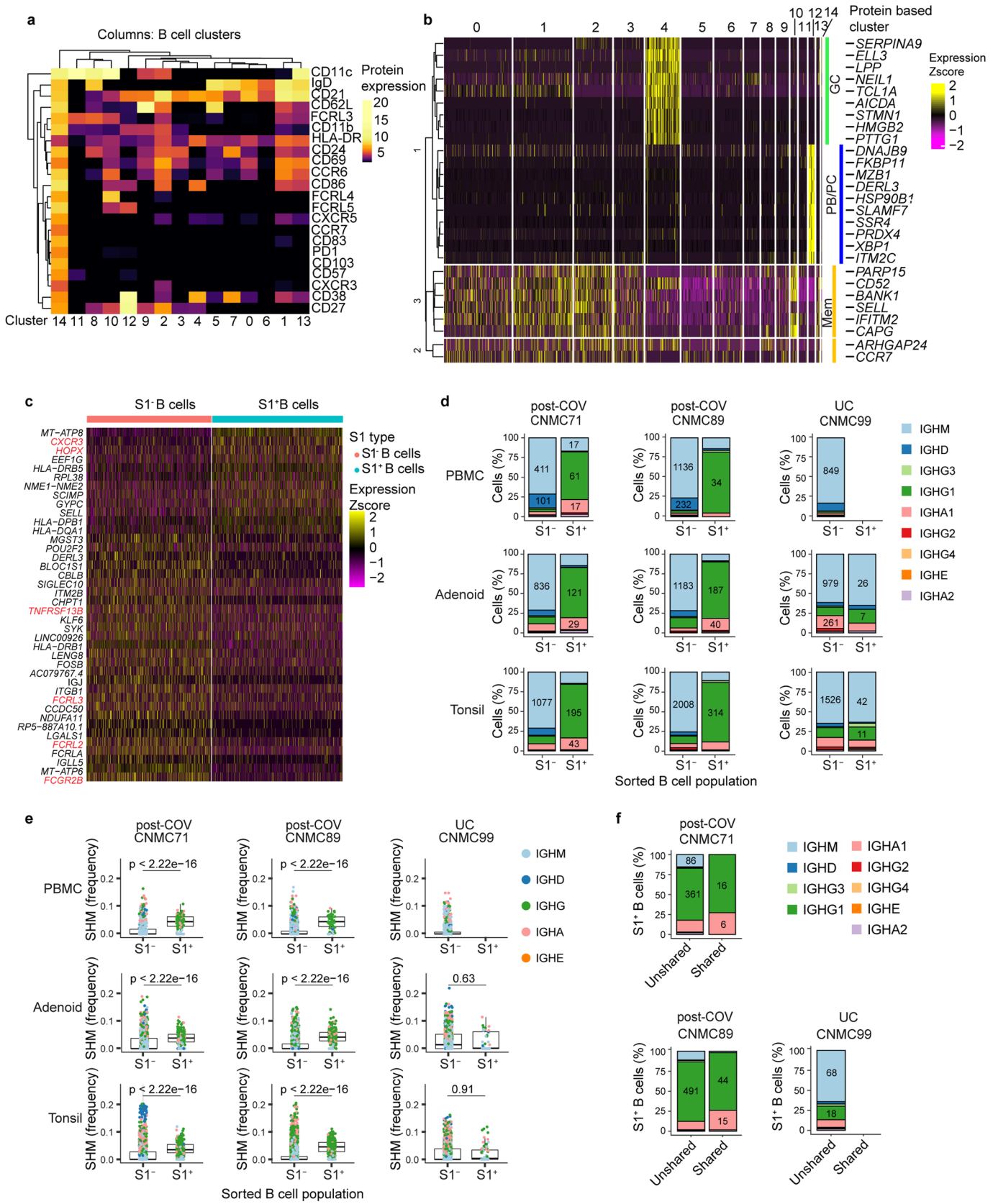

Extended Data Fig. 2 | See next page for caption.

https://doi.org/10.1038/s41590-022-01367-z

Extended Data Fig. 2 | CITE-seq analysis of SARS-CoV-2 antigen-specific B cells. a,b. Heat map of unsupervised clustering by CITE-seq antibody expression of $S1^+$ and $S1^-$ B cells from tonsils, adenoids and PBMCs from three donors (2 post-COV and 1 UC) yielding 15 clusters (**a**). Expression of signature gene sets for GC B cells, memory B (Mem) cells and plasma cells/plasmablasts (PC/PB) among all B cells ($S1^+$ and $S1^-$) organized by cluster (**b**). **c.** Heat map showing differentially expressed (DE) genes in $S1^+$ vs. $S1^-$ B cells from tonsils and adenoids from cluster 2 (which are $CD27^+$ B_{SM} cells), see Supplementary Table 5. **d.** Sub-isotype percentages among sorted $S1^+$ and $S1^-$ B cells from adenoids, tonsils and PBMCs of 2 post-COV donors (CNMC71 and 89) and one UC (CNMC99). Raw number of cells with a given sub-isotype are labeled only for sub-isotypes that make up >10% of a given category. **e.** Somatic hypermutation (SHM) frequency (calculated in V gene) among sorted $S1^+$ and $S1^-$ B cells of all isotypes from PBMCs, adenoids and tonsils of each donor. Median ± quartiles and p values shown in plots. Significance calculated with two-sided Mann–Whitney U-test. CNMC71 PBMC $S1^+$ n = 101, $S1^-$ n = 577 cells; CNMC89 PBMC $S1^+$ n = 44, $S1^-$ n = 1491 cells; CNMC99 PBMC $S1^-$ n = 1026 cells; CNMC71 adenoid $S1^+$ n = 191, $S1^-$ n = 1177 cells; CNMC89 adenoid $S1^+$ n = 261, $S1^-$ n = 1647 cells; CNMC99 adenoid $S1^+$ n = 40, $S1^-$ n = 1593 cells; CNMC71 tonsil $S1^+$ n = 286, $S1^-$ n = 1514 cells; CNMC89 tonsil $S1^+$ n = 416, $S1^-$ n = 2644 cells; CNMC99 tonsil $S1^+$ n = 66, $S1^-$ n = 2346 cells. **f.** Sub-isotype frequencies among $S1^+$ B cells from clones shared between tonsil and adenoid and unshared clones. Raw number of cells with a given sub-isotype are labeled only for sub-isotypes that make up >10% of a given category.

https://doi.org/10.1038/s41590-022-01367-z

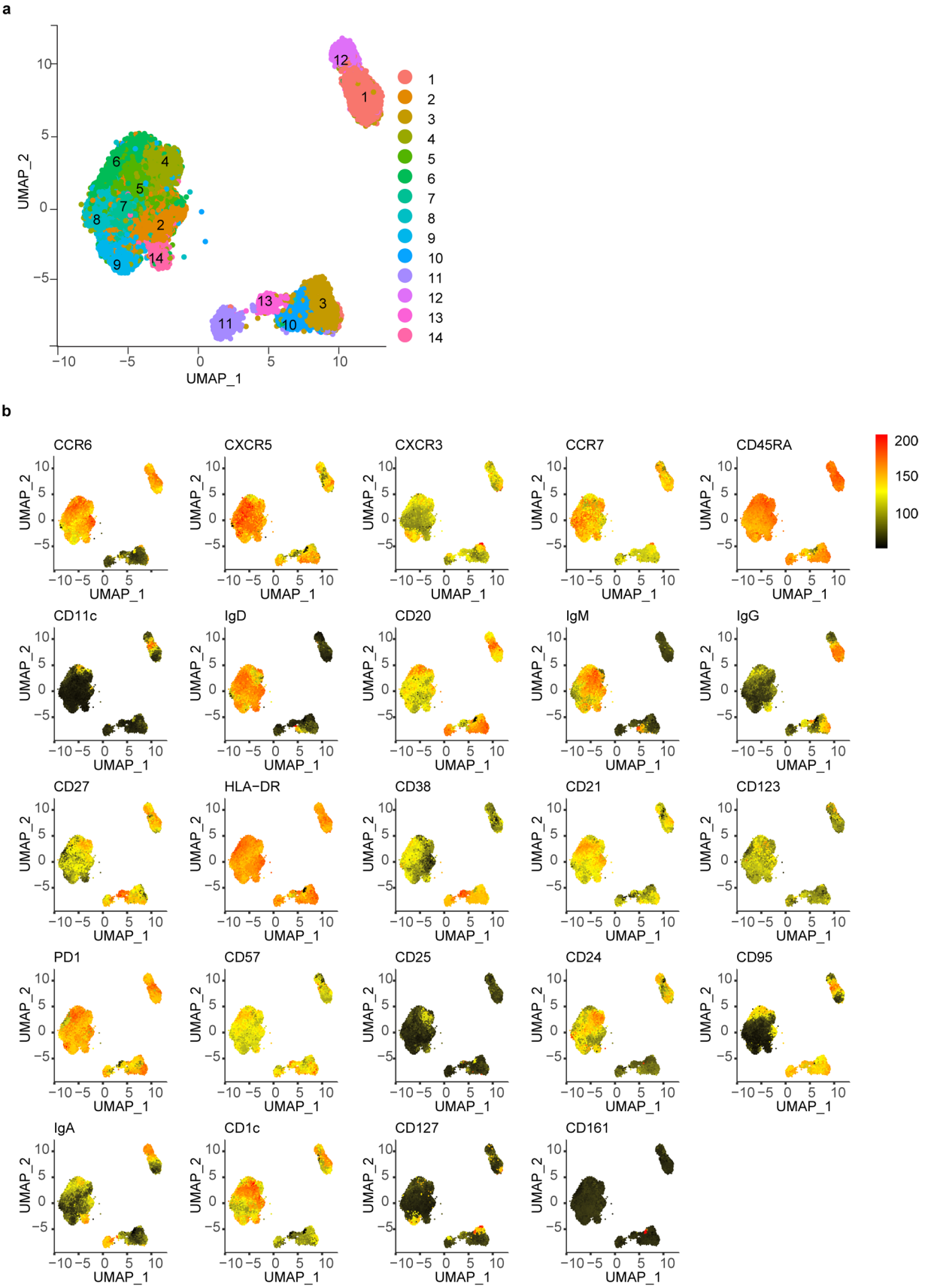

Extended Data Fig. 3 | UMAP of unsupervised clustering of B cells from tonsil and adenoid. a. Uniform manifold approximation and projection (UMAP) of unsupervised clustering of surface markers from flow cytometric analysis of $CD19^+$ B cells from adenoids and tonsils. **b**. Heatmaps of marker/antibody expression overlayed on UMAP.

https://doi.org/10.1038/s41590-022-01367-z

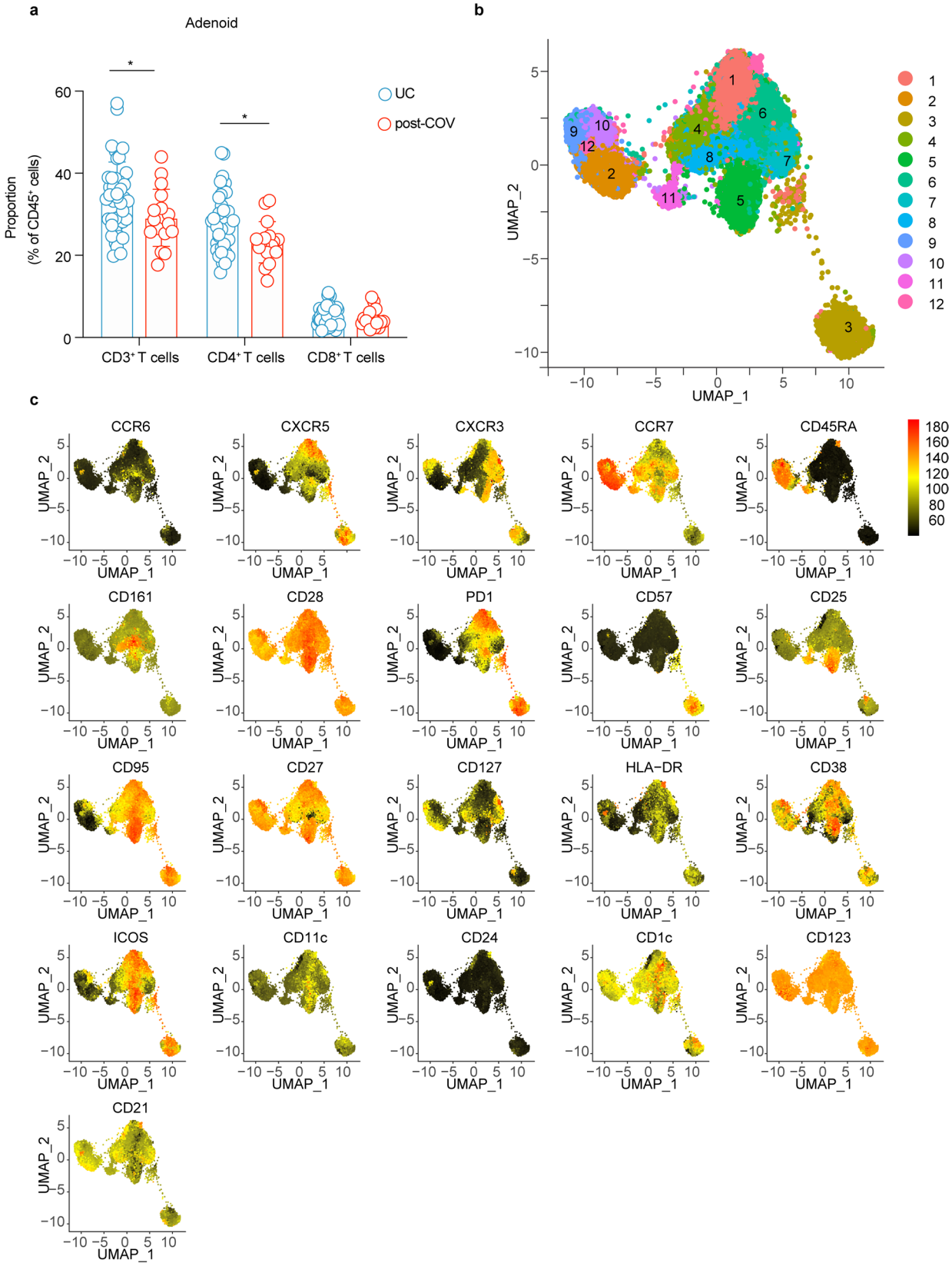

Extended Data Fig. 4 | UMAP of unsupervised clustering of CD4$^+$ T cells from tonsil and adenoid. a. Comparison of CD3$^+$, CD4$^+$ and CD8$^+$ T cell frequency in adenoid of post-COV (n = 17) and UC donors (n = 42), CD3$^+$ p value = 0.043, CD4$^+$ p = 0.017. **b,c.** UMAP of unsupervised clustering of surface markers from flow cytometric analysis of CD4$^+$ T cells from adenoid and tonsil (**b**) with heatmaps of marker/antibody expression overlayed (**c**).

https://doi.org/10.1038/s41590-022-01367-z

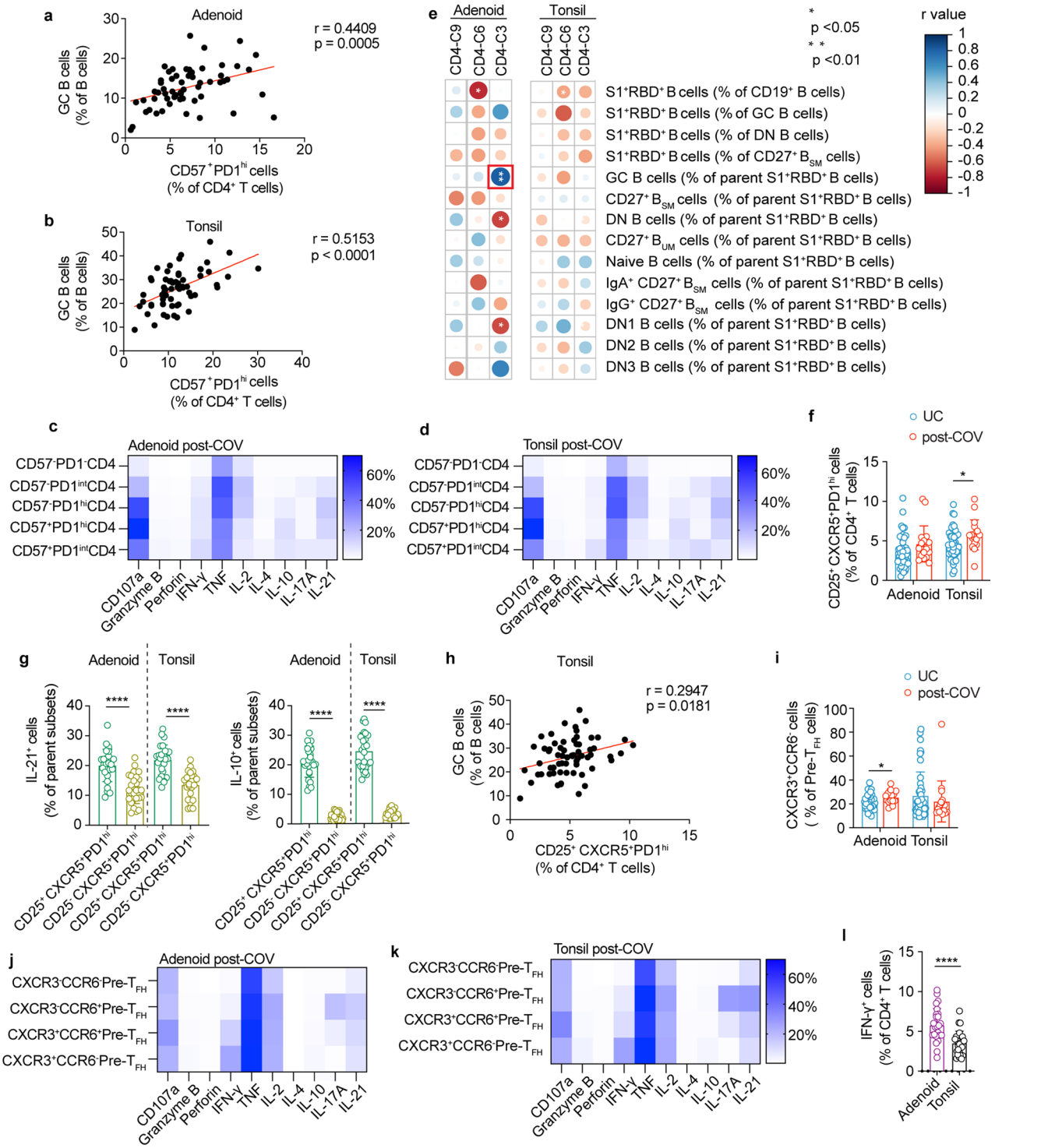

Extended Data Fig. 5 | Phenotyping of expanded CD4$^+$ T cell populations. a,b. Correlation between frequency of CD57$^+$PD-1^{hi} CD4$^+$ T cells and frequency of GC B cells in adenoids (**a**, n = 59) and tonsils (**b**, n = 64). **c,d.** Intracellular cytokine and cytotoxic factor expression in various CD4$^+$ T cell subsets gated on CD57 and PD-1 from post-COV adenoids (**c**, n = 13) and tonsils (**d**, n = 13) after PMA/ionomycin stimulation. Mean cell frequency shown in heat map. **e.** Correlations among various subsets of SARS-CoV-2-specific B cells (defined in Supplementary Figs. 1) and significantly different tissue CD4$^+$ T cell clusters (clusters 3, 6, 9 shown as % of CD4$^+$ T cells) from unsupervised analysis. **f.** Percentage of CD25$^+$CXCR5$^+$PD-1^{hi} cells among CD4$^+$ T cells in post-COV and UC adenoids and tonsils (p = 0.031). **g.** Cytokine production by CD25$^+$ and CD25$^-$ CXCR5$^+$PD-1^{hi} CD4$^+$ T cells in tonsils (n = 26) and adenoids (n = 26) following PMA/ionomycin stimulation, all p < 0.0001. **h.** Correlation between frequency of CD25$^+$CXCR5$^+$PD-1^{hi} CD4$^+$ T cell and GC B cell frequencies in tonsils (n = 64). **i.** Frequency of CXCR3$^+$CCR6$^-$ cells among pre-T$_{FH}$ cells (PD-1^{int}CXCR5$^+$ conventional CD4$^+$ T) in post-COV and UC adenoids (p = 0.042) and tonsils. **j,k.** Intracellular cytokine/cytotoxic factor expression in different pre-T$_{FH}$ cell subsets gated on CXCR3 and CCR6 from post-COV adenoids (**j**, n = 13) and tonsils (**k**, n = 13) after PMA/ionomycin stimulation. Mean cell frequency shown in heat map. **l.** Comparison of IFN-γ production by CD4$^+$ T cells in adenoids and tonsils following PMA/ionomycin stimulation (n = 26 including 13 post-COV and 13 UC samples of each tissue, p < 0.0001). For panels, f, and i: adenoids post-COV n = 17, UC n = 42; tonsils post-COV n = 18, UC n = 46. Each symbol represents one donor. Means ± S.D. displayed on bar plots. Significance calculated with two-sided Mann–Whitney U-test to compare two groups and Spearman's rank test for correlations (r is Spearman's coefficient). *p < 0.05, ****p < 0.0001.

https://doi.org/10.1038/s41590-022-01367-z

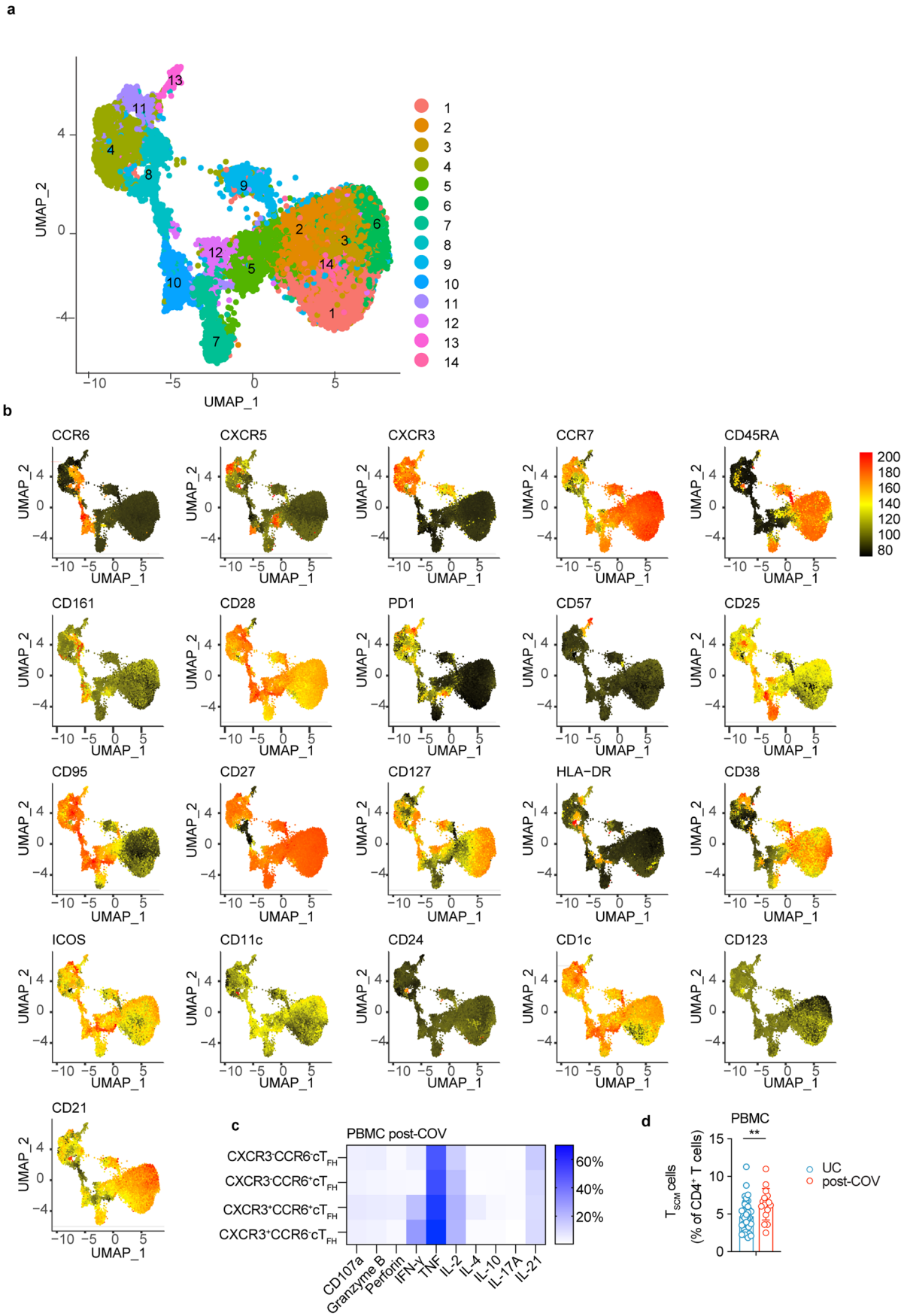

Extended Data Fig. 6 | See next page for caption.

https://doi.org/10.1038/s41590-022-01367-z

Extended Data Fig. 6 | cT_{FH} cell populations are expanded post-COVID-19 in PBMC. a,b. UMAP of unsupervised clustering of surface markers from flow cytometric analysis of $CD4^+$ T cells from PBMCs (**a**) with heatmaps of marker/antibody expression overlayed (**b**). **c**. Intracellular cytokine and cytotoxic factor production by various circulating T_{FH} cell (cT_{FH}) subsets in PBMC gated by CXCR3 and CCR6 from post-COV donors (n = 4) following PMA/ionomycin stimulation. Mean cell frequency shown in heat map. **d**. Frequency of $CD45RA^+CCR7^+CD28^+CD27^+CD95^+$ $CD4^+$ T stem cell-like memory (T_{SCM}) cells in PBMC of post-COV (n = 16) and UC (n = 41), p = 0.007. Each symbol represents one donor. Means ± S.D. displayed on bar plots. Significance calculated with two-sided Mann–Whitney U-test. **p < 0.01.

https://doi.org/10.1038/s41590-022-01367-z

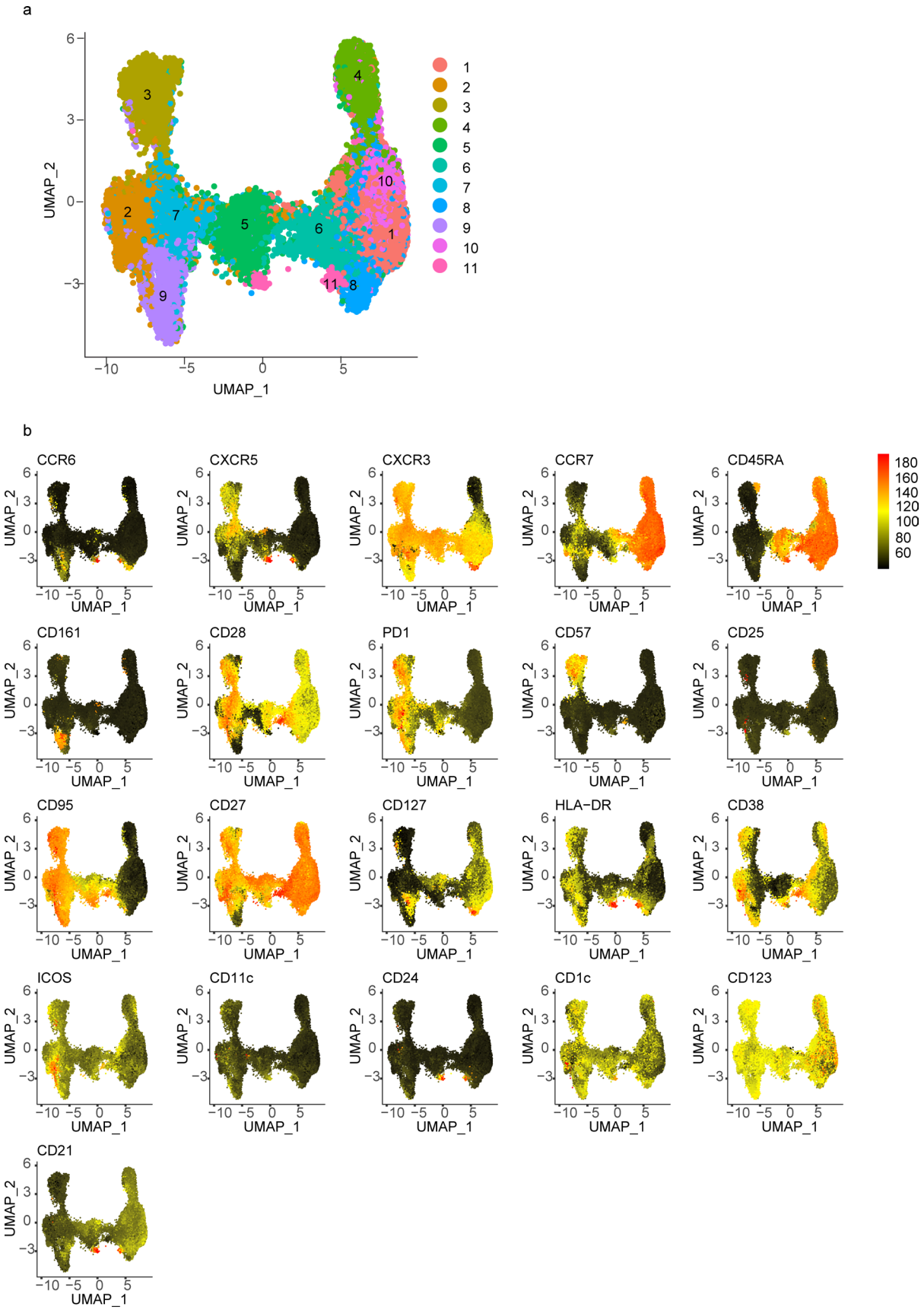

Extended Data Fig. 7 | UMAP of unsupervised clustering of CD8$^+$ T cells from tonsil and adenoid. a. UMAP of unsupervised clustering of surface markers from flow cytometric analysis of CD8$^+$ T cells from adenoids and tonsils. **b.** Heatmaps of marker/antibody expression overlayed on UMAP.

https://doi.org/10.1038/s41590-022-01367-z

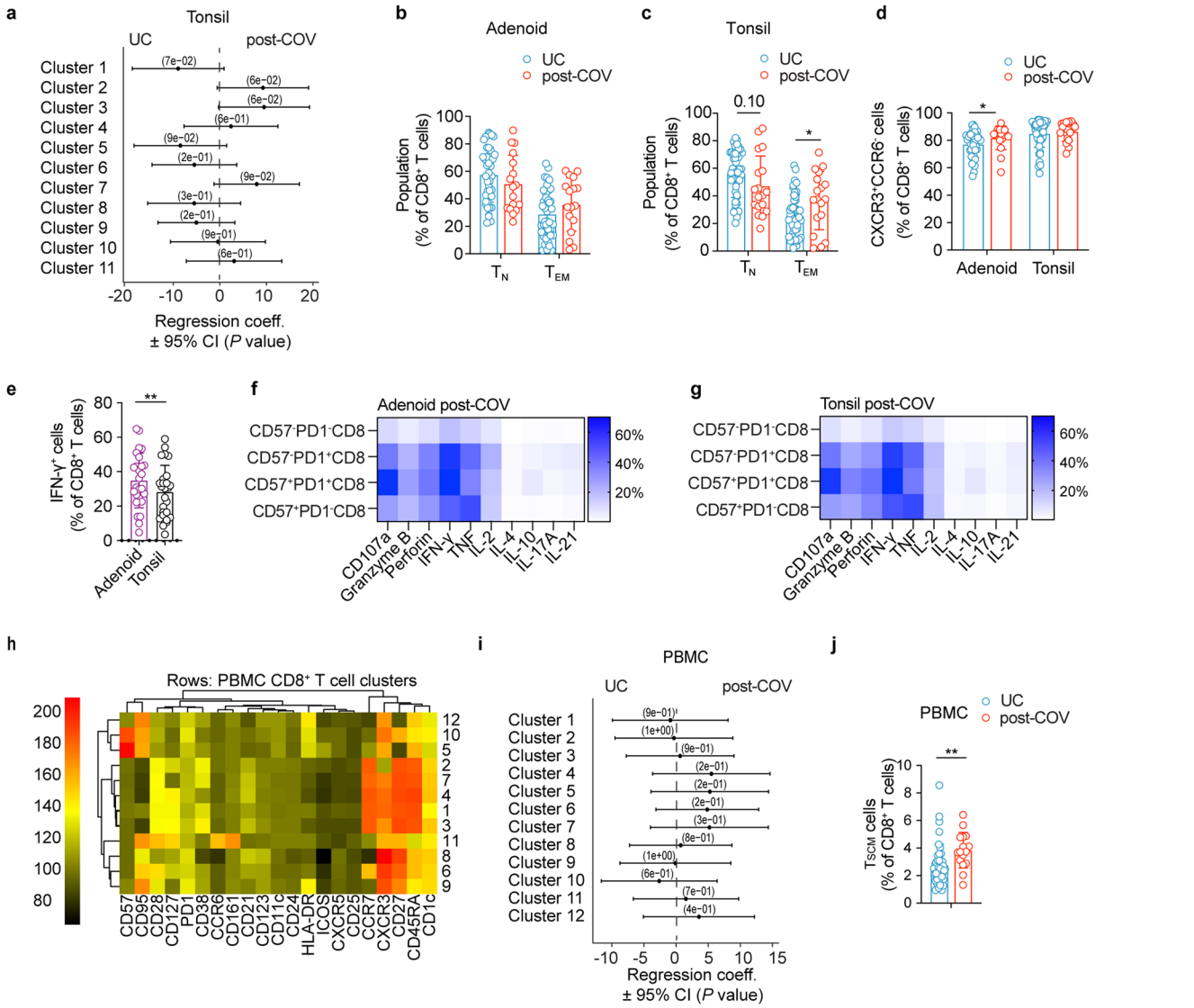

Extended Data Fig. 8 | Expanded CD8⁺ T cell populations after COVID-19. **a**. Quantification of the effect of previous SARS-CoV-2 infection on CD8⁺ T cell clusters in tonsil showing regression coefficients ± 95% confidence intervals (CI) and p values, estimated with a linear model controlling for age and sex (post-COV n = 15, UC n = 42). **b,c**. Frequencies of CD45RA⁺CCR7⁺CD8⁺ naïve T (T_N) and CD45RA⁻CCR7⁻CD8⁺ effector memory T (T_{EM}) cells in post-COV and UC adenoids (**b**) and tonsils (**c**, p = 0.035 for T_{EM}). **d**. Frequency of CXCR3⁺CCR6⁻ cells among CD8⁺ T cells in post-COV and UC adenoids (p = 0.022) and tonsils. **e**. Comparison of IFN-γ production by CD8⁺ T cells in adenoids and tonsils following PMA/ionomycin stimulation (n = 26 for each tissue, p = 0.003). **f,g**. Intracellular cytokine/cytotoxic factor production by different CD8⁺ T cell subsets gated by CD57 and PD-1 from post-COV adenoids (**f**, n = 13) and tonsils (**g**, n = 13). Mean cell frequency shown in heat map. **h**. Unsupervised clustering of CD8⁺ T cells from PBMCs according to surface antibodies from flow cytometric analysis. No clusters showed significant differences (p < 0.05) in post-COV (n = 13) and UC (n = 34) samples. **i**. Quantification of the effect of previous SARS-CoV-2 infection on CD8⁺ T cell clusters in PBMCs showing regression coefficients ± 95% CI and p values, estimated with a linear model controlling for age and sex. **j**. Frequency of CD45RA⁺CCR7⁺CD28⁺CD27⁺CD95⁺ CD8⁺ T stem cell-like memory (T_{SCM}) in post-COV (n = 16) and UC (n = 41) PBMCs (p = 0.002). For panels **b**–**d**, adenoids post-COV n = 17, UC n = 42, tonsils post-COV n = 18, UC n = 46. Each symbol represents one donor. Means ± S.D. displayed on bar plots. Significance calculated with two-sided Mann–Whitney U-test. *p < 0.05, **p < 0.01.

https://doi.org/10.1038/s41590-022-01367-z

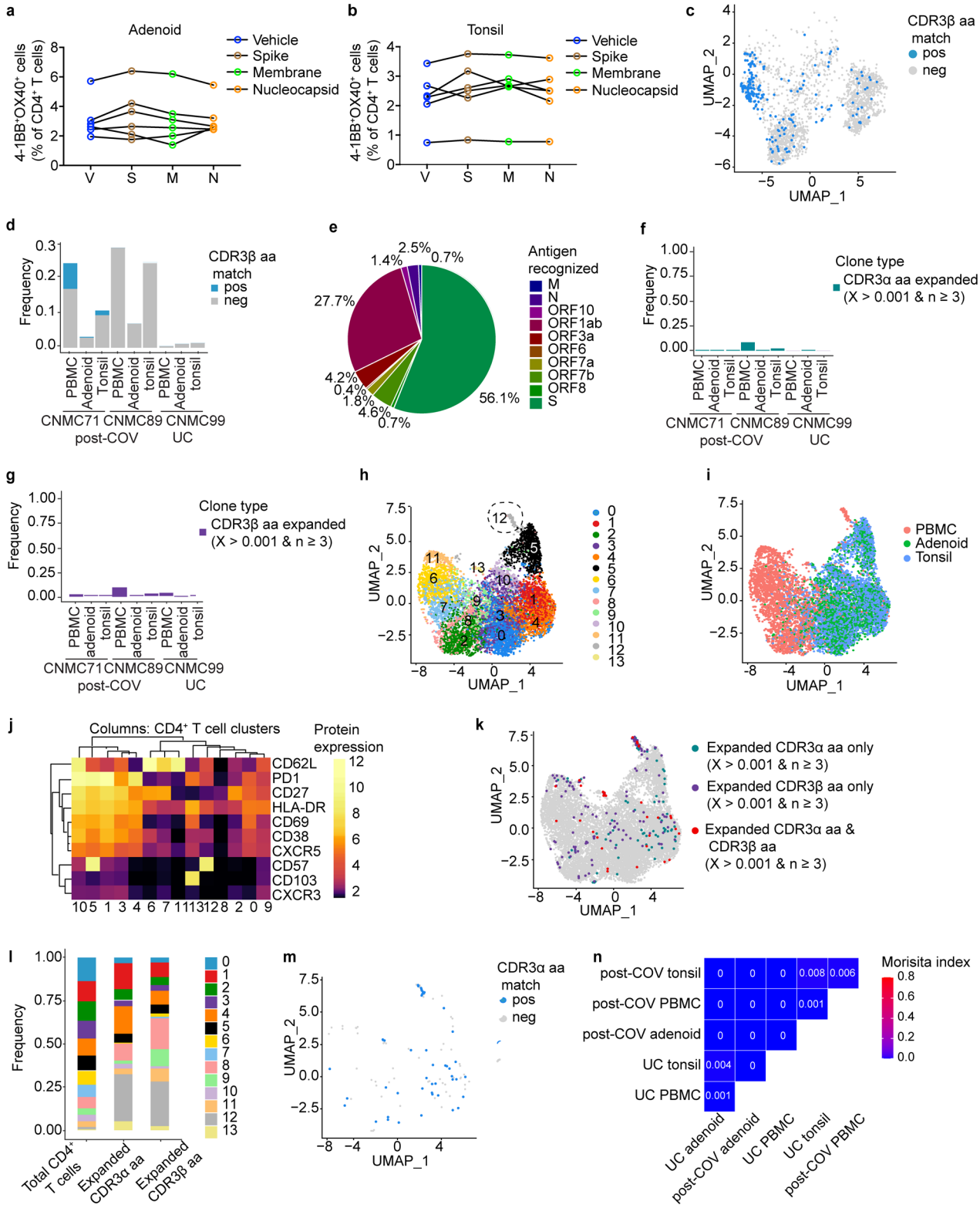

Extended Data Fig. 9 | See next page for caption.

https://doi.org/10.1038/s41590-022-01367-z

Extended Data Fig. 9 | SARS-CoV-2 antigen-specific T cells and TCR repertoire. a,b. Frequencies of AIM$^+$ (OX40$^+$4-1BB$^+$) CD4$^+$ T cells from adenoid (**a**) and tonsil (**b**) of post-COV tonsils (n = 6) and adenoids (n = 6) following SARS-CoV-2 spike (S), membrane (M) and nucleocapsid (N) peptide pool stimulation. DMSO (vehicle, V) is negative control. Significance calculated with two-sided Wilcoxon signed rank test for paired samples from the same donor. **c**. Among expanded CD8$^+$ T cell clones, those with TCRβ CDR3 amino acid (aa) sequences that match those publicly reported to be SARS-CoV-2-reactive are highlighted in the UMAP (clustering shown in Fig. 7h). **d**. Frequency of matches among expanded CD8$^+$ T cells from two post-COV donors (CNMC71 and 89) and one UC (CNMC99). More PBMCs were sorted than tonsil or adenoid cells in order to sort similar numbers of S1$^+$ B cells from each sample; therefore, more T cells were analyzed from PBMCs than tonsil or adenoid. **e**. Antigens recognized by CD8$^+$ T cells in post-COV samples with CDR3β aa sequences publicly reported to be SARS-CoV-2 reactive; proportion of cells recognizing each antigen is shown in the pie chart. **f,g**. Frequency of CD4$^+$ T cells that are part of expanded clonotypes (frequency >0.001 and absolute count ≥3) in tonsils, adenoids and PBMCs. Clones were defined by identical CDR3α (**f**) or CDR3β (**g**) aa sequences. **h**–**m**. UMAP (**h**), tissue distribution (**i**) and CITE-seq surface antibody expression (**j**) of 14 clusters of sorted CD95$^+$CD4$^+$ T cells from tonsils, adenoids and PBMCs of 2 post-COV donors and one UC. Expanded TCRα or β clonotypes (**k**) and distribution of expanded clones across clusters (**l**). Expanded TCRα clones with CDR3 sequences that match publicly reported SARS-CoV-2-specific sequences (**m**). **n**. Overlap of CD4$^+$ T cell clones among PBMCs, tonsils and adenoids from 2 post-COV donors and one UC; degree of overlap between TCRα/β CDR3 aa sequences was calculated with the Morisita index (shown in plot), ranging from 0 to 1, with 0 indicating no sharing and 1 indicating full overlap.

https://doi.org/10.1038/s41590-022-01367-z

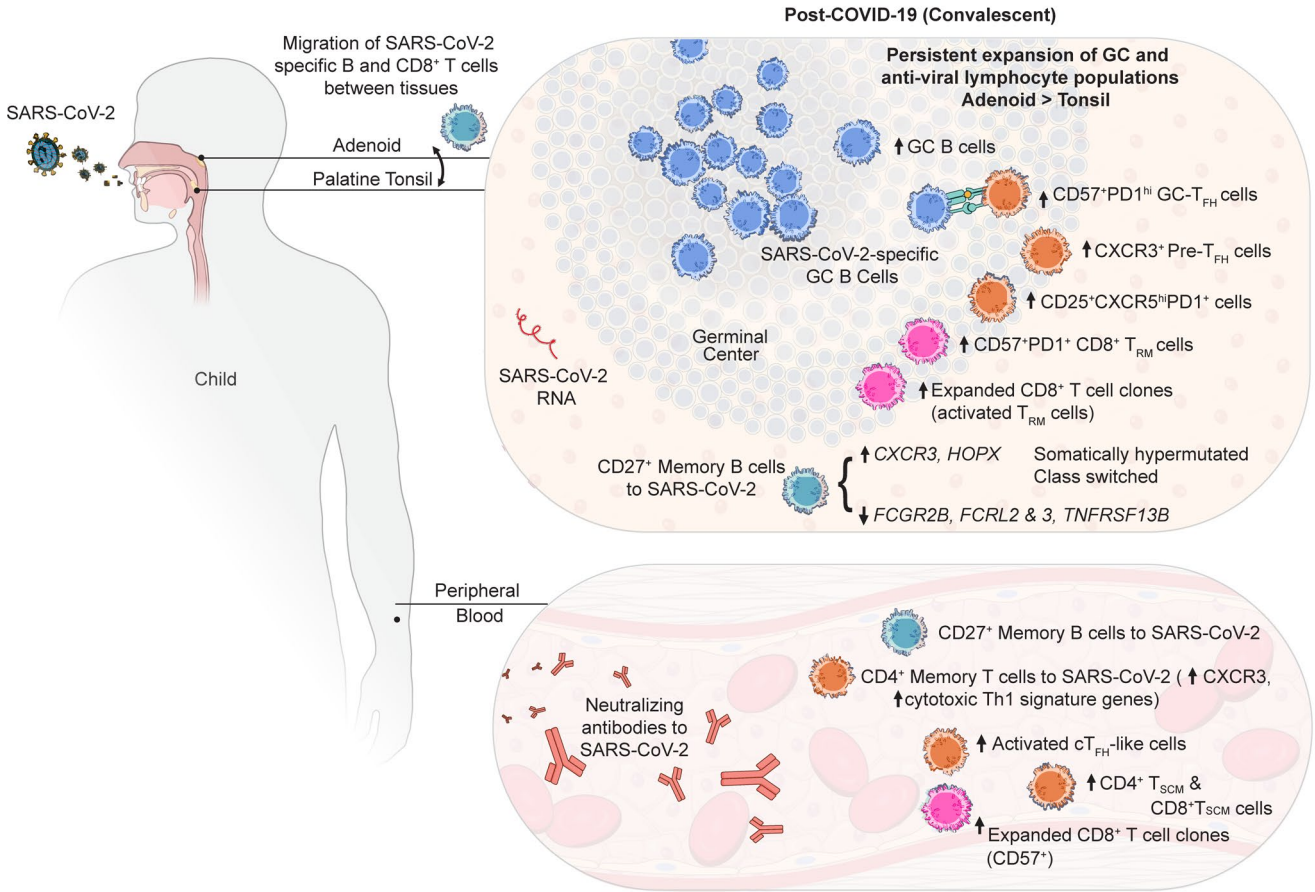

Extended Data Fig. 10 | Summary of findings. Schematic illustrating the immunologic profile of the pharyngeal lymphoid tissues and peripheral blood of COVID-19-convalescent children including (1) SARS-CoV-2-specific GC B, memory B and T cells with overlapping B and CD8⁺ T cell clones in the tonsils and adenoids, (2) persistent changes in lymphocyte populations involved in GC and anti-viral responses, which were most prominent in the adenoid, with type 1 (IFN-γ-associated) skewing of several T lymphocyte populations, and (3) persistence of viral RNA in the tissue.

nature portfolio

Corresponding author(s): Kalpana Manthiram, Pamela Schwartzberg

Last updated by author(s): 10/17/2022

Reporting Summary

Nature Portfolio wishes to improve the reproducibility of the work that we publish. This form provides structure for consistency and transparency in reporting. For further information on Nature Portfolio policies, see our Editorial Policies and the Editorial Policy Checklist.

Statistics

For all statistical analyses, confirm that the following items are present in the figure legend, table legend, main text, or Methods section.

n/a	Confirmed	
☐	☒	The exact sample size (*n*) for each experimental group/condition, given as a discrete number and unit of measurement
☐	☒	A statement on whether measurements were taken from distinct samples or whether the same sample was measured repeatedly
☐	☒	The statistical test(s) used AND whether they are one- or two-sided *Only common tests should be described solely by name; describe more complex techniques in the Methods section.*
☐	☒	A description of all covariates tested
☐	☒	A description of any assumptions or corrections, such as tests of normality and adjustment for multiple comparisons
☐	☒	A full description of the statistical parameters including central tendency (e.g. means) or other basic estimates (e.g. regression coefficient) AND variation (e.g. standard deviation) or associated estimates of uncertainty (e.g. confidence intervals)
☐	☒	For null hypothesis testing, the test statistic (e.g. *F*, *t*, *r*) with confidence intervals, effect sizes, degrees of freedom and *P* value noted *Give P values as exact values whenever suitable.*
☒	☐	For Bayesian analysis, information on the choice of priors and Markov chain Monte Carlo settings
☐	☒	For hierarchical and complex designs, identification of the appropriate level for tests and full reporting of outcomes
☐	☒	Estimates of effect sizes (e.g. Cohen's *d*, Pearson's *r*), indicating how they were calculated

Our web collection on statistics for biologists contains articles on many of the points above.

Software and code

Policy information about availability of computer code

Data collection

Participants' clinical data were collected and managed in REDCap web database platform.
Flow cytometric data were collected on a Cytek Aurora with manufacturer's software (SpectroFlo V1.1).
S1+/S1- B cells, CD95+CD4/CD8 were sorted from adenoid and tonsil on FACSAria Fusion SORP with manufacturer's software (BD FACSDiva Software V8.0.2).
S1+/S1- B cells, CD95+CD4/CD8 were sorted from PBMC on FACSAria III with manufacturer's software (BD FACSDiva Software V8.0.2).
ddPCR were performed on QX200 Droplet Reader (Bio-Rad) and analyzed using the freely available QuantaSoft Analysis Pro Software (Bio-Rad) to quantify copies of N1, N2, and RP genes per well, which was then normalized to RNA concentration input.
scRNA+CITEseq+TCR/BCRseq were acquired from Illumina NovaSeq platform.

Data analysis

1. For unsupervised analysis of flow cytometric data, FCS files (3.0) as well as FlowJo workspaces (10.7.2) were processed in R (4.1) via Rstudio (1.4.1717) and Bioconductor (3.13) using cytoverse (0.0.0.9000), including flowCore (2.4.0), flowWorkspace (4.4.0), ggcyto (1.20.0), openCyto (2.4.0), CytoML (2.4.0), cytolib (2.4.0) and cytoqc (0.99.2). Seurat (4.0.3), uwot (0.1.10) and leiden (0.3.9) were used in shared nearest neighbors graph building, t-UMAP projection, and meta-clustering, respectively, with default settings. t-UMAP projections as well as all confidence intervals of coefficients and their p-values (from two-tailed t-test of each coefficient within each model) are presented in plots built with ggplot2 (3.3.5).
2. Manual analysis of flow cytometric data was performed with FlowJo (v10.7.2).
3. Multiple intracytokine production analysis was performed with SPICE (V6).
4. NovaSeq sequencing data were analyzed using CellRanger (10x Genomics, v 6.0.0) to map cDNA libraries to the hg19 genome reference (10x Genomics hg19 CellRanger reference, v 1.2.0) and to count antibody tag features. Data were further processed using Seurat (v.4.0.1) running in R (v4.0.3). Surface protein library counts were transformed with dsb. ComplexHeatmap package and ggplot2 were used for visualization. Differentially expressed genes between S1+ and S1- B cells determined with Seurat after downsampling with seqtk v1.3.
5. V(D)J genes for each sequence were aligned to the IMGT reference database v3.1.29 using IgBlast v1.16.0 and Change-O v1.0.0. BCR analyses performed using R v.4.1.1 and scoper (v1.1.0), shazam (v1.1.0), alakazam (v1.1.0), dowser (v0.1.0) and IgPhyML(v1.1.3). Results were visualized with ggpubr (v0.4.0), ggplot2 (v3.3.5), dowser (v0.1.0) and ggtree (v3.0.4). BCRs were compared to the COV-AbDab database.

TCR repertoire was analyzed with scRepertoire (v1.6.0).
6. For image analysis, immunolabeling was performed with the PELCO BioWave Pro 36500-230 microwave equipped with a PELCO SteadyTemp Pro 50062 Thermoelectric Recirculating Chiller (Ted Pella) using a 2-1-2-1-2-1-2-1-2 program. After captured with an inverted Leica TCS SP8 X confocal microscope, a combination of automatic and manual surface/contour creation methods were used to define germinal center (GC) regions of interest (ROI) with Imaris software (Imaris version 9.8.0, Bitplane AG). The number and phenotype of T cells inside and outside of the B cell follicle/GC were quantified using histo-cytometry and analyzed with FlowJo v10.6.1. Imaging data were exported and processed in Excel (Microsoft Office v16.65) and GraphPad Prism 8.2.1.
7. Correlations assessed using the Spearman rank correlation were visualized by corrplot (v0.92).
7. Statistical analysis was done in SPSS(IBM, version 28.0.0.0) or R(4.1). Scatter and bar plots were generated in GraphPad Prism v8 and 9. Scripts used have been deposited in github: https://github.com/kalpanamanthiram/Covid-Tonsil

For manuscripts utilizing custom algorithms or software that are central to the research but not yet described in published literature, software must be made available to editors and reviewers. We strongly encourage code deposition in a community repository (e.g. GitHub). See the Nature Portfolio guidelines for submitting code & software for further information.

Data

Policy information about availability of data

All manuscripts must include a data availability statement. This statement should provide the following information, where applicable:

- Accession codes, unique identifiers, or web links for publicly available datasets
- A description of any restrictions on data availability
- For clinical datasets or third party data, please ensure that the statement adheres to our policy

Raw CITE-seq data has been deposited into GEO, accession GSE215802. Source data are provided with the article are in the supplementary tables or upon request from the corresponding authors. SARS-CoV-2-specific TCR sequences were downloaded from the immuneCODE database, VDJdb database, and recent manuscripts (cited in the text).

Field-specific reporting

Please select the one below that is the best fit for your research. If you are not sure, read the appropriate sections before making your selection.

☒ Life sciences ☐ Behavioural & social sciences ☐ Ecological, evolutionary & environmental sciences

For a reference copy of the document with all sections, see nature.com/documents/nr-reporting-summary-flat.pdf

Life sciences study design

All studies must disclose on these points even when the disclosure is negative.

Sample size	No sample size calculation was performed given the exploratory nature of the study. We collected peripheral blood, tonsils, and adenoids from 110 participants which were determined by surgeon operating room schedules and availability of study staff to consent participants. Sample sizes for studies of particular tissues, especially PBMCs, were limited by availability of adequate amount of tissue/blood.
Data exclusions	For flow cytometry analyses, exclusion criteria for controls: 1. Exclude those without sleep disordered breathing (SDB) or obstructive sleep apnea (OSA) and exclude those with frequent tonsillitis (> 6 episodes/year): CNMC 4, 6, 12, 26, 30, 38, 40, 53, 66, 67, 68, 75, 79, 88, 93, 105,106,107 2. CNMC 43 (had positive nasopharyngeal PCR, but negative serology, neutralization titers, and no SARS-CoV-2 specific B cells by flow cytometry) 3. CNMC 58 and 76 (indeterminate serology, but negative neutralization titers and no SARS-CoV-2 specific B cells by flow cytometry) 4. Exclude those with sickle cell anemia: CNMC 25, 37, 92 5. Exclude those taking the following immunodulating medications within 2 weeks of surgery: montelukast, cetirizine, or oral corticosteroids - CNMC 2, 3, 60, 19, 33, 61 6. Particular tissue or blood samples were not collected 7. Too few cells on flow cytometry acquisition 8. Low cell viability after sample processing 9. Exclude samples with obvious shift on manual gating 10. For unsupervised clustering analysis: Prior to statistical modeling of cluster frequencies, principal component analysis of frequencies (rank-normalized) was used in QC. Upon visual inspection of the first two principal components, single outlier samples located outside the main structure of the data were excluded. For AIM assay (peptide pool stimulation), intracytokine staining after PMA/ionomycin stimulation, and imaging, COVID-19 convalescent and control samples were matched based on confounding factors including age, sex, and clinical disorder and based on the availability of adequate amount of sample. For CITEseq, samples were selected based on adequate availability of the cells from each tissue.
Replication	In order to avoid losing cell populations during freeze-thaw, we stained and acquired flow cytometric data from freshly processed cells. Two study personnel performed all of these laboratory studies. Unsupervised analysis and manual gating of flow cytometry data was independently performed by two investigators and revealed similar results. The study design does not lend itself to replication.

Randomization

We approached patients scheduled to undergo tonsillectomy regarding study participation without exclusion based on COVID-19 history or demographics. Only two participants were recruited later in the collection period specifically because they had a known history of COVID-19. they Samples were processed the day after collection and flow cytometry panels were stained and acquired the day after collection as they arrived. For functional studies, imaging, ddPCR, and CITE-seq, samples were selected based on their SARS-CoV-2 infection status.

Blinding

Researchers were not blinded to the COVID-19-exposure status of participants as participants were queried about exposure history; however, many participants, and therefore the research team, were unaware of prior infection. For functional studies, imaging, and CITE-seq, researchers were not blinded because samples were selected for the experiment based on their exposure status. Samples for the CITE-seq experiment were pooled in order to minimize batch effect.

Reporting for specific materials, systems and methods

We require information from authors about some types of materials, experimental systems and methods used in many studies. Here, indicate whether each material, system or method listed is relevant to your study. If you are not sure if a list item applies to your research, read the appropriate section before selecting a response.

Materials & experimental systems

n/a	Involved in the study
☐	☒ Antibodies
☐	☒ Eukaryotic cell lines
☒	☐ Palaeontology and archaeology
☒	☐ Animals and other organisms
☐	☒ Human research participants
☒	☐ Clinical data
☒	☐ Dual use research of concern

Methods

n/a	Involved in the study
☒	☐ ChIP-seq
☐	☒ Flow cytometry
☒	☐ MRI-based neuroimaging

Antibodies

Antibodies used

Number Reagent Source Catalog number Clone Dilution (PBMC, ul/200ul) Dilution (Adenoid and Tonsil, ul/200ul)
1 Anti-CD11c-BUV395 BD 563787 B-ly6 3 ul 4.5 ul
2 Anti-CD71-BUV661 BD 749818 L01.1 0.5 ul 1.6 ul
3 Anti-CD138-BUV737 BD 612834 MI15 1 ul 2.4 ul
4 Anti-CD45-BUV805 BD 612891 HI30 2 ul 3.3 ul
5 Anti-CD62L-BV750 BD 747422 DREG-56 0.6 ul 0.6 ul
6 Anti-FCRL5/FCRL3-AF647 BD 564343 307307 2.5 ul 4.5 ul
7 Anti-CD86-AF700 BD 561124 2331 (FUN-1) 1 ul 2.5 ul
8 Anti-CD20-APC-H7 BD 560734 2H7 2 ul 3.3 ul
9 Anti-CD10-BV510 BD 563032 HI10a 2 ul 1.6 ul
10 Anti-CD19-BV650 BD 563226 SJ25C1 3 ul 7.5 ul
11 Anti-CD95-PE-Cy5 BD 340480 DX2 1 ul 0.8 ul
12 Anti-IgG-PE-Cy7 BD 561298 G18-145 2 ul 6.5 ul
13 Anti-CD3-BV570 BioLegend 300436 UCHT1 3 ul 3.3 ul
14 Anti-IgD-BV605 BioLegend 348232 IA6-2 2 ul 2.5 ul
15 Anti-IgM-BV711 BioLegend 314540 MHM-88 2 ul 5 ul
16 Anti-CD27-BV785 BioLegend 302832 O323 3 ul 1.6 ul
17 Anti-CD14-Spark Blue 550 BioLegend 367148 63D3 2.5 ul 3.3 ul
18 Anti-CD21-FITC BioLegend 354910 Bu32 2 ul 1.6 ul
19 Live dead dye-Zombie NIR BioLegend 423106 0.25 ul 0.25 ul
20 CoV2-RBD-Biotin BioLegend 793906 2.5 ul of conjugated antibody 2.5 ul of conjugated antibody
21 SAv-BV421 BioLegend 405225
22 CoV2-S1-Biotin BioLegend 793806 5 ul 5 ul
23 SAv-APC ThermoFisher S32362
24 Anti-CD38-APC-Fire810 BioLgend 303550 HIT2 1 ul 1 ul
25 Anti-IgA-VioBlue Miltenyi 130-113-479 IS11-8E10 2 ul 1.3 ul
26 Anti-CD85j-Super bright 436 ThermoFisher 62-5129-42 HP-F1 2.5 ul 6.5 ul
27 Anti-FCRL4-PerCP-eFluor710 ThermoFisher 46-3079-42 413D12 5 ul 2.4 ul

2. Broad immunophenotying flow panel:
Number Reagent Source Catalog Number Clone Dilution (PBMC, ul/180ul) Dilution (Adenoid and Tonsil, ul/180ul)
1 Anti-CD141-BB515 BD 566017 1A4 2.5 ul 2.5 ul
2 Anti-CD16-BUV496 BD 612944 3G8 0.6 ul 0.6 ul
3 Anti-TCR γδ-BB700 BD 745944 11F2 1 ul 4 ul
4 Anti-CD11c-BUV661 BD 612967 B-ly6 3.5 ul 3.5 ul
5 Anti-IgG-BV605 BD 563246 G18-145 5 ul 5 ul
6 Anti-CD127-APC-R700 BD 565185 HIL-7R-M21 6 ul 5 ul
7 Anti-IgD-BV480 BD 566138 IA6-2 0.6 ul 1 ul
8 Anti-CD56-BUV737 BD 612766 NCAM16.2 3.5 ul 3.5 ul
9 Anti-CXCR5-BV750 BD 747111 RF8B2 1.2 ul 1.2 ul
10 Anti-CD8-BUV805 BD 612889 SK1 1.2 ul 1.2 ul

11 Anti-ICOS-BUV563 BD 741421 DX29 0.6 ul 1.2 ul
12 Anti-CD45RA-BUV395 BD 740315 5H9 0.3 ul 0.6 ul
13 SAv-BUV615 BD 613013 0.9 ul 0.9 ul
14 Anti-CD14-Spark Blue 550 BioLegend 367148 63D3 2.5 ul 2.5 ul
15 Anti-CD25-PE BioLegend 302606 BC96 10 ul 10 ul
16 Anti-CD28-BV650 BioLegend 302946 CD28.2 2.5 ul 5 ul
17 Anti-CXCR3-PE-Cy7 BioLegend 353720 G025H7 5 ul 5 ul
18 Anti-PD-1-BV785 BioLegend 329930 EH12.2H7 5 ul 2.5 ul
19 Anti-CCR6-BV711 BioLegend 353436 G034E3 1.2 ul 1.2 ul
20 Anti-CCR7-BV421 BioLegend 353208 G043H7 5 ul 5 ul
21 Anti-CD19-Spark NIR 685 BioLegend 302270 HIB19 1.2 ul 2.5 ul
22 Anti-CD38-APC/Fire 810 BioLegend 303550 HIT2 1 ul 1 ul
23 Anti-CD57-FITC BioLegend 359604 HNK-1 1.2 ul 1.2 ul
24 Anti-CD1c-Alexa Fluor 647 BioLegend 331510 L161 5 ul 1.2 ul
25 Anti-HLA-DR-APC-Fire 750 BioLegend 307658 L243 2.5 ul 2.5 ul
26 Anti-IgM-BV570 BioLegend 314517 MHM-88 2.5 ul 4 ul
27 Anti-CD24-PE/Dazzle 594 BioLegend 311134 ML5 5 ul 5 ul
28 Anti-CD3-BV510 BioLegend 317332 OKT3 5 ul 5 ul
29 Anti-CD21-PerCP CY5.5 BioLegend 354908 Bu32 1.2 ul 2.5 ul
30 Anti-CD4-CF568 Cytek R7-20041 SK3 1.2 ul 1.2 ul
31 Anti-IgA-Biotin Jackson ImmunoResearch 109-066-011 Polyclonal 5 ul 5 ul
32 Anti-CD123-Super Bright 436 ThermoFisher 62-1239-42 6H6 3.5 ul 3.5 ul
33 Anti-CD95-PE-Cy5 ThermoFisher 15-0959-42 DX2 0.6 ul 0.6 ul
34 Anti-CD45-PerCP ThermoFisher MHCD4531 HI30 1.2 ul 1.2 ul
35 Anti-CD20-Pacific Orange ThermoFisher MHCD2030 HI47 2.5 ul 7.5 ul
36 Anti-CD161-eFluor 450 ThermoFisher 48-1619-42 HP-3G10 5 ul 5 ul
37 Anti-CD27-APC ThermoFisher 17-0279-42 O323 5 ul 2.5 ul
38 Live dead dye-Blue ThermoFisher L23105 0.225 ul 0.225

3. Imaging panel
Number Panel Step Antibodies Conjugate
1 GC 1 Hoechst 33342 NA Biotium 40046 NA 1: 5000
2 GC 3 CD20 Alexa Fluor 488 ThermoFisher 53-0202-82 L26 1: 100
3 GC 3 Ki-67 Biotin Novus NB500-170B Polyclonal 1 :10
4 GC 4 See Above Streptavidin Alexa Fluor 532 ThermoFisher S11224 NA 1: 200
5 GC 1 CD138 Unconjugated R&D AF2780 Polyclonal 1: 50
6 GC 2 Donkey anti-goat IgG Alexa Fluor 555 ThermoFisher A21432 Polyclonal 1: 200
7 GC 3 CD68 iFluor 594 Caprico Biotechnologies 1064135 KP1 1: 40
8 GC 1 CD21 Unconjugated Abcam Ab240987 SP186 1: 200
9 GC 2 Donkey anti-rabbit IgG Alexa Fluor 680 ThermoFisher A10043 Polyclonal 1: 200
10 T 1 Hoechst 33342 NA Biotium 40046 NA 1: 5000
11 T 3 CD57 Unconjugated BioLegend 359602 HNK-1 1: 50
12 T 4 Donkey anti-mouse IgM Alexa Fluor 488 Jackson ImmunoResearch 715-545-020 Polyclonal 1: 200
13 T 3 Ki-67 Biotin Novus NB500-170B Polyclonal 1: 10
14 T 4 See Above Streptavidin iFluor 514 AAT Bioquest 16956 NA 1: 50
15 T 1 CD8 Unconjugated ThermoFisher 14-0085-82 C8/144B 1: 10
16 T 2 Donkey anti-mouse IgG Alexa Fluor 555 ThermoFisher A31570 Polyclonal 1: 200
17 T 1 CD3 Unconjugated Abcam Ab205228 SP7 1: 100
18 T 2 Donkey anti-rabbit IgG Alexa Fluor 594 ThermoFisher A21207 Polyclonal 1: 200
19 T 3 HLA-DR AF647 Novus NBP2-47670AF647 LN-3 1: 150
20 T 1 PD-1 Unconjugated R&D AF1086 Polyclonal 1: 20
21 T 2 Donkey anti-goat IgG Alexa Fluor 680 ThermoFisher A-21084 Polyclonal 1: 200

4. T cell cytokine panel
Reagent Source Catalog number Clone Dilution (PBMC, ul/180ul) Dilution (Adenoid and Tonsil, ul/180ul)
1 Anti-CD45RA-BUV395 BD 740315 5H9 0.6 ul 0.6 ul
2 Anti-CD56-BUV737 BD 612766 NCAM16.2 3.5 ul 3.5 ul
3 Anti-CD8-BUV805 BD 612889 SK1 1 ul 1.2 ul
4 Anti-CXCR5-BV750 BD 747111 RF8B2 1 ul 1 ul
5 Anti-CD25-BB515 BD 564467 2A3 10 ul 10 ul
6 Anti-CD95-BB700 BD 566542 DX2 0.6 ul 0.6 ul
7 Anti-CD103-BUV661 BD 749993 Ber-ACT8 5 ul 2.5 ul
8 Anti-CD69-BUV563 BD 748764 FN50 1 ul 1 ul
9 Anti-CXCR3-PECy5 BD 551128 1C6/CXCR3 5 ul 5 ul
10 Anti-Granzyme B-PE BD 561142 GB11 1.8 ul 3.6 ul
11 Anti-IL4-PerCP Cy5.5 BD 561234 8D4-8 7.2 ul 3.6 ul
12 Anti-IL21-Alexa Fluor 647 BD 560493 3A3-N2.1 36 ul 36 ul
13 SAv-BUV615 BD 613013 0.9 ul 0.9 ul
14 Anti-CCR7-BV421 BioLgend 353208 G043H7 5 ul 1 ul
15 Anti-CD3-BV510 BioLgend 344828 SK7 2.5 ul 2.5 ul
16 Anti-CCR6-BV711 BioLgend 353436 G034E3 1 ul 1 ul
17 Anti-PD1-BV785 BioLgend 329929 EH12.2H7 5 ul 1.2 ul
18 Anti-CD57-FITC BioLgend 359604 HNK-1 1.2 ul 1.2 ul
19 Anti-CD14-Spark Blue 550 BioLgend 367148 63D3 1 ul 2.5 ul
20 Anti-HLA-DR-APC/Fire 750 BioLgend 307658 L243 2 ul 2 ul
21 Anti-CD38-APC/Fire810 BioLgend 303550 HIT2 1 ul 1 ul

22 Anti-CD19-Spark NIR 685 BioLgend 302270 HIB19 1.2 ul 1.2 ul
23 Anti-IL17A-BV605 BioLgend 512326 BL168 3.6 ul 3.6 ul
24 Anti-IL2-BV650 BioLgend 500334 MQ1-17H12 5.4 ul 10.8 ul
25 Anti-IFNγ-Pacific Blue BioLgend 502522 4S.B3 3.6 ul 3.6 ul
26 Anti-IL10-PE/Dazzle 594 BioLgend 506812 JES3-19F1 3.6 ul 3.6 ul
27 Anti-Perforin-APC BioLgend 353312 B-D48 9 ul 9 ul
28 Anti-TNFa-PE-Cy7 BioLgend 502930 MAb11 0.36 ul 0.36 ul
29 Anti-CD107a (LAMP-1) -Biotin BioLgend 328604 H4A3 1ul with 200ul culture medium 2 ul in 200ul culture medium
30 Anti-CD4-CD568 Cytek R7-20041 SK3 0.6 ul 2.5 ul
31 Anti-CD45-PerCP ThermoFisher MHCD4531 HI30 0.5 ul 1.2 ul
32 Anti-CD27-Super Bright 436 ThermoFisher 62-0279-42 O323 5 ul 5 ul
33 Live dead dye-Blue ThermoFisher L23105 0.225 ul 0.225 ul

5. Activation induced marker panel
Number Reagent Source Catalog number Clone Dilution (PBMC, ul/180ul) Dilution (Adenoid and Tonsil, ul/180ul)
1 Anti-CXCR3-PE/Cy5 BD 551128 1C6/CXCR3 5 ul 5 ul
2 Anti-CXCR5-BV750 BD 747111 RF8B2 1 ul 1 ul
3 Anti-CD45RA-BUV395 BD 740315 5H9 0.6 ul 0.6 ul
4 Anti-ICOS-BUV563 BD 741421 DX29 0.6 ul 1.2 ul
5 Anti-CD56-BUV737 BD 612766 NCAM16.2 3.5 ul 3.5 ul
6 Anti-CD8-BUV805 BD 612889 SK1 1 ul 1.2 ul
7 Anti-CD40L-PE BD 557299 TRAP1 10 ul 15 ul
8 Anti-CD25-PE-CF594 BD 562403 M-A251 2 ul 2 ul
9 Anti-CCR7-BV421 BioLegend 353208 G043H7 1 ul 1 ul
10 Anti-CCR6-BV711 BioLegend 353436 G034E3 1 ul 1 ul
11 Anti-CD4-BV605 BioLegend 317438 OKT4 1 ul 1 ul
12 Anti-CD69-BV650 BioLegend 310934 FN50 2 ul 2.5 ul
13 Anti-PD1-BV785 BioLegend 329930 EH12.2H7 5 ul 1.2 ul
14 Anti-CD57-FITC BioLegend 359604 HNK-1 2 ul 1 ul
15 Anti-CD14-Spark Blue 550 BioLegend 367148 63D3 1 ul 2.5 ul
16 Anti-CD45-PerCP BioLegend 368506 2D1 0.5 ul 1.2 ul
17 Anti-4-1BB-PeCy7 BioLegend 309818 4B4-1 2.5 ul 2.5 ul
18 Anti-CD19-Spark NIR 685 BioLegend 302270 HIB19 1.2 ul 2.5 ul
19 Anti-CD38-APC/Fire 810 BioLegend 303550 HIT2 1 ul 1 ul
20 Anti-HLA-DR-APC/Fire 750 BioLegend 307658 L243 2 ul 2.5 ul
21 Anti-OX40-APC BioLegend 350008 Ber-ACT35 5 ul 5 ul
22 Live dead dye- Blue ThermoFisher L23105 0.9 ul 0.9 ul
23 CD40 Antibody, anti-human Miltenyi 130-094-133 130-094-133 0.5ug/ml 0.5ug/ml

6. S1+ /S1- B cell and CD95+ CD4/CD8 T cell sorting panel
Number Reagent Source Catalog number Clone Dilution (PBMC, 30mill in 200ul) Dilution (Adenoid & Tonsil, 30mill in 200ul)
1 Anti-CD19-PeCy7 BIoLegend 302216 HIB19 1: 20 1: 20
2 Anti-CD56-BV510 BIoLegend 362533 5.1H11 1: 10 1: 10
3 Anti-CD14-BV510 BIoLegend 367124 63D3 1: 10 1: 10
4 Anti-CD3-Alexa Fluor 488 BIoLegend 317310 OKT3 7: 100 1: 20
5 Anti-CD8-PE BIoLegend 303804 QA18A37 1: 20 1: 20
6 Anti-CD95-PE/Dazzle 594 BIoLegend 305634 DX2 1: 40 1: 40
7 CoV2-S1-Biotin BIoLegend 793806 1: 5 of conjugated antibody 1: 5 of conjugated antibody
8 BIoLegend 405225
9 Anti-CD45-PerCP-Vio 700 Miltenyi 130-110-636 REA747 1: 20 1: 20
10 Anti-CD4-APC-eFLuor 780 ThermoFisher 47-0048-42 OKT4 1: 10 1: 10
11 Live dead dye-Aqua ThermoFisher L34957 7: 200 7: 200
12 SAv-APC ThermoFisher S32362 1: 5 of conjugated antibody 1: 5 of conjugated antibody

7. CiteSeq antibody panel
Number Reagent Source Catalog number Barcode Clone Dilution (ul/30mill PBMC in 200ul volume) Dilution (ul/30mill Adenoid & Tonsil in 200ul volume)
1 TotalSeq™-C0384 anti-human IgD Antibody BioLegend 348245 CAGTCTCCGTAGAGT IA6-2 8 ul 16 ul
2 TotalSeq™-C0389 anti-human CD38 Antibody BioLegend 303543 TGTACCCGCTTGTGA HIT2 16 ul 32 ul
3 TotalSeq™-C0154 anti-human CD27 Antibody BioLegend 302853 GCACTCCTGCATGTA O323 4 ul 8 ul
4 TotalSeq™-C0181 anti-human CD21 Antibody BioLegend 354923 AACCTAGTAGTTCGG Bu32 2 ul 4 ul
5 TotalSeq™-C0053 anti-human CD11c Antibody BioLegend 371521 TACGCCTATAACTTG S-HCL-3 2 ul 4 ul
6 TotalSeq™-C0828 anti-human CD307d (FcRL4) Antibody BioLegend 340213 CGATTTGATCTGCCT 413D12 8 ul 16 ul
7 TotalSeq™-C0829 anti-human CD307e (FcRL5) Antibody BioLegend 340309 TCACGCAGTCCTCAA 509f6 4 ul 8 ul
8 TotalSeq™-C0826 anti-human CD307c/FcRL3 Antibody BioLegend 374413 GCCTAGTTTGAACGC H5/FcRL3 8 ul 16 ul
9 TotalSeq™-C0006 anti-human CD86 Antibody BioLegend 305447 GTCTTTGTCAGTGCA IT2.2 2 ul 4 ul
10 TotalSeq™-C0147 anti-human CD62L Antibody BioLegend 304851 GTCCCTGCAACTTGA DREG-56 2 ul 4 ul
11 TotalSeq™-C0146 anti-human CD69 Antibody BioLegend 310951 GTCTCTTGGCTTAAA FN50 16 ul 32 ul
12 TotalSeq™-C0159 anti-human HLA-DR Antibody BioLegend 307663 AATAGCGAGCAAGTA L243 16 ul 32 ul
13 TotalSeq™-C0161 anti-human CD11b Antibody BioLegend 301359 GACAAGTGATCTGCA ICRF44 16 ul 32 ul
14 TotalSeq™-C0359 anti-human CD83 Antibody BioLegend 305341 CCACTCATTTCCGGT HB15e 8 ul 16 ul
15 TotalSeq™-C0088 anti-human CD279 (PD-1) Antibody BioLegend 329963 ACAGCGCCGTATTTA EH12.2H7 8 ul 16 ul
16 TotalSeq™-C0168 anti-human CD57 Recombinant Antibody BioLegend 393321 AACTCCCTATGGAGG "
QA17A04" 16 ul 32 ul
17 TotalSeq™-C0145 anti-human CD103 (Integrin αE) Antibody BioLegend 350233 GACCTCATTGTGAAT Ber-ACT8 8 ul 16 ul
18 TotalSeq™-C0180 anti-human CD24 Antibody BioLegend 311143 AGATTCCTTCGTGTT ML5 16 ul 32 ul

19 TotalSeq™-C0140 anti-human CD183 (CXCR3) Antibody BioLegend 353747 GCGATGGTAGATTAT "
G025H7 " 16 ul 32 ul
20 TotalSeq™-C0148 anti-human CD197 (CCR7) Antibody BioLegend 353251 AGTTCAGTCAACCGA G043H7 16 ul 32 ul
21 TotalSeq™-C0143 anti-human CD196 (CCR6) Antibody BioLegend 353440 GATCCCTTTGTCACT G034E3 8 ul 16 ul
22 TotalSeq™-C0144 anti-human CD185 (CXCR5) Antibody BioLegend 356939 AATTCAACCGTCGCC J252D4 8 ul 16 ul

Validation

All antibodies used for flow cytometry, CITE-seq, and histo-cytometry were from manufacturers/companies used in immunology studies. These companies have validated their antibodies in human PBMCs, tissues, or cell lines and the information from their websites is summarized.

All FACS antibodies were titrated for each panel to maximize specific signal and minimize background separately for PBMC or adenoid/tonsil cells. Note that the antibody concentrations used for CITE-seq were optimized by the manufacturer based on healthy PBMC samples, and thus may not be optimal for tissue samples. We have not independently verified the specificity of each antibody in our CITE-seq panel. Antibody concentrations were based on titration from flow cytometry.

Antibody validation from each manufacturer are given below.
Biolegend: For flow cytometry reagents, each lot product is validated by QC testing with a series of titration dilutions by BioLegend. Reactivity is verified in human PBMC (flow cytometry plots or histograms shown on website). For TotalSeq™ Antibodies, bulk lots are tested by PCR and sequencing to confirm the oligonucleotide barcodes. They are also tested by flow cytometry to ensure the antibodies recognize the proper cell populations. Bottled lots are tested by PCR and sequencing to confirm the oligonucleotide barcodes. Antibodies are verified in humans.

BD: Validated for flow cytometry (routinely tested) in human PBMCs (histogram or flow cytometry plots shown on website for each one) and QC tested.

Miltenyi: Validated for flow cytometry (routinely tested) in human PBMCs (flow cytometry plots shown on website) and QC tested .

Cytek: CD4 CFB548 manufactured and provided by Biotium, Inc. under an Agreement between Biotium and Cytek.

Biotium implements a Quality System, certified by QAS according to Standard QAS ISO 9001:2015. Histogram is showing staining on human PBMCs is shown.

Jackson ImmunoResearch: Biotinylated- IgA antibody: Based on immunoelectrophoresis and/or ELISA, the antibody reacts with the heavy chain of human IgA but not with human IgG or IgM. No antibody was detected against non-immunoglobulin serum proteins. The antibody may cross-react with IgA from other species.
IgM: Based on immunoelectrophoresis and/or ELISA, the antibody reacts with the heavy chain of mouse IgM but not with mouse IgG or the light chains of mouse immunoglobulins. No antibody was detected against non-immunoglobulin serum proteins. The antibody may cross-react with IgM from other species.

R&D: Reactivity shown in human tissue sections on website.

Thermofisher:Reactivity shown in human tissue sections (including some with tonsil) on website.

Caprico Biotechnologies: Verified for use in human PBMCs (histogram shown on website).

AAT Bioqust: Verified in human HeLa cells on website

Novus: Verified for use in immunohistochemistry of human tissues

Abcam: Antibodies were verified by relative expression to ensure that the antibodies binds to the antigen stated.

Eukaryotic cell lines

Policy information about cell lines

Cell line source(s)	293_ACE2_TMPRSS2 cell line was generated and sourced from the lab of Carol Weiss at FDA [see reference Neerukonda, S.N. et al. (2021) PLoS One 16, e0248348].
Authentication	Cell lines were checked for expression of ACE2 and validated by FACS analysis. None of the cell lines were authenticated by karyotyping or other genomic techniques.
Mycoplasma contamination	Negative for mycoplasma
Commonly misidentified lines (See ICLAC register)	No commonly misidentified cell lines were used in this study.

Human research participants

Policy information about studies involving human research participants

Population characteristics	Participant characteristics are given in Supplemental Tables 1-3.
Recruitment	We recruited 110 children who underwent tonsillectomy and/or adenoidectomy at Children's National Hospital (CNH) in Washington, DC, USA. All children scheduled to undergo tonsillectomy at CNH were eligible. The first 102 participants were recruited from late September 2020 to early February 2021 without screening for prior COVID-19. An additional 2 participants were subsequently recruited with known history of COVID-19, plus 6 additional subjects (one of whom turned out to be positive by serology) were recruited in May and June 2021. Experienced ENT surgeons assessed the clinical diagnoses of each participant. Informed onsent was obtained by the clinical research research team at CNH.
Ethics oversight	This study was approved by the Institutional Review Board (IRB) at Children's National Hospital (IRB protocol number 00009806). Written informed consent was obtained from parent/guardians of all enrolled participants, and assent was obtained from minor participants over 7 years of age.

Note that full information on the approval of the study protocol must also be provided in the manuscript.

Flow Cytometry

Plots

Confirm that:

☒ The axis labels state the marker and fluorochrome used (e.g. CD4-FITC).

☒ The axis scales are clearly visible. Include numbers along axes only for bottom left plot of group (a 'group' is an analysis of identical markers).

☒ All plots are contour plots with outliers or pseudocolor plots.

☒ A numerical value for number of cells or percentage (with statistics) is provided.

Methodology

Sample preparation

Blood and tissue collection
Tonsil and adenoid tissues were stored in RPMI media with 5% FBS (VWR), gentamicin 50mg/mL (Gibco), and 1X antibiotic/antimycotic solution (Gibco) on ice immediately after collection. Tissues were processed the day after collection. A 3-5mm portion of tonsil and adenoid tissue was cut and fixed in 5mL of 10% buffered formalin (Avantik) for 24-48 h. The fixed tissue was then incubated in 70% ethanol until it was paraffin-embedded. The remainder of the tissue was mechanically disrupted and filtered through a 100µm cell strainer to create a single cell suspension, lysed with ACK buffer (Gibco), and washed with PBS three times. Freshly isolated PBMCs and tonsil and adenoid cells were surface stained and analyzed with flow cytometry as described below on the day of processing. The remaining cells were stored in liquid nitrogen in the presence of fetal bovine serum (FBS, VWR) with 10% DMSO.

Frozen cell thawing method
Banked PBMC, tonsil and adenoid cells were thawed from liquid nitrogen in a 37°C water bath for 2-3 mins. 2 mL of media consisting of RPMI with 10% of FBS, 0.1mg/ml DNase I (Roche) and 10mM HEPES was added drop-by-drop to the thawed cells. Cells were further diluted by incremental addition of a 1:1 volume of media up to 8 mL, then centrifuged at 1600 rpm for 5 min. Cells were then resuspended in 300 µL of media, incubated at RT for 5 min, washed with media without DNase I, and filtered through a 100um strainer before spinning down for culture and resuspending in staining buffer (PBS + 1% BSA for CITEseq, PBS with 2% FBS and 2 mM EDTA for FACS).

High-dimensional flow cytometry: SARS-CoV-2 antigen specific B cell detection
5 million cells per sample of PBMC, adenoid, or tonsil were resuspended in PBS with 2% FBS and 2 mM EDTA (FACS buffer). Biotinylated S1 and RBD probes (BioLegend) were cross-linked with fluorochrome-conjugated streptavidin in a molar ratio of 4:1. Fluorochrome-conjugated streptavidin was split into 5 aliquots and conjugated to biotinylated probes by mixing for 20 min for each aliquot at 4°C. Cells were first stained with the viability dye, Zombie NIR (1:800 dilution, BioLegend), for 15 min at RT, washed twice and then incubated with True-Stain Monocyte Blocker (BioLegend) for 5 min. An antibody cocktail containing the rest of the surface antibodies, the S1 and RBD probes, and Brilliant Stain Buffer Plus (BD) were then added directly to the cells and incubated for 30 min at RT in the dark (200uL staining volume). Cells were washed three times and fixed in 1% paraformaldehyde for 20 min at RT before washing again and collecting on a spectral flow cytometer (Aurora, Cytek).

High-dimensional flow cytometry: broad immunophenotyping flow cytometry panel
2 million cells per sample of PBMC and 5 million cells per adenoid or tonsil were resuspended in FACS buffer. Cells were first stained with LIVE/DEAD Blue (1:800, ThermoFisher) for 15 min at RT, washed twice and then incubated with True-Stain Monocyte Blocker (BioLegend) for 5 min. Antibodies for chemokine receptors and TCRgd were sequential added at RT (anti-CCR7 for 10 min, anti-CCR6, anti-CXCR5 and anti-CXCR3 together with Brilliant Stain Buffer Plus for 5 min, anti-TCRgd for 10 min). An antibody cocktail containing the rest of the surface antibodies and Brilliant Stain Buffer Plus (BD) were then added directly to the cells and incubated for 30 min at RT in the dark (total staining volume 182uL). Cells were washed three times and stained with fluorescence conjugated streptavidin for 15 min at RT. Then, cells were washed twice times and fixed in 1%

paraformaldehyde for 20 min at RT before washing again and acquiring on a spectral flow cytometer (Aurora, Cytek).

Processing for CITE-seq
Banked PBMC, tonsil and adenoid from 2 donors with history of COVID-19 (CNMC 71 and 89) and one control (CNMC 99) were thawed from liquid nitrogen in a 37°C water bath for 2-3 mins. 2 mL of media consisting of RPMI with 10% of fetal bovine serum, 0.1mg/ml DNase I (Roche) and 10mM HEPES was added drop-by-drop to the thawed cells. Cells were further diluted by incremental addition of a 1:1 volume of media up to 8 mL, then centrifuged at 1600 rpm for 5 min. Cells were then resuspended in 300 µL of media, incubated at RT for 5 min, washed with media without DNase I, and filtered through a 100um strainer before spinning down and resuspending in staining buffer (PBS + 1% BSA). Cells were then incubated with Fc blocker (Human TruStain FcX, BioLegend), stained with TotalSeq-C human hashtag antibodies (BioLegend) to uniquely label the sample origin (by tissue and donor), and washed with PBS + 0.04% BSA. Adenoids and tonsils from the 3 donors (6 samples in total) were pooled together and PBMCs from 3 were pooled together separately. The number of cells to pool from each tissue and donor was calculated with the aim of pooling a similar number of S1+ positive B cells from each sample. Pooled cells were first incubated with Fc blocker at 4°C for 10 min followed by CITE-seq and sorting antibody cocktails in the following order at 4°C: TotalSeq anti-CXCR3 antibody for 10 min, TotalSeq chemokine cocktail (anti-CCR7, CCR6, CXCR5 antibodies) for 10 min, and the rest of CITE-seq antibodies and fluorescence-labeled sorting antibodies and viability dye (Aqua) for 30 min (Supplementary Table 10). Cells were then washed with PBS+0.04% BSA and resuspended in PBS+2% FBS. S1+ and S1- B cells were sorted from each pool on a BD Aria sorter (BD Biosciences, San Jose, CA). Cells were sorted into PBS +2% FBS. Note that the antibody concentrations used for CITE-seq were optimized by the manufacturer based on healthy PBMC samples, and thus may not be optimal for tissue samples. We have not independently verified the specificity of each antibody in our CITE-seq panel. Antibody concentrations were based on titration from flow cytometry.

Whole slide multiplexed imaging of FFPE tissue sections
Tissue and slide processing and staining
5 µm tissue sections were cut from FFPE samples and placed onto glass slides. Following sectioning, glass slides (with tissue) were baked in a 60°C oven for 1 hour. Deparaffinization was performed as described previously: 2 exchanges of 100% xylene (10 minutes per exchange) followed by 100% ethanol for 10 minutes, 95% ethanol for 10 minutes, 70% ethanol for 5 minutes, and 10% formalin for 15 minutes. Antigen retrieval was performed by incubating slides in AR6 buffer (Akoya Biosciences) for 40 minutes in a 95°C water bath. After 40 minutes, slides were removed from the water bath and allowed to cool on the bench for 20 minutes. Sections were permeabilized, blocked, and stained in PBS containing 0.3% Triton X-100 (Sigma-Aldrich), 1% bovine serum albumin (Sigma-Aldrich), and 1% human Fc block (BD Biosciences). Immunolabeling was performed with the PELCO BioWave Pro 36500-230 microwave equipped with a PELCO SteadyTemp Pro 50062 Thermoelectric Recirculating Chiller (Ted Pella) using a 2-1-2-1-2-1-2-1-2 program. In general, primary antibodies were applied first, washed 3 times in PBS, and incubated with appropriate secondary antibodies. Directly conjugated primary antibodies were applied last after blocking with host sera (5%). Endogenous biotin was blocked using the Avidin/Biotin Blocking Kit (Abcam). Cell nuclei were visualized with Hoechst (Biotium) and sections were mounted using Fluoromount G (Southern Biotech).

Activated induced marker (AIM) assay
Banked frozen PBMC and tonsil and adenoid cells were thawed as described above in “Processing for CITE-seq.” Two million mononuclear cells from tonsil or adenoid or one million PBMC from each donor were cultured in a 96 well round bottom plate at a concentration of 1x10E7 cells/mL in AIM media consisting of RPMI plus 5% human AB serum (Omega), 2 mM L-glutamine, 0.055 mM beta-mercaptoethanol, 1% penicillin/streptomycin, 1 mM sodium pyruvate, 10 mM HEPES, and 1% non-essential amino acids. Prior to addition of peptide pools, cells were blocked at 37°C for 15 min with 0.5µg/mL of anti-CD40 mAb (Miltenyi). Following this, cells were stimulated with SARS-CoV-2 peptide pools for 18 hours at 37°C in 5% CO2 incubator. The following peptide pools were reconstituted per instructions and used for stimulation (Miltenyi): PepTivator SARS-CoV-2 Prot_S+, PepTivator SARS-CoV-2 Prot_S1, PepTivator SARS-CoV-2 Prot_S, PepTivator SARS-CoV-2 Prot_N, PepTivator SARS-CoV-2 Prot_M. Prot_S+, Prot_S1 and Prot_S were pooled into one megapool of spike peptides at concentration of 0.6 nmol/ml for each pool. PHA-L (Millipore) at 5µg/ml was used as positive control. Negative control wells lacking peptides were supplemented with an equivalent volume of DMSO and ddH2O. After stimulation, cells were first stained with a viability dye (LIVE/DEAD Blue, ThermoFisher) for 15 min at RT, washed twice and then incubated with True-Stain Monocyte Blocker (BioLegend) for 5 min. Antibodies for chemokine receptors (anti-CXCR3 for 10 min, anti-CCR7 for 10 min, anti-CXCR5 and anti-CCR6 together for 5 min) were sequential added at RT. The antibody cocktail containing the rest of the surface antibodies and Brilliant Stain Buffer Plus (BD) was then added directly to the cells and incubated for 30 min at RT in the dark (total staining volume 180uL). Stained cells were washed three times and fixed in 1% paraformaldehyde for 20 min at RT before collecting on a spectral flow cytometer (Aurora, Cytek).

T cell functional assays - intracellular cytokine staining
Frozen cells were thawed as described in “Processing for CITE-seq.” 2 million PBMC, adenoid, or tonsil cells from each sample were resuspended in 200 uL of complete RPMI medium containing 10% FBS (VWR), 2 mM glutamine, 0.055 mM beta-mercaptoethanol, 1% penicillin/streptomycin, 1 mM sodium pyruvate, 10 mM HEPES, and 1% non-essential amino acids. Cells were stimulated with PMA (50ng/ml, Sigma), ionomycin (1000ng/ml, Sigma) for 2.5 h in the presence of anti-CD107a (BioLegend), GolgiSTOP (monensin, BD), and GolgiPlug (BFA, BD). After stimulation, surface markers were stained as described above in the AIM assay. Surface-stained cells were washed and fixed with Cytofix Fixation Buffer (BD) at RT for 20 min and washed with permeabilization buffer (eBioscience) twice. Then, the intracellular cytokine antibody mix was added for 30 min at RT (staining volume 50uL). Stained cells were collected on a spectral flow cytometer (Aurora, Cytek).

Instrument

Flow data were collected on a 5 laser Aurora (Cytek).
S1+/S1- B cells, CD95+ CD4/CD8 cells were sorted from adenoid and tonsil on FACSAria Fusion SORP.
S1+/S1- B cells, CD95+ CD4/CD8 cells were sorted from PBMC on instrument FACSAria III.
Single cell RNA sequenced on Illumina NovaSeq platform.

Software	FACSDiva Software(BD, V8.0.2) for sorting; Spectroflo (Cytek) for FACS data collection from Cytek Aurora.
Cell population abundance	S1+/- B cells (S1+ are ~0.1% of CD19+ B cells) were sorted from pooled adenoid/tonsil or pooled PBMC samples. CD95+CD4/CD8 cells were sorted from pooled adenoid/tonsil or pooled PBMC samples.
Gating strategy	Gating strategies are presented in the supplementary figures 1-3, 6, and 9.

☒ Tick this box to confirm that a figure exemplifying the gating strategy is provided in the Supplementary Information.